PREPARATION OF FUNCTIONAL BIODEGRADABLE COMPOSITE POLYMERIC MICRO-/NANO-PARTICLES FOR BIOMEDICAL APPLICATIONS

By

Anna Song

A DISSERTATION

Submitted to
Michigan State University
in partial fulfillment of the requirements
for the degree of

Materials Science and Engineering-Doctor of Philosophy

2018

ABSTRACT

PREPARATION OF FUNCTIONAL BIODEGRADABLE COMPOSITE POLYMERIC MICRO-/NANO-PARTICLES FOR BIOMEDICAL APPLICATIONS

By

Anna Song

Biodegradable polymers are a group of promising materials for various applications such as packaging, cosmetics, food, pharmaceutical and biomedical engineering. Due to their good biocompatibility and biodegradability, biodegradable polymers are often used to fabricate micro-/nano-particles as vehicles of drugs, growth factor, cosmetics ingredients, antimicrobials and so on. Among these, poly(lactic acid) (PLA) is one of the most commonly used biodegradable polymer and thus is used here to study the fabrication of various kinds of PLA composite micro-/nano-particles. In this study, various types PLA composite micro-/nano-particles were prepared based on the one-step double (W/O/W) emulsion method developed in our group.

Firstly, biodegradable magnetic particles with different sizes were prepared via the adaptable emulsion setup for the potential applications in magnetic resonance imaging (MRI) and magnetic drug delivery. Via the simple adjustment of emulsification temperature to high temperature or room temperature, a transformation of PLA-iron oxide nanoparticles (IONPs) composite particles from hollow microparticles to solid nanospheres can be achieved. This study presents a fast and easily adaptable process to encapsulate either hydrophobic or hydrophilic IONPs into the hydrophobic polymeric particles, with different shapes and sizes, by simply adjusting the emulsification temperature at the specific mixing condition in the one-step W/O/W emulsion process.

Secondly, a new system of heterogeneous PLA-polystyrene (PS) bioblend thin hollow microparticles with uniform hemispherical multicompartments and the subsequently formed PLA porous (Cagelike) microparticles were firstly developed via the one-step W/O/W emulsion combined with solvent-induced phase separation (SIPS) method. The driven forces for this unique multicompartmental structure are the dramatic change of the solubility of PS in ethyl acetate and the rapid solvent removal rate from the diffusion process. The overall microparticle size decreased with increasing amount of PS while the relative size of PS protrusion particle increased along with increasing PS. By replacing the solvent with a different solvent (toluene) or the PS with a different polymer (polycaprolactone, PCL), different anisotropic particles were obtained.

Lastly, PLA/nanoclay (various types) composite microparticles were developed and the key factors of controlling particle morphology were studied by both experiments and design of experiment (DOE) factorial analysis. Surfactant concentration was identified as the most effective parameter, compared to other factors including nanoclay/PLA ratio, pH of the water phase, viscosity and emulsion duration. The TGA analysis showed a relatively high content (~43%) of hydrophilic nanoclay (MMT) in the final PLA/nanoclay composite particles. A model drug (diclofenac) was encapsulated to study the nanoclay-drug interaction because of the high cation exchange capacity of nanoclay. The result showed that negatively charged natural nanoclay is not ideal for anionic or non-ionic drugs.

This thesis is dedicated to my grandfather and grandmother.
Thank you for being the first mentor of my life.

TABLE OF CONTENTS

LIST OF TABLES

LIST OF FIGURES

1 INTRODUCTION

1.1 BIODEGRADABLE POLYMERIC MICRO-/NANO-PARTICLES

Biodegradable polymers have become more and more popular in almost all the fields to replace the conventional petroleum-based, non-biodegradable polymers. Compared with the conventional commercial polymers, biodegradable polymers are environmentally friendly and less dependent on non-renewable resources. Generally, there are two types of biodegradable polymers: synthetic and bio-based. The form is from the conventional synthesis of bio-derived (polylactide) or synthetic monomers (polycaprolactones, polyesteramides). The latter one includes a wide range of natural macromolecules like polysaccharides (starch, cellulose, chitosan, alginate *etc.*), proteins and lipids, and microorganisms [1].

In recent decades, biodegradable polymeric micro-/nnao-particles have attracted numerous attention as controlled release (CR) vehicles for drug delivery, gene therapy, tissue engineering, cosmetics, and food packaging [2]. There are several advantages including 1) biocompatibility and biodegradability; 2) the ability for target delivery; 3) good dispersibility; 4) high encapsulation efficiency; 5) easy for scale up and so on [1]. There are two types of polymeric nanoparticles (NPs) as shown in Figure 1.1. One is the nanocapsules with a core-shell structure, in which the drug sits in the cavity coated by the polymer shell, or absorbed on the particle surface. The other one is called nanospheres, in which drugs disperse uniformly in the particle matrix, or absorbed on the particle surface [1, 3].

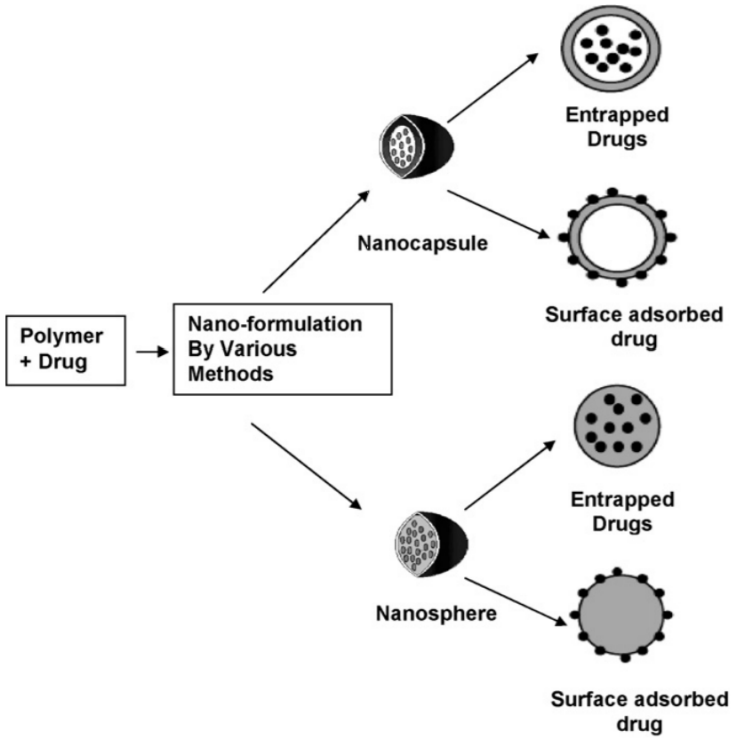

Figure 1. 1 Types of biodegradable polymeric nanoparticles drug delivery vehicles. Reproduced with permission from [3].

1.1.1 Particles from synthetic biodegradable polymers

Two types of methods have been mainly used to prepare micro-/nano-particles from synthetic biodegradable polymers: emulsion based and precipitation based nanoparticles [1, 4]. The emulsion-based method is to prepare an oil-in-water (O/W) emulsion followed by the solvent removal process (Figure 1.2). In the emulsion-solvent evaporation method, the organic solvent evaporates under reduced pressure, leading to the formation of solidified polymer particles. This emulsion-solvent evaporation method has also been modified to obtain nanocapsules with an oil/perfluorocarbon core [5]. In the emulsion-diffusion method, a partially water-miscible solvent is used as the oil phase, which is mixing saturated with water before the emulsion process. After adding the O/W emulsion into a large amount of water, the equilibrium of the system changes, which causes the diffusion of the solvent to the outer water phase [6]. This emulsion-diffusion

process has also been modified to fabricate nanocapsules by introducing oil into the solvent phase [7]. Another technique is the reverse salting-out process by using a water-soluble polymer as a stabilizer. The advantage of this method is that no surfactant and heating needed, which can be applied to biopolymers or temperature-sensitive drugs [8].

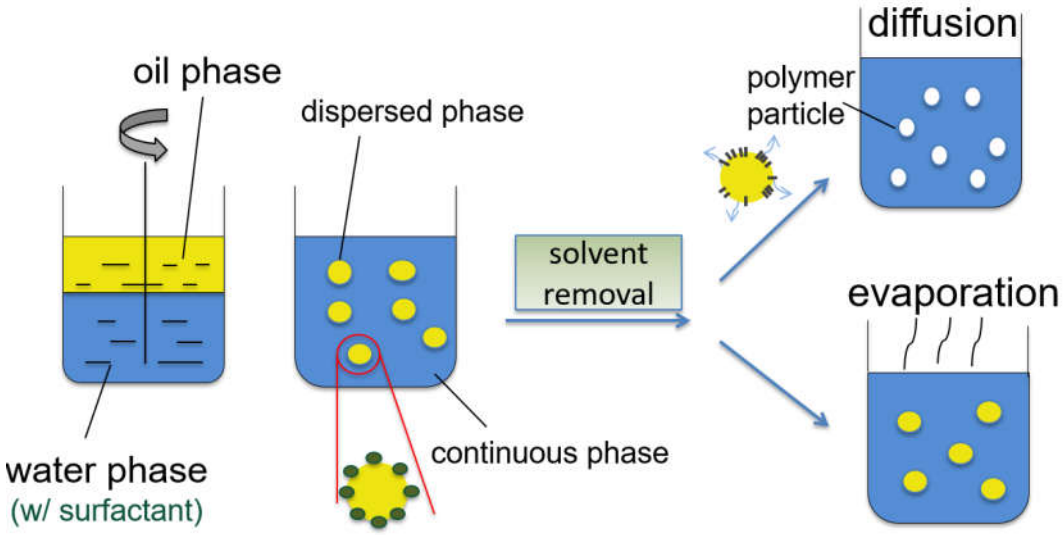

Figure 1. 2 Schematic of polymer particles prepared by emulsion solvent-removal method.

In order to encapsulate hydrophilic drugs, a double emulsion method, water-in-oil-in-water (W/O/W), has been developed with drugs sitting in the inner water phase [9]. The main advantage telling this method from others is an efficient encapsulation of hydrophilic drugs. The conventional double emulsion needs two steps as shown in Figure 1.3 (left). Recently, a one-step double emulsion has been developed with a modified Taylor-Couette Nanomixer in our group as shown in Figure 1.2 (right) [10]. This new technique is more suitable for scaling up due to its facile process and short time emulsion (2 min).

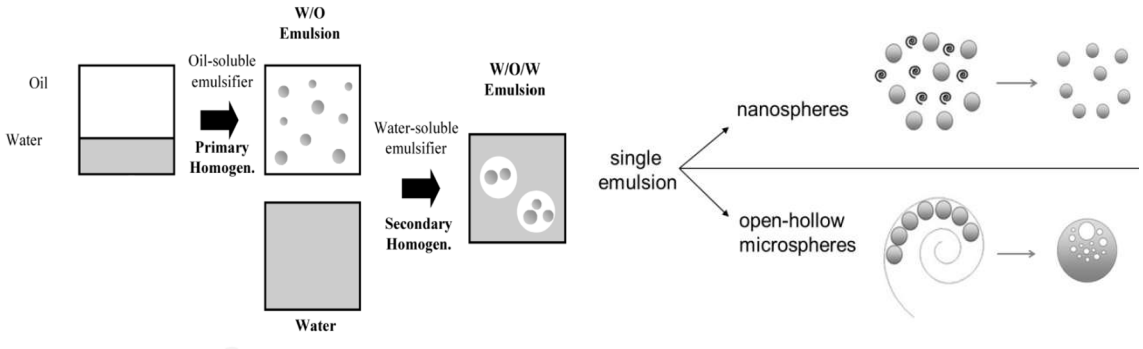

Figure 1. 3 Comparison of conventional two-step double-emulsion process and innovative one-step double emulsion. Reproduced with permission from [10, 11].

The second type of method is developed by Fessi et al. and is called nanoprecipitation [12]. This process is based on the fact that the polymer will precipitate when the non-solvent is added to the polymer solution. The solvent and non-solvent must be mutually miscible. Nanocapsules can be prepared with a similar process by interfacial deposition of the biodegradable polymer, followed by the removal of solvent through diffusion [13].

1.1.2 Particles from biopolymers

Biopolymers like collagen, chitosan, alginate, gelatin, starch etc. have attracted a lot of attention due to their natural biocompatibility and bioavailability. There are several common methods for the fabrication of protein and polysaccharide based biopolymer nanoparticles including emulsification, desolvation, coacervation and electrospray drying [14]. In addition, different methods have been developed based on the unique properties of different materials. Calvo et al. developed a method called ionic gelation to prepare chitosan nanoparticles. In this method, a polyanion sodium tripolyphosphate (TTP) has been used to interact with the positively charged amino group of chitosan. Ionic gelation is a mild process shown good association with proteins [15]. Another way to prepare chitosan NPs is the emulsion-droplet coalescence method (Figure

1.4). In this method, a water-in-oil emulsion of chitosan was formed followed by the addition of another emulsion of NaOH solution. Chitosan NPs was obtained when contacted with NaOH [16].

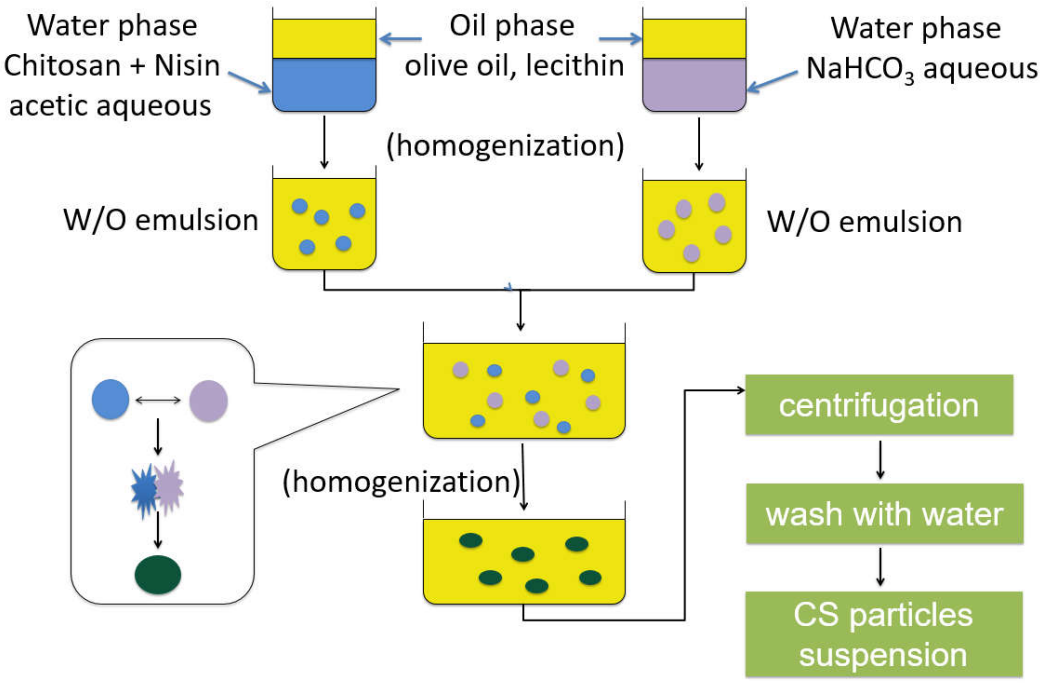

Figure 1. 4 Schematic of Nisin-loaded chitosan nanoparticles prepared via emulsion-droplet coalesce method.

1.2 EMULSION

The emulsion is defined as two immiscible liquids forming a colloid after some sort of energy input. Thermodynamically, the colloid will change back to two separate phases eventually. Thus, surfactants are often used to keep the emulsion stable for longer time. Regarding the structure of emulsion droplets, several types of the emulsion droplets are available: single emulsion (water-in-oil, oil-in-water), multiple emulsion (water-in-oil-in-water), and emulsion with a solid core [17].

The emulsion phenomenon is often combined with some solvent removal process to prepare solidified polymeric particles, which was discussed in section 1.1.1. In order to generate nano-

sized particles, the initial energy input such as agitation is significant to determine the initial droplet size and thus the particle size.

1.2.1 Emulsion homogenizer

Efficient mixing is an important part of any emulsion process as it directly affects the initial droplet size and stability. Commonly used mixers, namely, homogenizers for emulsion are blade type, rotor-stator, bead homogenizer (mechanical homogenizers), ultrasonic homogenizer, high pressure and other types of physical forces [18].

In this research, a high-speed Nanomixer used to provide a uniform, high shear stress for emulsion process and the exfoliation of nanoclay. As shown in Figure 1.5, Nanomixer consists of a stainless-steel inner cylinder with uniform holes and an outer cylinder as the vessel. The inner cylinder is connected to a high-speed rotor and thus our Nanomixer can be simplified as a Taylor-Couette (concentric rotating cylinders) mixer.

Because of the high-speed turbine provide by the Nanomixer, the centrifugal force is greater than gravity, causing the fluid flow to be pressed strongly against the inside wall of the vessel. The fluid is thus mixed in a closed-in space where a significant energy can be applied to it. The high speed and the holes on the rotor ensure the turbulent fluid flow in the vessel. Therefore, numerous turbulent eddies are generated during the process and the size of the eddies directly affect the size and distribution of the emulsion droplets. Based on the definition of Re for fluids, regimes in turbulent flow can be categorized as turbulent viscous and the turbulent inertial regime, which leads to different sizes of turbulent eddies [19, 20].

A large amount of heat is generated inside the Nanomixer vessel during the mixing process because of high speed and high shear stress. In order to control the temperature, cooling water

circulated around the mixing chamber as shown in Figure 1.5 (left). Results show that mixing temperature is a very important parameter to control the size of the polymer particles.

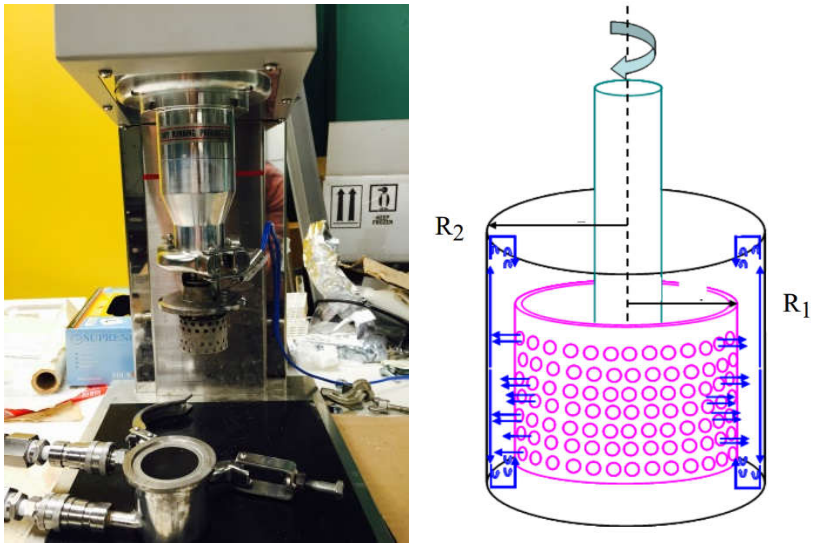

Figure 1. 5 (left) Image of Nanomixer; (right) Schematic of Nanomixer chamber geometry. The solution is in the gap between $R_1$and R_2. Reproduced (right) with the permission from [10].

1.3 INTRODUCTION OF MODEL DRUGS

1.3.1 Introduction of diclofenac

Diclofenac (DCF) is a phenylacetic acid derivative (Figure 1.6), known as a non-steroidal anti-inflammatory drug (NSAID). It was introduced as early as in 1974 and has been used in 120 countries since then. Because of its low solubility in aqueous solution, the salt formation (e.g., diclofenac sodium) is normally used to enhance its solubility, dissolution rate, and bioavailability. As a potent pain-killer drug in the NSAID category, DCF is one of the commonly used drugs in the treatment of rheumatoid arthritis, degenerative joint disease, and osteoarthritis and ankylosing spondylitis [21, 22]. The administration of DCF into the intra-articular cavity is a common treatment for a patient who has chronic joint pain. However, the short-term residence of DCF in the intra-articular cavity will reduce the effect and increase the frequency of administration, which

increases the patient's pain for the treatment. Therefore, using a drug delivery system (e.g., microspheres) can prolong the residence of DCF inside the human body and then reduce the administration times.

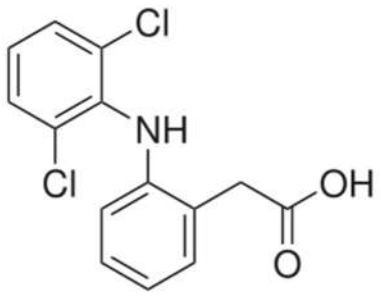

Figure 1. 6 Chemical structure of Diclofenac

1.3.2 Introduction of Nisin

Nisin, as one of the bacteriocins produced from food-grade lactic acid and considered as a natural polypeptide, was approved as a food preservative in 1969 by the Joint Food and Agriculture Organization/World Health Organization (FAO/WHO) [23, 24]. Since then, it has been widely used in the food industry including dairy products, eggs, meat, vegetables, seafood [25]. Nisin is a member of a class of antimicrobial substances called lantibiotics because of the unusual amino acid lanthionine. Indeed, lantibiotics have the potential to act as food preservatives but nisin has been the only one approved as a food preservative [26]. Nisin is a low molecular weight polypeptide composed of 34 amino acids. Generally, nisin has two variants A and Z, which differ in a single amino acid residue at position 27 where is histidine in nisin A and asparagine in nisin Z [27]. The amino acid sequence and proposed structure of nisin Z are given in Figure 1.7 [28, 29].

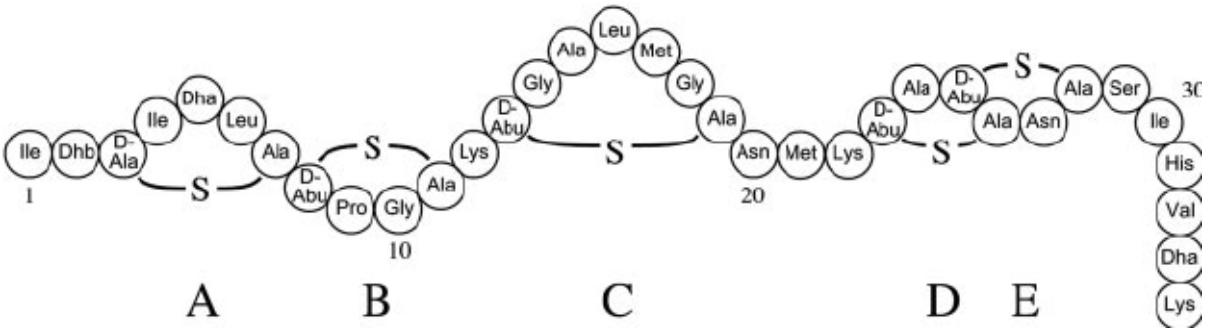

Figure 1. 7 The structure of nisin Z showing amino acid units (adapted from [30])

Nisin is a broad-spectrum antimicrobial towards Gram-positive bacteria, especially spores [23, 31]. The action mode of nisin is that it forms a complex with Lipid II, which is the precursor molecule of the bacterial membrane formation. This nisin-Lipid II complex then goes into the bacteria and then produces pores in the bacteria wall leading to the inhibition and death of bacteria [31]. The reason why nisin is not effective in inhibiting Gram-negative bacteria is that Gram-negative bacteria have thicker cell wall than Gram-positive bacteria [31]. Thus, in conjunction with any treatment, such as heating, osmotic shock, freezing and exposure to chelating agents, which can make the Gram-negative bacterial cell walls more permeable, it is possible to suppress the Gram-negative bacteria in food [23, 31]. In recent studies, purified nisin Z showed effective inhibition for both Gram-positive and Gram-negative bacteria [32].Thus, a ultrapure nisin Z product was mainly used to implement the drug encapsulation experiment in this research.

When used in food industry, the effect of nisin in free form is limited due to the interaction with food matrix, chemical degradation, and low solubility at pH above 6.0 [33]. Incorporation of nisin in food packaging and edible films can improve the antibacterial efficiency by avoiding interactions between food and nisin, and achieving the prolonged release of nisin [34-36]. However, the cost of such films is relatively high, leading to a high price. Micro/nano-encapsulation of antimicrobials with controlled release function has received increasing attention in recent years as

discussed in section 1.1. Therefore, encapsulation of nisin into biodegradable polymeric micro/nanoparticles was developed in this study to achieve the prolonged release of nisin as well as improve the antimicrobial efficiency.

2 ENCAPSULATION OF HYDROPHOBIC OR HYDROPHILIC IRON OXIDE NANOPARTICLES INTO POLY-(LACTIC ACID) MICRO/NANOPARTICLES VIA ADAPTABLE EMULSION SETUP

2.1 MOTIVATION

Magnetic nanoparticles have attracted significant interest from a wide range of research areas, including biomedicine and drug delivery [37], magnetic resonance imaging (MRI) [38], magnetic fluids [39], catalysis [40] and environmental remediation [41, 42]. In the biomedical field, magnetic nanoparticles have been used for magnetic targeting delivery. As early as the 1970s, microspheres entrapped with iron oxide were used in targeted cancer therapy by applying a magnetic field [43, 44]. Magnetic nanoparticles have also been studied as diagnostic agents to increase image contrast for both *in vivo* and *in vitro* diagnosis, like Magnetic Resonance Imaging (MRI) tumor detection [45].

For the successful application of magnetic nanoparticles, it is necessary to overcome several problems associated with particle stability, such as aggregation, undesirable chemical activity, and losses of dispersibility and magnetism [46]. So far, several protection strategies such as coating the magnetic nanoparticles with surfactants and polymers, coating with an inorganic layer such as silica or carbon, and embedding magnetic nanoparticles into a matrix have been developed to prevent the agglomeration and corrosion of naked magnetic nanoparticles [46]. For example, Ferumoxide, an FDA-approved IONP formulation with a size range of 100-150 nm, contains a 5-10 nm IONP core. Similar to other coating methods, it results in a core-shell structure for each

magnetic nanoparticle [47]. These individually protected IONPs have good dispersibility, yet low content (around 0.01%) of IONPs in the whole core-shell particle, which leads to low cell labeling efficiency [48, 49].

Compared with this core-shell type of IONPs, direct entrapment of IONPs into a matrix provides a higher loading efficiency. Commercially available micron-sized iron oxide particles (MPIOs, Bangs Laboratories, Fishers, IN) have been developed with around 50 wt.% iron oxide content [50, 51]. However, current commercialized MPIOs use the inert matrix, polystyrene/divinylbenzene, to encapsulate IONPs, limiting their biomedical applications. Recently, M. K. Nkansah *et al.*[52] reported the use of a biodegradable polymer, poly(lactide-co-glycolide) (PLGA), to encapsulate IONPs for MRI cell tracking. In this study, both micro- and nano-sized magnetic PLGA particles have been prepared to fulfill different applicable requirements [52]. Nanoparticles are more suitable for the intracellular magnetic labeling [53], however, the higher surface-to-volume ratio of nanoparticles leads to lower encapsulation efficiency and a faster rate of degradation, resulting in higher iron content loss after the same amount of time [52]. On the other hand, microparticles have higher encapsulation efficiency and a more delayed and attenuated aggregation peak [52]. In order to prepare IONPs encapsulated PLGA microparticles and nanoparticles, different experimental setups were employed in their study: microparticles (~2μm) were fabricated by oil-in-water (O/W) emulsion using homogenization, while nanoparticles (~105 nm) were obtained via tip sonication induced O/W emulsion [52]. In addition, due to the hydrophobic nature of PLGA, this method is limited to encapsulating hydrophobic IONPs.

For the purpose of extending the application of IONPs for targeted therapy and in *vivo* diagnosis, encapsulation of hydrophilic IONPs is necessary. Because IONPs must have a good

dispersion in the aqueous environment [54]. And a hydrophilic surface of the IONPs can increase its circulatory half-life in the blood stream from minutes to hours or days [43]. Typically, the encapsulation of hydrophilic IONPs into hydrophobic polymer particles is carried out by a conventional W/O/W double emulsion method, in which IONPs sit in the inner water phase [55]. But it has some significant drawbacks to scale up for industrial production. First, it takes two steps for emulsion formation: an internal W/O emulsion, then an O/W emulsion; Second, it mostly generates only micron-/submicron-sized particles (>200nm) rather than nanoparticles (50 – 200nm) [56]. Lastly, with the existence of internal water phase, no solid spheres are generated as the hydrophilic IONPs carriers [57]. This reduces the capability for designing particles tailored toward different release behaviors.

In this study, PLA particles encapsulating IONPs were produced using a fast (~2min emulsion) and adaptable one-step W/O/W emulsion method under a viscous turbulent shear flow, controlled by the addition of glycerol to the aqueous continuous phase. This method makes it possible the preparation of either micron-sized or nano-sized PLA particles encapsulated with either hydrophobic or hydrophilic IONPs, through the adjustment of the viscosity of water phase and emulsification temperature. PLA nanospheres (~80nm) with hydrophilic IONPs were generated via the dynamic HT-RT emulsion, processed initially under high temperature (HT, 60°C) condition and then at room temperature (RT, 25°C). Given the simplicity and short processing time, this method can present a commercially viable solution to a successful scale-up.

2.2 INTRODUCTION

2.2.1 Synthesis of magnetic nanoparticles

Magnetic nanoparticles have attracted a great interest due to its wide application in magnetic fluids, catalysis, magnetic resonance imaging (MRI), environmental remediation and so on. There are a number of methods developed for the synthesis of magnetic nanoparticles [46].

2.2.1.1 Co-precipitation

Co-precipitation is one of the most commonly used methods to synthesize iron oxides (either Fe_3O_4 or γ-Fe_2O_3) from aqueous Fe^{2+}/Fe^{3+} solutions by the addition of a base under an inert atmosphere at the proper temperature. The morphology and composition of the magnetic nanoparticles are related to the Fe^{2+}/Fe^{3+} ratio, the reaction temperature, the pH value, and the ionic strength of the media. The advantage of the co-precipitation method is that the quality of nanoparticles is reproducible as long as the synthetic condition is fixed [46]. However, the stability of the magnetic particles is a problem (magnetite particles can be oxidized to maghemite). The use of organic additives can stabilize the newly produced magnetic nanoparticles [58]. A recent study showed that oleic acid is the best coating material for the stabilization of Fe_3O_4 [59].

2.2.1.2 Thermal decomposition

Monodisperse magnetic nanoparticles with smaller size can be synthesized through the thermal decomposition of organometallic compounds in high-boiling organic solvents with surfactants. This method was inspired by the synthesis of semiconductor nanocrystals via thermal decomposition with well-controlled size and shape. Oleic acid and hexadecyl amine are often employed as surfactants in this method. Organometallic precursors are needed for the reaction. To

control the morphology of magnetic nanoparticles, the ratio of starting reagents including organometallic compounds, surfactant, and the solvent is primarily important. Other conditions like reaction temperature and reaction time might be crucial as well [46, 60].

This method can also be used to prepare metallic nanoparticles. Compared to metal oxides, metallic nanoparticles have larger magnetization, which is especially useful for data storage application [61].

2.2.1.3 Microemulsion

A microemulsion, which is usually a reverse emulsion (water-in-oil), can be used as a nanoreactor to prepare nanoparticles when adding solvent to the microemulsions, which lead to precipitation of nanoparticles. This method allows the preparation of metallic cobalt, cobalt/platinum alloys, and gold-coated cobalt/platinum nanoparticles [62]. Not only spherical particles can be prepared by this method, but also tubes were prepared. The disadvantage of the microemulsion is that the resulting particle size and shape are in a wide range due to the nature of emulsion. In addition, its production yield is low compared to other methods such as co-precipitation and thermal decomposition [46].

2.2.1.4 Hydrothermal synthesis

The hydrothermal synthesis method synthesizes nanocrystals by a liquid-solid-solution reaction. The system consists of metal linoleate (solid), an ethanol-linoleic acid liquid phase, and a water-ethanol solution at different reaction temperatures under hydrothermal condition. This method is based on the phase transfer and separation at the interfaces of the three phases during the synthesis

process [63]. A broad range of nanostructured materials can be formed under hydrothermal conditions [46].

2.3 EXPERIMENT

2.3.1 Materials

Iron (II) chloride tetrahydrate ($FeCl_2$•$4H_2O$) (Reagent grade 99%), iron (III) chloride ($FeCl_3$) (Reagent grade 97%), oleic acid (analytical standard) and Pluronic F68 (PF68) (average Mw=8,400 Da) were purchased from Sigma-Aldrich. Citric acid monohydrate powder was purchased from Fisher Scientific Co. Poly (D, L-lactic acid) (Mw=51,000 Da, Tg= 52.5 °C) was obtained from LakeShore Biomaterials. Ethyl acetate (EA), glycerol, and ammonium hydroxide (NH_4OH) were purchased from J.T. BAKER and used as received. Deionized (DI) water used in all the process was supplied by a Barnstead nanopure Diamond-UV purification unit equipped with a UV source and final 0.2 μm filter at 18.2 MΩ purity.

2.3.2 Preparation of hydrophilic and hydrophobic IONPs

Hydrophilic IONPs (Fe_2O_3) used in the study were prepared following the method suggested in the previous study [64, 65]. Briefly speaking, the mixture of Fe^{2+} and Fe^{3+} (1:2 molar ratio) with 40 ml water was heated to 80 °C under nitrogen purging. 5 ml NH_4OH was introduced by syringe while maintaining the temperature of the mixture at 80 ^{0}C for another 30 mins. 1 ml citric acid (CA) (2.38 M) was added to the mixture and the temperature was raised to 95 °C. Heating is continued for another 90 min. IONPs were cooled, separated and washed with a mixture of acetone and water three times by centrifugation. The IONPs were dispersed in DI water and stored at room temperature for use.

Hydrophobic IONPs were prepared in the same way, except using oleic acid (0.15 ml) in place of citric acid for a hydrophobic coating. The resulting IONPs were washed with a mixture of hexane and acetone (1:1) for three times to obtain stable IONPs colloid. The purified suspension was then dispersed into hexane for storage.

2.3.3 Preparation of hydrophilic/hydrophobic IONPs encapsulated PLA particles

EA and DI water were mutually saturated before being used for emulsion experiment. PLA solution (oil phase) was prepared by dissolving 15 mg/ml PLA into water-saturated EA. Aqueous solution (water phase) was prepared by dissolving 15 mg/ml PF68 in the EA-saturated water/glycerol (50% v/v) system. For the encapsulation of hydrophobic IONPs, IONPs were dispersed into the oil phase. For hydrophilic IONPs, IONPs were dispersed into the water phase. 6 ml oil phase was emulsified with 18 ml water phase using Nanomixer at the speed of 12500 s^{-1} for 2 min under HT or RT, by controlling the cooling system circulating around the Nanomixer tank. The resulting emulsion was then poured into 90 ml pure DI water to induce the diffusion of EA and the solidification of polymer particles. The final colloid dispersion after overnight diffusion was transferred to a glass vial and used for further characterization.

2.3.4 Scanning and Transmission Electron Microscopies

Scanning Electron Microscope (SEM) (JEOL 7500F) was used to observe particles morphology. The polymer particles dispersion was filtered using 0.1μm or 0.03μm pore size filter paper, air dried and sputter coated with platinum for the SEM characterization. SEM images were taken under 3kV electron accelerating voltage, ~4.5 mm working distance. Transmission electron microscopy (TEM) (JEOL 2200FS) was carried out to observe the distribution of magnetic NPs in

the polymer matrix. Freeze-drying microparticles were embedded into resin and then microtomed to give the cross-sectional view. For nanoparticles, the particle suspension was moved into a dialysis membrane tube, under a slow stirring water bath to gently remove glycerol and excessive surfactant PF68. After 3 days of dialysis, the suspension was then diluted 1:10 with DI water. Then several drops of the dilution were dripped on the carbon coated copper grid and air dried.

2.3.5 Particle size distribution and Zeta potential measurement

The particle size was measured using ImageJ from randomly collecting the diameter of a large number (300 each) of particles from the SEM images. The mean particle size and standard deviation were obtained directly from ImageJ. The histogram was plotted with a 30 nm bin from 0 to 300 nm.

ZetaPALS (Brookhaven Instruments Corporation) was employed to measure the surface charge of particles. The electrode was conditioned to reach 13200 mV of conductance with 1.5 ml sodium chloride (NaCl) solution (0.9 wt./vol. %). Particles suspension was diluted to 1:10 with the NaCl solution. In order to get a reliable data, each sample was subjected to 10 runs, and each run was composed of 30 cycles.

2.4 RESULTS AND DISCUSSION

2.4.1 One-step W/O/W-emulsion formation method

Figure 2.1 describes the overall schematic encapsulation methods and procedures used in this work. Figure 2.1(a) demonstrates the encapsulation of hydrophilic IONPs into PLA particles via our one-step W/O/W emulsion. The W/O/W double emulsion is widely used to encapsulate hydrophilic substances into hydrophobic polymer particles [66, 67]. Conventionally, to form a W/O/W

emulsion, two sequential emulsion processes are used with usually different recipes of inner and outer water phases [57]. The complexity of this method limits the loading efficiency and thus decreases the commercial scale-up possibility in the pharmaceutical industry. To produce polymeric particles encapsulating hydrophilic particles, the procedure of W/O/W emulsion needs to be simplified.

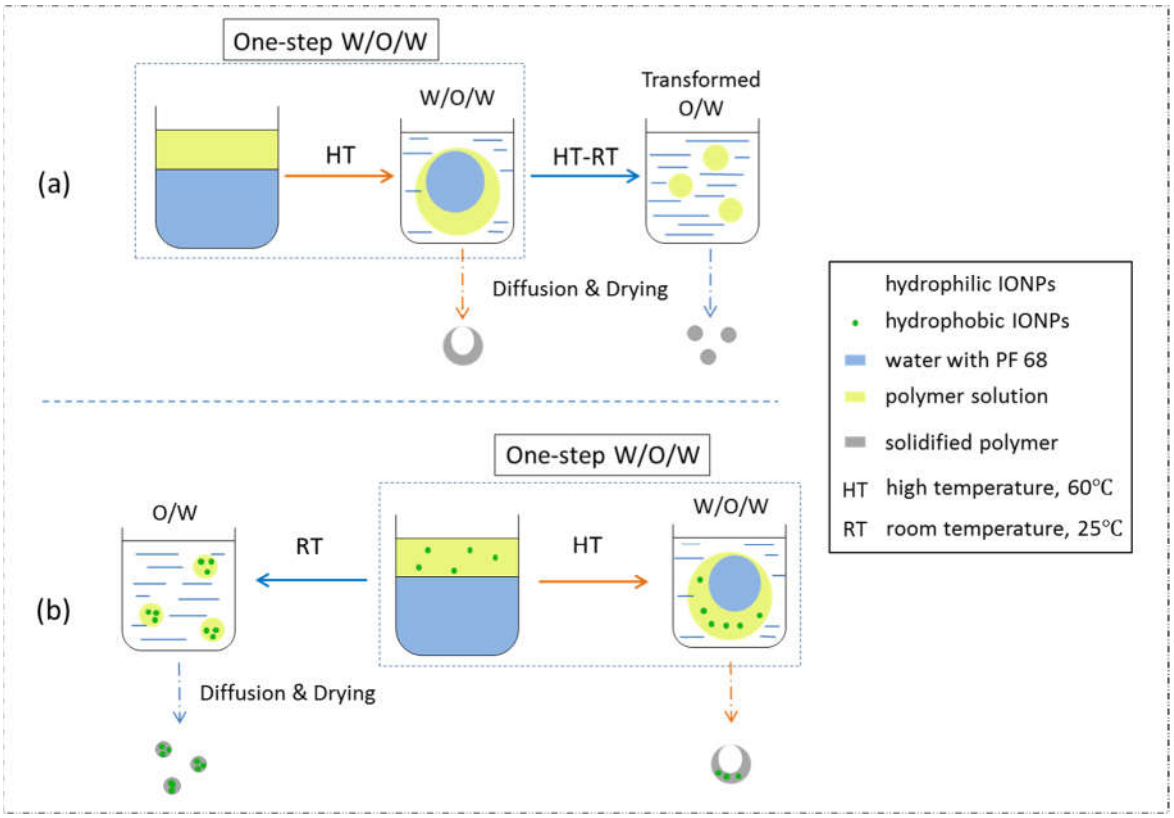

Figure 2. 1 Schematic preparation procedures of (a) PLA-hydrophilic IONPs micro-/nano-particles, (b) PLA-hydrophobic IONPs micro-/nano-particles.

In our previous study, a novel, one-step W/O/W-emulsion formation method was developed via a modified Taylor-Couette mixer [10]. Compared to the conventional two-step W/O/W formation, the present method significantly reduced the particles preparation duration time and simplified process. The modified Taylor-Couette mixer used in this study, also called Nanomixer,

consists of two concentric cylinders with the inner perforated turbine and the outer cylindrical vessel. The gap between two cylinders is ~ 2 mm and thus generates a high shear force in the closed vessel, leading to a turbulent fluid flow mixing condition. Under the turbulent condition, the dispersed emulsion droplets may undergo deformation, breakup or coalescence upon the action of viscous or inertial stress. The dominant stress in the flow is determined by the size of the smallest turbulent eddies, λ. When λ is smaller than the initial droplet size, the mixing condition is inertial turbulent regime; when λ is larger than the maximum initial droplet size, the mixing is under the viscous turbulent regime. According to "Kolmogorov Scale" [68], the eddy diameter is proportional to the viscosity of the continuous phase. In this study, the viscosity of continuous phase was controlled by adding different volume fractions of glycerol into the water phase while the overall ratio of oil phase to water phase fixed at 1:3. This was discussed in detail in our previous study where the eddy size increased with the increasing amount of glycerol. The results showed that the eddy size was larger than the maximum initial droplet size when the fraction of glycerol was beyond ~40% (v/v). When the water phase contained 40% (v/v) glycerol or less (viscosity~1.5cP), solid nanospheres were obtained, suggesting the formation of O/W single emulsion in which oil droplets containing PLA were dispersed. When 50% (v/v) or more glycerol was applied, open-hollow microparticles were formed, which implied the formation of W/O/W double emulsion (Figure 2.1(a), HT). Therefore, under the same emulsification temperature (HT, 60°C), the transitional behavior between O/W emulsion and W/O/W emulsion were dependent on the viscosity of continuous phase [10]. In addition to viscosity, emulsification temperature was another key factor in the formation of one-step W/O/W emulsion. When the temperature was greater than its glass transition temperature ($T_{g,PLA}$=52°C), the mobility of PLA chain segments

greatly increased and thus oil droplets tended to coalesce among multi-droplet collisions. The reason why we chose 60℃ is that the boiling point of ethyl acetate is 77 ℃.

In summary, the HT condition and the change in viscosity resulted in a viscous turbulent regime. The sizes of eddies formed were larger than the initial O/W droplets. When droplets were caught inside a large-size eddy, O/W droplets engaged with collision and coalescence to form W/O/W double emulsion droplets (Figure 2.2(a)). This process is considered the one-step W/O/W emulsion (adaptable emulsion, Figure 2.1(a)) method in this study. When the emulsification temperature was reduced to room temperature (RT), the mixing condition changed back to the inertial turbulent flow, in which the eddy size was smaller than the droplet size. Thus, large-size W/O/W droplets were broken up into small O/W droplets by shear force (Figure 2.2(b)) [69] and this resulted in the formation of nanoparticles (Figure 2.1(a), HT-RT).

Meanwhile, in the case of hydrophobic IONPs, the emulsification at HT generated open-hollow microparticles in the same way as hydrophilic IONPs (Figure 2.1(b)). At RT, nanoparticles with hydrophobic IONPs were generated based on the typical O/W emulsion as shown in Figure 2.1(b). In this work, the percentage of glycerol was fixed at 50% (v/v) in order to control the emulsion droplet transformation between W/O/W and O/W only by emulsification temperature (Figure 2.1). Then, micro- and nano-polymeric particles incorporating IONPs were generated under HT and RT, respectively.

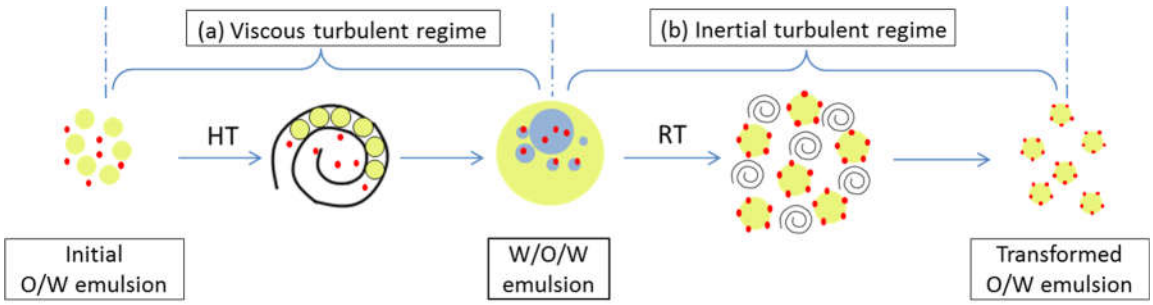

Figure 2. 2 Schematic mechanism of encapsulating hydrophilic IONPs into PLA particles.

Table 2. 1 Emulsion conditions of PLA and PLA-IONPs particles

Sample No.	Particle composition	Preparation Parameters			
		C_{PLA} (mg/ml)	**IONPs location**	**Glycerol (% v/v)**	**Emulsion Temp.**
A	PLA MP[a]	15	N	50	HT
B	PLA NP[b]	15	N	50	HT-RT
C	PLA-hydrophilic IONPs MP	15	Water phase	50	HT
D	PLA-hydrophilic IONPs NP	15	Water phase	50	HT-RT
E	PLA-hydrophobic IONPs MP	15	Oil phase	50	HT
F	PLA-hydrophobic IONPs NP	15	Oil phase	50	RT
G	PLA-hydrophobic IONPs NP	15	Oil phase	0	RT

[a]Microparticle. [b]Nanoparticle.

2.4.2 Generation of PLA-hydrophilic IONPs micron-/nano-sized particles

Based on the preparation method mentioned in the previous section, polymeric (PLA) particles encapsulating hydrophilic IONPs were prepared under different emulsification temperature conditions (Table 2.1), resulting in particles of different shapes and sizes. For comparison, PLA particles without IONPs were generated (Figure 2.3 (a-b)). At HT, PLA particles with open-hollow structure were generated (Sample A, Table 2.1) as shown in Figure 2.3 (a). The hollow structure resulting from the drying of the inner water phase of W/O/W droplet is as shown in Figure 2.1(a). The opening of particles was caused by polymer solidification during the solvent diffusion process. During the diffusion of solvent (ethyl acetate), spherical W/O/W emulsion droplets shrunk to smaller size. When the droplet size was close enough to the inner water bubble size, polymer content was not sufficient to form a resistant layer around the incompressible inner water phase [57]. PLA nanoparticles (Sample B, Table 2.1) were obtained at HT-RT due to the transformation of W/O/W emulsion to O/W emulsion. The nanoparticles were solid and spherical as shown in Figure 2.3 (b).

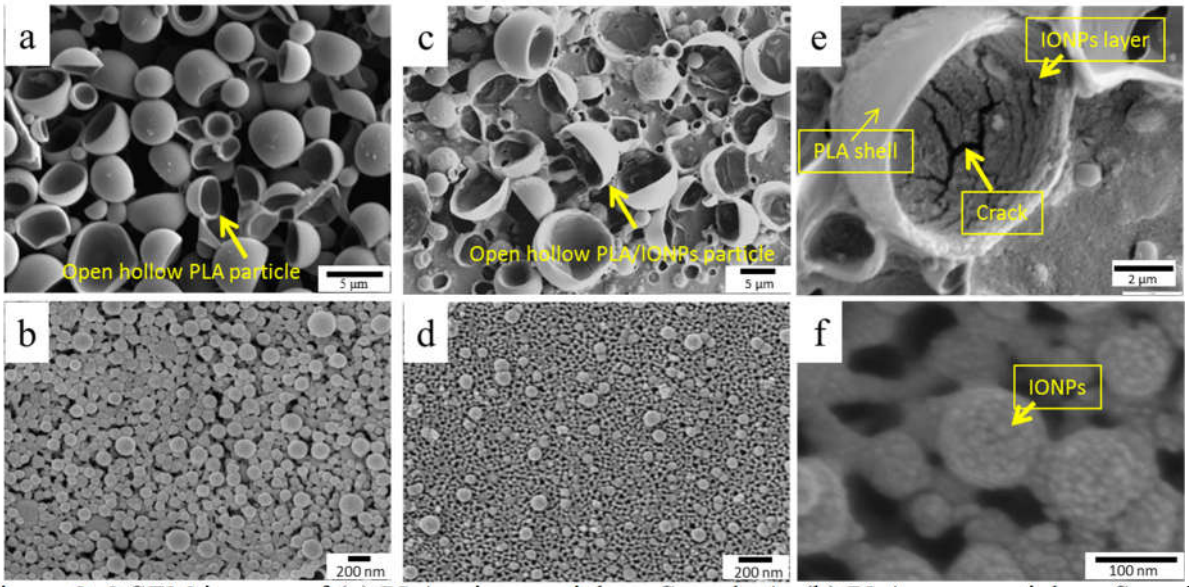

Figure 2. 3 SEM images of (a) PLA microparticles - Sample A, (b) PLA nanoparticles - Sample B, (c,e) PLA-hydrophilic IONPs microparticles - Sample C, (d,f) PLA-hydrophilic IONPs nanoparticles - Sample D.

PLA-hydrophilic IONPs microparticles and nanoparticles were obtained by the process shown in Figure 2.1(a) and Figure 2.2, in which hydrophilic IONPs were initially dispersed in the water phase. Composite microparticles (Figure 2.3(c,e)) were obtained from W/O/W emulsion in HT step followed by the diffusion-drying process. As shown in Figure 2.3(c), compared to pure PLA microparticles, the addition of hydrophilic IONPs did not change the open-hollow structure and the overall particle size distribution (~5μm). This is because the hydrophilic IONPs could not go into the oil phase and thus do not affect the polymer phase concentration. In the formation of W/O/W emulsion droplets, most hydrophilic IONPs were sitting in the inner water phase and were trapped into particle shell during the diffusion and drying process (Figure 2.1(a)). During the solvent diffusion process, PLA was gradually precipitated around the inner water droplet, forming the shell of capsule-structure particle. The hydrophilic IONPs were retained on the shrinking polymer shell when the inner water phase transferred across the dynamic solidifying polymer shell of the micro-sized particles [70]. PLA shell formed a hydrophobic wall to retard the leakage of hydrophilic IONPs into the outer water phase. When applying higher magnification on the individual composite particle (Figure 2.3(e)), NPs (~10nm) were observed on both the inner and outer surface of PLA particle. The inner particle surface was rougher than the outer, with the appearance of cracks. It has been reported that the magnetic NPs at the interface could induce the buckling instability of emulsion droplets during the solvent removal, causing the shrinkage of particles [71]. This is consistent with our proposed W/O/W emulsion formation, namely, hydrophilic IONPs have been captured into the inner water phase (Figure 2.2).

PLA-hydrophilic IONPs nanoparticles (Figure 2.3(d,f)) were prepared via an HT followed by RT (HT-RT) step (Figure 2.1(a)). That is, the W/O/W emulsion was emulsified again under the room temperature (RT emulsion). As shown in Figure 2.2, when an RT emulsion step was carried

out after the HT emulsion step, the W/O/W droplets might undergo deformation by the small-sized eddies. Under deformation, breakup and coalescence of the droplets occurred competitively, turning W/O/W droplets into single emulsion (O/W) droplets. The flow-induced deformation promoted the interaction between the inner and outer interfaces, enhancing the entrapment of hydrophilic IONPs inside droplets [67]. During this process, IONPs stayed more on the outside of the oil droplet. The SEM image of higher magnification (Figure 2.3(f)) demonstrates individually distributed NPs (~10 nm) on the PLA particle surface. Most PLA particles were covered with IONPs like a "raspberry". Compared with the limited previous study on hydrophilic IONPs encapsulated polymeric particles [55, 72, 73], the particles prepared by our method had a higher concentration of IONPs. In addition, IONPs distribute more uniformly in our method [55].

In order to confirm the successful encapsulation of hydrophilic IONPs into PLA particles, TEM was applied to PLA-hydrophilic IONPs composite microparticles and nanoparticles (Figure 2.4). Figure 2.4(a) shows a black (embedded IONPs) open-ring structure, which is consistent with our SEM observation of open-hollow microparticles (Figure 2.3(c,e)). The higher magnification TEM image (Figure 2.4(b)) provides details of the local region of this microparticle. The thickness of the black region was approximately 120 nm, which was composed of IONPs with approximately 10 nm in diameter while the thickness of PLA/IONPs particle shell from the SEM image (Figure 2.3(e)) was about 150 nm. As shown in Figure 2.4(a), the inner particle surface was relatively smooth, which suggests that IONPs were mostly embedded within the PLA shell, with few sitting on the inner surface. The IONPs seemed individually distributed, aggregate with each other and densely stacked along the length of PLA shell. Figure 2.4(c-d) demonstrates the stacking entrapment of hydrophilic IONPs inside the PLA nanoparticles. Nanoparticles were not

homogenously spherical (Figure 2.4(c)), suggesting that IONPs locate more on particle surfaces as shown in the SEM observation (Figure 2.3(f)).

To test the magnetic performance of microparticles with hydrophilic IONPs, the resulting particle suspension was collected into a vessel and set next to a magnetic bar. PLA-hydrophilic IONPs composite microparticles slowly moved towards the magnet bar (less than 15 min) as shown in Figure 5. Meanwhile, the particle suspension became transparent, which suggests a high loading efficiency of hydrophilic IONPs into PLA microparticles.

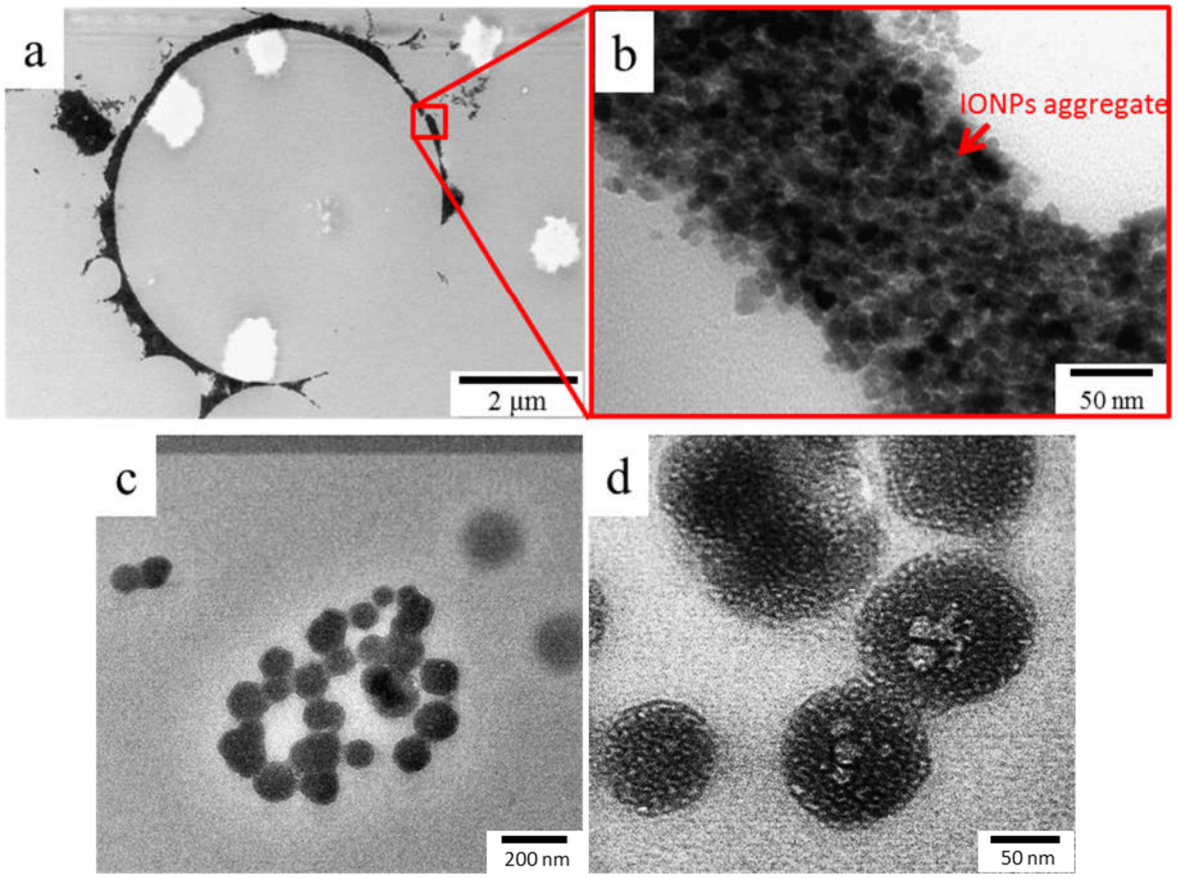

Figure 2. 4 TEM images of (a-b) PLA-hydrophilic IONPs hollow microparticles, (c-d) PLA-hydrophilic IONPs nanospheres.

Figure 2. 5 Migration of PLA-hydrophilic IONPs composite particles under the magnetic field by a magnet; before (left) and after (right).

2.4.3 Generation of PLA-hydrophobic IONPs micron-/nano-sized particles

The PLA-hydrophobic IONPs micron-/nano-particles were prepared via the process shown in Figure 2.1(b). The SEM results (Figure 2.6) show the samples E-G from Table 2.1. Figure 2.6(a-c) shows that the addition of hydrophobic IONPs significantly changed the microparticle structure and size. Compared with the plain PLA and PLA-hydrophilic IONPs composite particles, PLA-hydrophobic IONPs particles have a closed microparticle structure and smaller mean particle size (~2μm) (Figure 2.6a). This is probably because hydrophilic IONPs were added into the water phase while hydrophobic ones were added into the oil phase which dissolved PLA. Therefore, during the solvent diffusion process, the PLA-hydrophobic IONPs particles maintained a spherical shape because the concentration of the oil phase (polymer plus hydrophobic IONPs) was high enough to form a resistant layer around the inner water droplet [57]. This led to the formation of the closed-hollow microparticles after drying (Figure 2.6c). IONPs-induced anisotropic shrinkage [71] caused cracks on the surface or collapse of polymer particles as shown in a higher

magnification (Figure 2.6b). To encapsulate hydrophobic IONPs into PLA nanoparticles, the one-step W/O/W emulsion was not necessary and RT was enough to capture hydrophobic IONPs (Figure 2.1(b), RT), corresponding to sample F in Table 2.1 (Figure 2.6d). As a comparison, a conventional O/W single emulsion, without glycerol in the water phase, was carried out (Figure 2.6e).

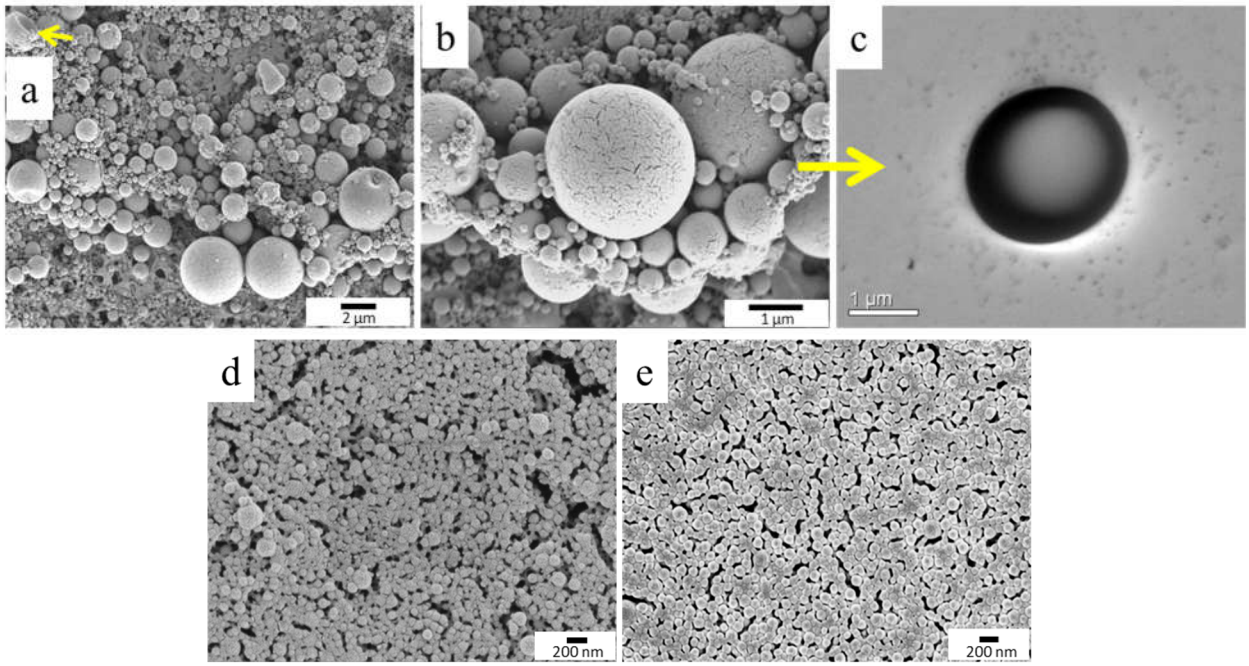

Figure 2. 6 (a-b) SEM images of PLA-hydrophobic IONPs microparticles - Sample E, (c) TEM image of PLA-hydrophobic IONPs microparticle - Sample E, (d) SEM image of PLA-hydrophobic IONPs nanoparticles - Sample F (with glycerol), (e) SEM image of PLA-hydrophobic IONPs nanoparticles - Sample G (without glycerol).

Figure 2.7 shows the TEM images of sample F and G. In Figure 2.7(a-b), which represent PLA/hydrophilic IONPs nanoparticles with 50% (v/v) glycerol (Sample F), the hydrophobic IONPs sit more on the edge of the particle rather than in the middle. On the other hand, in Figure 7 (c-d) (Sample G), the concentration of IONPs was denser in the middle than in the particle edge. To confirm such a difference in the location of IONPs, the surface property was measured using the zeta potential (Table 2.2). The surface charge of pure PLA particle is -10.18 mV. Hydrophobic

IONPs used in this study is anionic because of the oleic acid coating. Nanoparticles prepared with glycerol (Sample F) showed a larger absolute zeta potential value than the one without glycerol (Sample G), which was consistent with the TEM observation. The reason might be that the diffusion of solvent for sample F is slower because of the existence of glycerol in the outer water phase. The motion of IONPs was mainly driven by the diffusion of ethyl acetate towards the outer water phase. In sample F, the addition of glycerol increased the viscosity of the outer water phase and thus hindered the diffusion, leading to a slower movement of IONPs along the diffusion direction. This feature can be used to tailor the distribution and thus the release behavior of IONPs. In addition, further slowing down the diffusion process may increase the zeta potential of PLA particles and thus improve the colloidal stability.

For polymeric particles with hydrophobic IONPs, no matter how the emulsion was generated (an o/w droplet or w/o/w droplet forms), the hydrophobic IONPs were encapsulated within the polymer matrix (Figure 2.6) and the particle size was controllable from micron-size to nano-size.

Table 2. 2 Zeta potential (mV) of PLA-hydrophobic IONPs composite nanoparticles

Samples	**Zeta potential (mV)**
Sample F	-30.87±1.51
Sample G	-26.90±1.26
Pure PLA NPs	-10.18±1.19

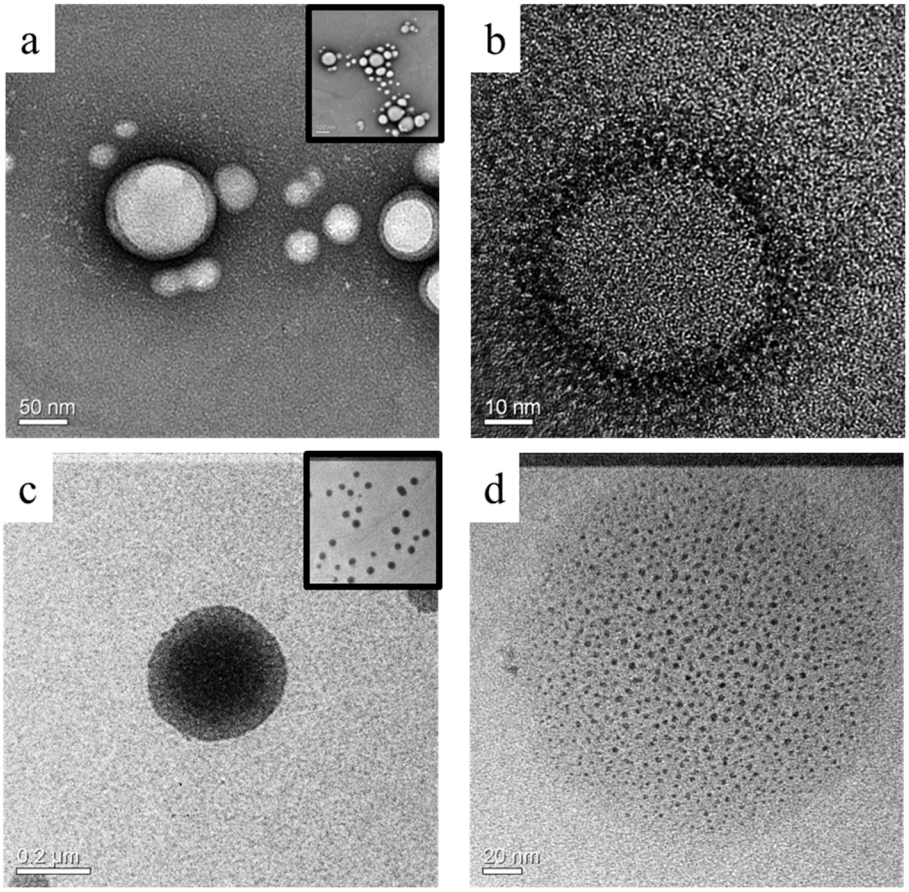

Figure 2. 7 TEM images of PLA-hydrophobic IONPs composite nanoparticles (a-b) prepared with glycerol in Water phase - Sample F, (c-d) prepared without glycerol - Sample G. Black dots represent IONPs.

2.4.4 Analysis of particle size

2.4.4.1 Effect of dynamic HT-RT process on particle size

From the previous results [10], with the same experimental setup, pure PLA nanoparticles generated from the HT-RT process (~104 nm) showed a smaller mean particle size than that from RT emulsion (~164 nm) (Figure 2.1(b)-RT). On the other hand, PLA nanoparticles prepared from HT-RT process showed a higher polydispersity. This gives us a tool to reduce the size of nanoparticles: more repeated HT-RT processes lead to smaller particle size.

Our dynamic HT-RT process has the advantage in preparing composite nanoparticles which are better suited for cell labeling since the NPs need to go through the cell membrane [53].

As shown in Figure 2.8(b), the obtained PLA-hydrophilic IONPs nanoparticles have a much lower average particle size (~80nm) than that has been reported by literature (~ 200 nm) [55, 72]. From the diagram, 90% of the particles are within 100 nm with the minimum particle size is about 30 nm.

2.4.4.2 Effect of IONPS on particle size

For microparticles, the addition of hydrophilic IONPs in water phase did not significantly affect the composite particle shape and size while hydrophobic IONPs sitting in oil phase decreased the overall particle size and changed the particle to a closed-sphere shape. As mentioned before, this is because hydrophobic IONPs increased the overall oil phase concentration. Thus, during the solvent diffusion process, polymer/IONPs formed a continuous layer and the diameter of a spherical particle was smaller than a hemisphere of the same volume. For nanoparticles, as shown in Figure 2.8, the addition of IONPs, no matter hydrophilic or hydrophobic, decreased the composite particle size compared to pure PLA nanoparticles (Figure 2.3(b)). The mean particle sizes of PLA-IONPs nanoparticles were about 20 nm smaller than that of pure PLA particles. The possible reason would be that the existence of IONPs resulted in Pickering emulsion (solids-stabilized emulsion).[74] Under the turbulent-inertial flow, droplets were stabilized by IONPs and thus kept as smaller droplets.

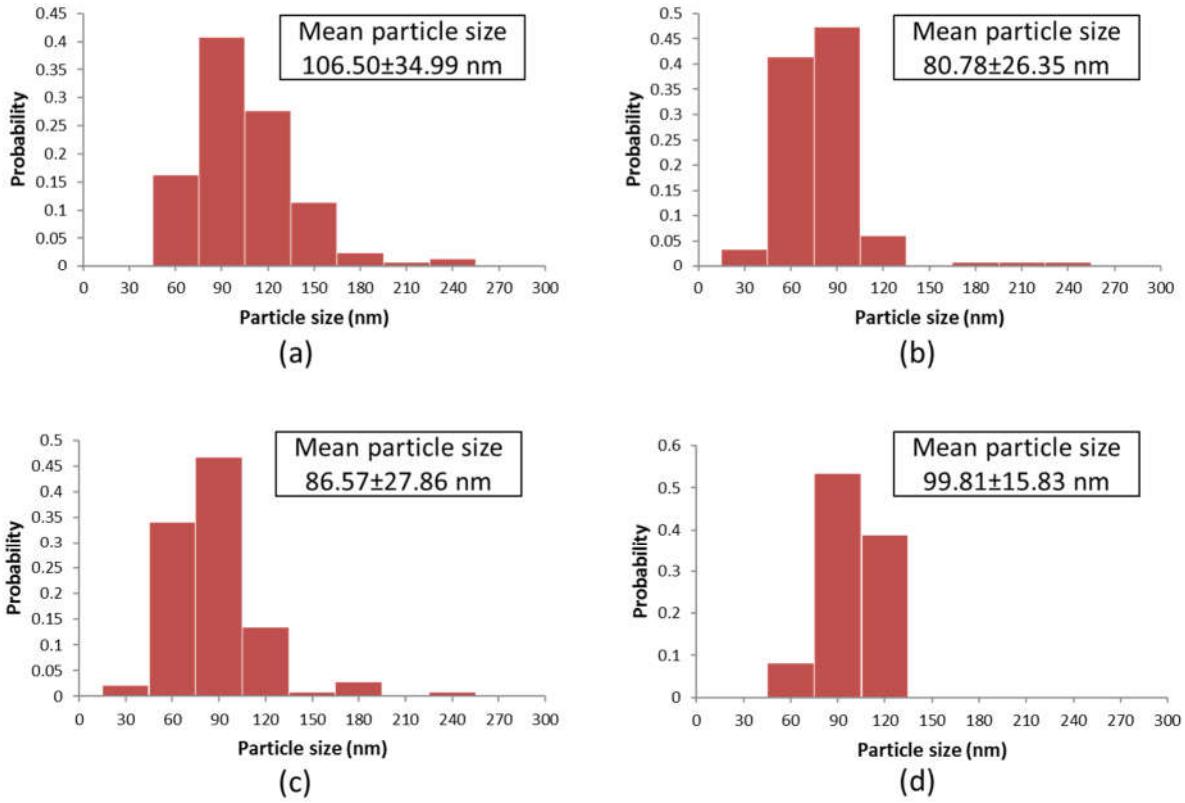

Figure 2. 8 Particle size distributions. (a) plain PLA NPs - Sample B, (b) PLA-hydrophilic IONPs NPs, - Sample D, (c) PLA-hydrophobic IONPs NPs - Sample F, (d) PLA-hydrophobic IONPs NPs - Sample G.

2.5 CONCLUSIONS

Magnetic PLA microparticles and nanospheres were successfully prepared by a fast, one-step W/O/W emulsion method without introducing any surface coating or modification. The formation of multiple-emulsion droplets entrapping hydrophilic IONPs in the inner compartments as well as the diffusion of these NPs to the polymer matrix during the solvent removal and drying process played an important role in dispersing hydrophilic NPs in the hydrophobic polymer. The particle sizes and shapes were well controlled by operating different emulsion conditions. The SEM and TEM results revealed the well-dispersed IONPs in the polymer shell and sphere. The flexible encapsulation of hydrophobic and hydrophilic IONPs and controllable particle size preparation allow achieving different applications. This process can also be applied to prepare carriers of water

soluble drugs or molecules of interest, e.g. penicillin and doxorubicin hydrochloride, with an improved compatibility of composite components. The facile and fast process operation sheds light on the potential scale-up production of biodegradable magnetic particles.

3 PREPARATION OF ANISOTROPIC PLA-PS HOLLOW MICROPARTICLES AND CAGE-LIKE POROUS PLA MICROPARTICLES VIA EMULSION-DIFFUSION METHOD COMBINED WITH SOLVENT-INDUCED PHASE SEPARATION

3.1 MOTIVATION

Anisotropic particles have attracted great attention recently in several applications such as biomedical engineering, enzyme engineering, switchable display devices and biological/optical sensors because they can provide dual- and multifunction within one unit [75-77]. Among these, polymeric micro- and nanoparticles with complex shapes demonstrated great potential in drug delivery [78], medical imaging and remote control of cellular behavior [75]. For example, among all the anisotropic particles, multicompartment particles are useful in dual-drug delivery, in which two or more drugs need to be released in a certain order and need independent release kinetics.

Common methods for chemically and morphologically anisotropic polymeric particles preparation include stretching of spherical particles, copolymer self-assembly micelle, emulsion combined with phase separation, microfluidics, non-wetting template molding, electrohydrodynamic (EHD) co-jetting [75, 76]. While the stretching method can generate distinctly different shapes particles (>20), it requires special stretching devices and does not usually make chemically anisotropic particles [76]. The current top-down methods, including, non-wetting template and EHD co-jetting, can prepare precisely compartmentalized particles (some with patchy surfaces) with uniform size. However, they have complicated manipulation process and small yield, which is not suitable for scalable production [77, 79]. Conventional methods based

on phase separation of polymer blends were used to prepare anisotropic bi- or multicompartmental particles but without well-controlled shapes. While spherical particles can be routinely prepared by droplet-based methods, a few examples show that non-spherical particles can be prepared with conventional droplet-based methods [76]. Besides, it is hard to combine two immiscible polymers in one unit due to the thermodynamic of the dual-liquid system [79]. Even though, compared with the top-down methods, emulsion based polymeric particle preparation is easy to scale up, having relatively uniform size and ability to adapt to various architecture anisotropic particles [77]. Anisotropic polymeric particles based on poly(lactic acid) (PLA) has a high potential in biomedical applications.

In order to prepare functional micro- or nano- PLA particles, to lower the cost, and to expand the practical application of PLA, numerous materials have been blended with it. Among these, PLA-polystyrene (PS) bioblend has been identified as one promising cost-effective, thermally stable, and semi-biodegradable composite. In this study, well-controlled, uniformly compartmental PLA-PS bioblend hollow microparticles were prepared with a facile, fast and one-step double-emulsion method.

Porous microparticles have numerous advantages in drug delivery and tissue engineering because they show a better rate of drug release and low mass density. The current porous particles prepared by the commonly used salt-leaching method have an interconnected porous structure which is hard for tissues to penetrate [80, 81].

In our study, after forming the PLA-PS multicompartmental particles, subsequent PLA porous microparticles were prepared by selective solvent extraction of PS using cyclohexane. This cage-like PLA microparticle has a great potential in the growth factor delivery built in the tissue engineering scaffolds.

3.2 INTRODUCTION

3.2.1 Anisotropic particles

Multifunctional anisotropic particles have a great potential in many fields such as drug delivery, medical imaging, cosmetics, painting and so on [75, 76, 82] (Figure 3.1). Generally speaking, anisotropic particles are particles that are the non-spherical shape. In the current literature, there are three types of anisotropic particles: patchy, multicompartment, and Janus particles (Figure 3.2). Patchy particles have precisely controlled patches with different chemical compositions in the corona [75, 83]. Multicompartment particles are particles with physically phase separated architecture in the core [75]. Janus particles, named after the double-faced Roman god, have two phase-separated domains either in the core or in the corona [75]. There is some overlap between these particles in terms of their definitions. For example, in Figure 3.2, D and E are patchy particles as well as Janus particles or multicompartment particles, respectively.

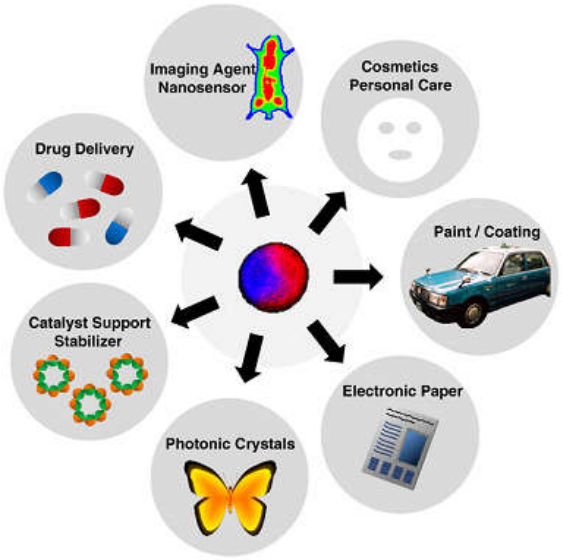

Figure 3. 1 Anisotropic particles and their emerging applications. Reproduced with permission from [76].

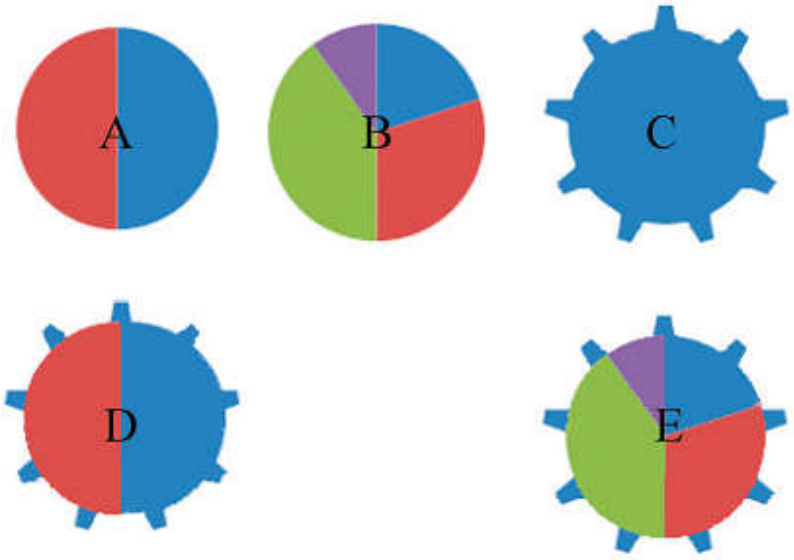

Figure 3. 2 Schematic representation of anisotropic particles: (A) Janus particles; (B) multi-compartment particles; (C) patchy particles; (D) patchy Janus particles; (E) patchy multi-compartment particles. Reproduced with permission from [75].

Various methods were developed to prepare micro- or nano- anisotropic particles complex in shapes, surfaces, and compartments. There are mainly two categories: top-down method and bottom-up method. The top-down method has the advantage of creating novel and customized shapes. But the operation process is complicated and often associated with high cost and low yield. On the other hand, the conventional bottom-up method is easy to scale up and cost efficient. However, it is hard to control particle shapes precisely. Despite the numerous research in this area, accurate engineering of anisotropy in submicron particles is still challenging [76]. Here, common preparation methods are summarized (Figure 3.3, overview).

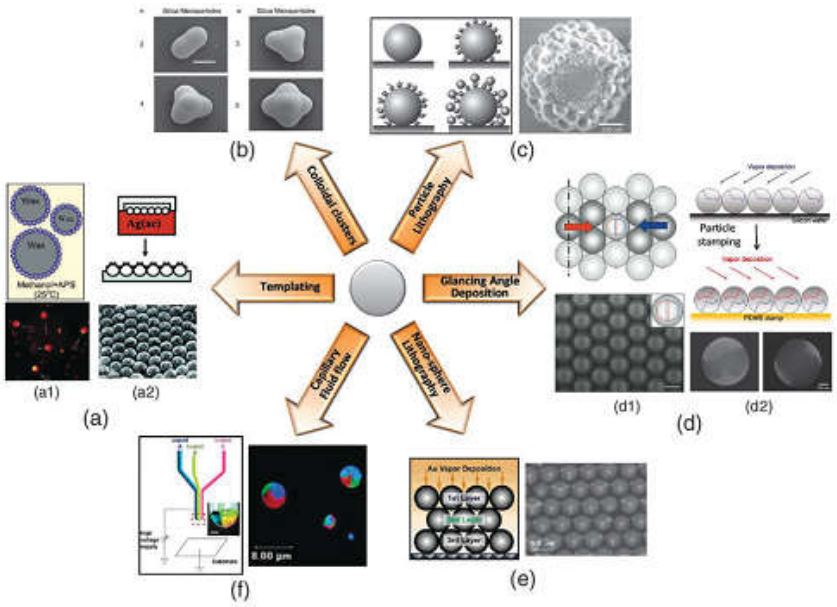

Figure 3. 3 Techniques for the fabrication of patchy particles. (a) templating; (b) colloidal assembly; (c) particle lithography; (d) glancing-angle deposition; (e) nanosphere lithography; (f) electrospray using a bi-phase nozzle. Reproduced with permission from [75, 84].

3.2.1.1 Self-assembly of colloids

Self-assembly of colloids with liquid protrusions was developed to prepare well-controlled and tunable patchiness. Cross-linked polymer spheres with a liquid protrusion or wet layer assembled into colloidal molecules by coalescence of the liquid protrusions or layers as shown in Figure 3.4 [85]. The self-assembly method is also known as the "bottom-up" manufacturing process. It is promising in terms of overcoming the size limitations and process restrictions of the "top-down" method like photolithography [84]. However, a sorting process is necessary for obtaining homogeneous samples due to the various particle shapes generated in one batch [79]. Besides, large-scale fabrication of anisotropic particles via self-assembly method is still elusive and requires further study [84, 86].

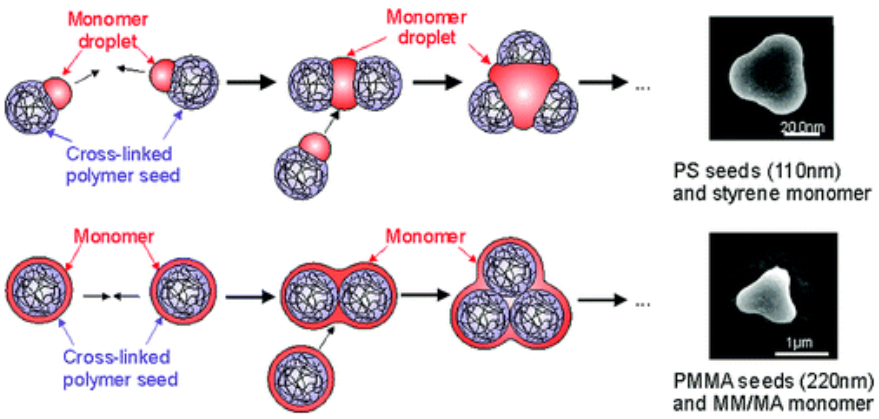

Figure 3. 4 Schematic of coalescence of liquid protrusions or wet layers, yielding colloidal molecules. Reproduced with permission from [85].

3.2.1.2 Self-assembly of block copolymers

Patchy multicompartment particles can be obtained by self-assembly of amphiphilic block copolymers in aqueous solution, in which the hydrophobic polymer chain forms the core and the hydrophilic chain forms the patchy architecture [75, 87]. An extension of this approach was to mix two different diblock copolymers with a common hydrophobic block. Upon mixing these two diblock polymers, patchy spherical micelles were formed in water [88]. Another interesting method was to use a triblock copolymer with two outer hydrophilic blocks to form a mixed micelle, after which the hydrophilic-to-hydrophobic transition resulted in the formation of multicompartment micelles (the procedure is in Figure 3.5) [89]. The self-assembly of block copolymers is a relatively new area compared to other anisotropic particle fabrication methods. The first self-assembled multicompartment polymer micelles were reported in 2004 by Lodge, Hillmyer, and coworkers [90]. Since then, they reported numerous elegant multicompartment polymer micelles prepared with star polymers [91-93]. However, the synthesis of star polymers is complicated compared to linear block copolymers [94]. Therefore, the linear triblock copolymers

self-assembly has been studied and shown great potential [95-97]. The limitation, however, is that the fabrication process is multi-steps and needs a sophisticated operation.

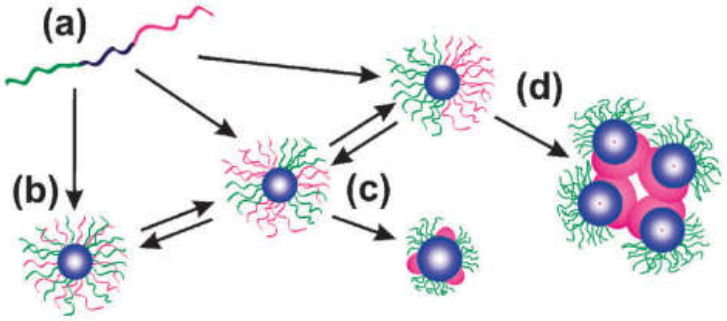

Figure 3. 5 Schematic of a triblock copolymer with two outer hydrophilic blocks that can self-assemble into multicompartment micelles. Reproduced with permission from [98].

3.2.1.3 Phase separation of polymer blends

Phase separation between two incompatible polymers during the solvent evaporation in the aqueous solution allows the formation of Janus particles [99]. The shape of the resulting anisotropic particles is determined by the combination of a pair of polymers, the solvent evaporation speed, and the type of surfactant used [82, 100]. As shown in Figure 3.6, the mechanism behind this method is simple and the preparation setup is easy to repeat. However, in reality, the particle shape and size from one batch are often not uniform. Besides, the selection of the combination of polymers and the solvent is complicated. Huang et al. reported a multicompartment particle made of a single polymer via a one-pot double emulsion induced by partial wetting [79].

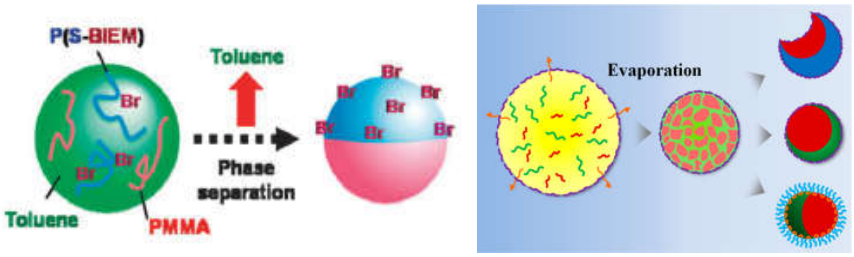

Figure 3. 6 (Left) Schematic of Janus particles via polymer blends separation; (right) various anisotropic particles via phase separation. Reproduced with permission from [82, 99].

3.2.1.4 Top-down methods

Emerging top-down methods, such as microfluidics [77, 82, 100, 101], electrohydrodynamic (EHD) co-jetting [102], non-wetting template [103], provide sophisticated and versatile ways to fabricate anisotropic multicompartment particles that can be precisely controlled in dimension and composition. So far, microfluidics and EHD co-jetting have been predominantly used for multicompartment particles research because they can provide well-defined droplets, which will lead to uniform size and repeatable results. Both approaches use the laminar flow of two or more polymer solutions [76]. For example, using microfluidics to prepare multicompartment particles involves steps including the introduction of laminar flow of different polymer solutions, the formation of polymer solution droplets (Figure 3.7a), and then the solidification of droplets into particles by photocrosslinking (Figure 3.7b) or other methods [101]. EHD co-jetting method not only produces multicompartment particles but also cylinders. It has the advantage of producing truly complex anisotropic particles [76]. Lahann and coworkers have investigated the EHD co-jetting method to prepare bi- or tri- anisotropic particles [104, 105]. The challenges for these methods are that it requires a complicated operation process and high cost with a low yield, which limits the spreading of their application.

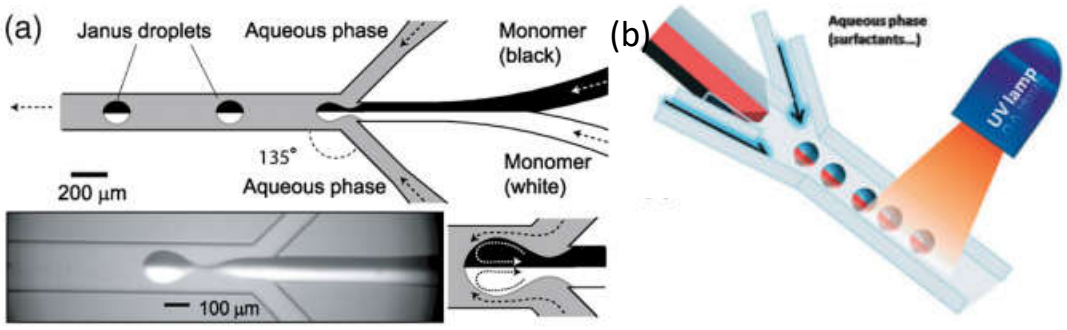

Figure 3. 7 Schematic of using microfluidics to prepare Janus particles: (a) the introduction of laminar flow; (b) solidification by photocrosslinking. Reproduced with permission from [75, 77].

3.2.1.5 Other methods

Other than the commonly used methods, researchers have developed numerous interesting methods to generate anisotropic particles such as co-encapsulation of multiple types of nanoparticles (Figure 3.8a), stretching (Figure 3.8b), micromolding (Figure 3.8c), matrix embedment (Figure 3.8d), glancing angle deposition (Figure 3.3d).

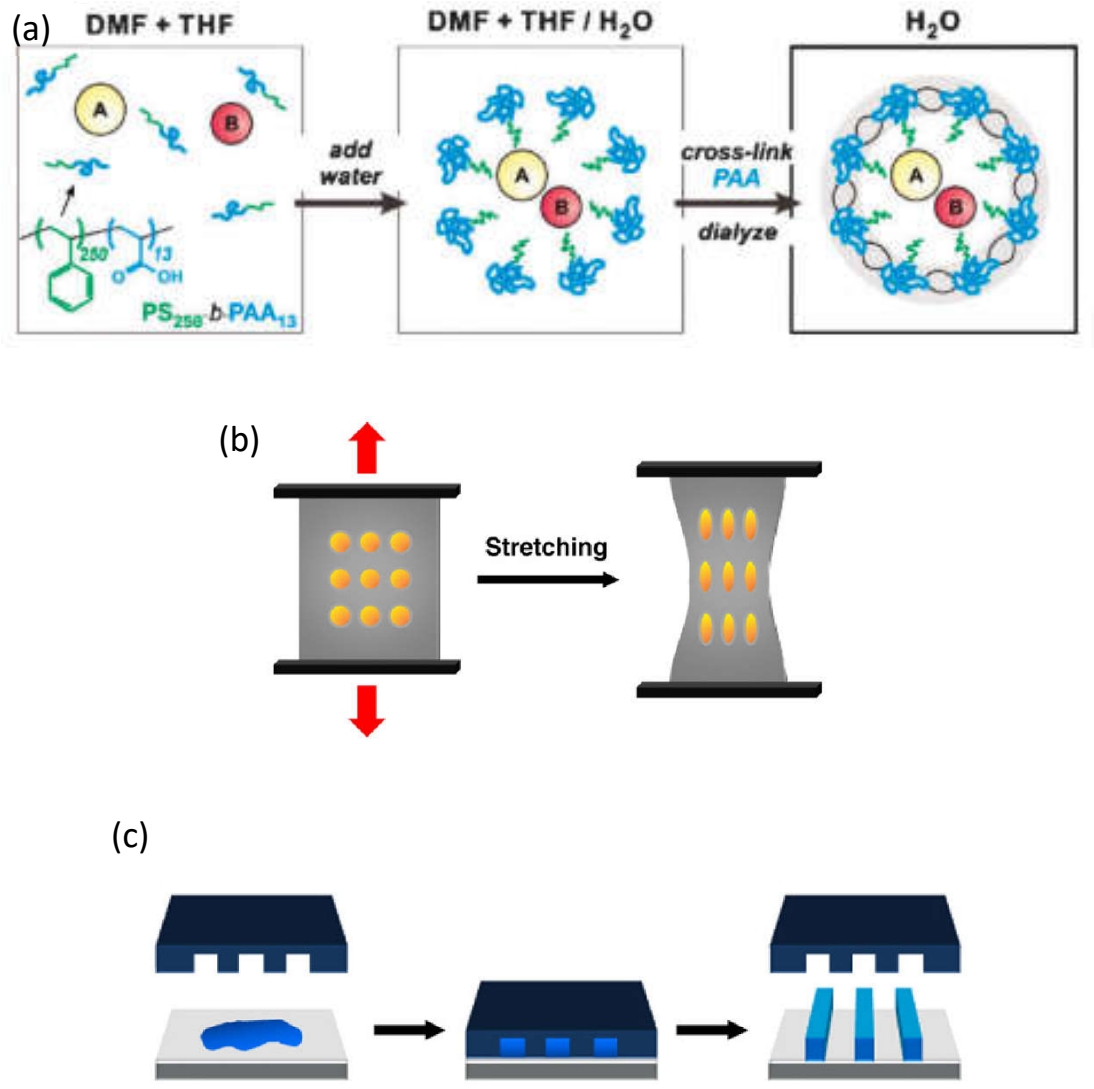

Figure 3. 8 (a) Preparation of multifunctional hybrid nanostructures by co-encapsulation of multiple types of nanoparticles (A and B) within a cross-linkable block copolymer micelle; (b) Particle stretching method; (c) Micromolding method; (d) Preparation of anisotropic particles by embedded matrix. Reproduced with permission from [76, 106].

Figure 3.8 (cont'd)

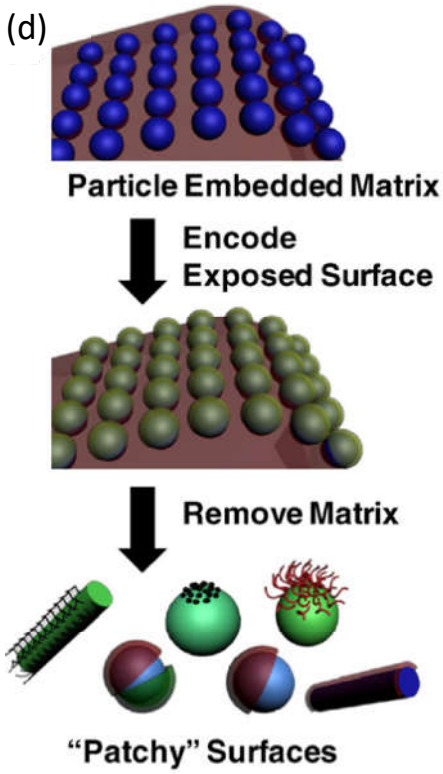

3.2.2 Functional porous particles

Polymer particles with porous structures have a great potential in various fields such as drug delivery [107, 108], tissue engineering scaffolds [109], microsensors [110], catalytic supports [111, 112], hydrogen/lithium storage vehicle [113, 114], CO2 capture and separation [115], solid phase extraction [116], and microreactors [117]. Depending on the size of pores, porous particles are categorized as macro- (>50 nm), meso- (50-2 nm), microporous (<2 nm), respectively. The main features of porous particles include high surface area, the ability to uptake various solvents with different polarity, and increased brittleness [118]. The commonly used preparation methods are suspension polymerization combined with a porogen, precipitation and dispersion polymerization, multistage heterogeneous polymerization, membrane/microchannel emulsification, microfluidics and so on [118].

Suspension polymerization (Figure 3.9) combined with porogen is widely used in industry because of its low cost and the upscaling possibility. Due to the droplet collision and breakup throughout the process, particles obtained are polydisperse, which is the main drawback of this method [118]. The selection of different porogen could result in different types of pore structures. For example, when using a good solvent (e.g. Toluene) as the porogen, micro- or mesopores are predominant, resulting in the high surface area but low porous volume. On the other hand, when using a nonsolvent, macropores are predominant with the significant low surface area but high porous volume. The critical step of forming porous structure is the phase separation before (nonsolvent) or after (good solvent) the gelation point [119]. Other commonly used porogen include linear polymers [120, 121], water [122], solids [123].

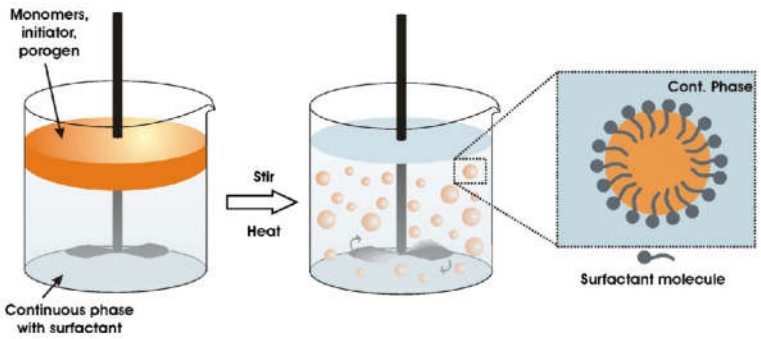

Figure 3. 9 Schematic of the suspension polymerization method. Reproduced with permission from [118].

Precipitation and dispersion polymerizations are techniques that start with completely homogeneous solutions. However, in the early stage, phase separation takes place as the result of polymerization. While precipitation and dispersion polymerizations have similar mechanisms, a crosslinker is necessary and used in a large proportion in precipitation polymerization. Thus, precipitation polymerization (Figure 3.10) is more suitable to prepare highly crosslinked and porous particles while dispersion polymerization is mainly used for non-crosslinked, non-porous

particles production. Compared to suspension polymerization, the advantage of these two techniques is the production of monodisperse particles in the range of 0.1-10 μm [118].

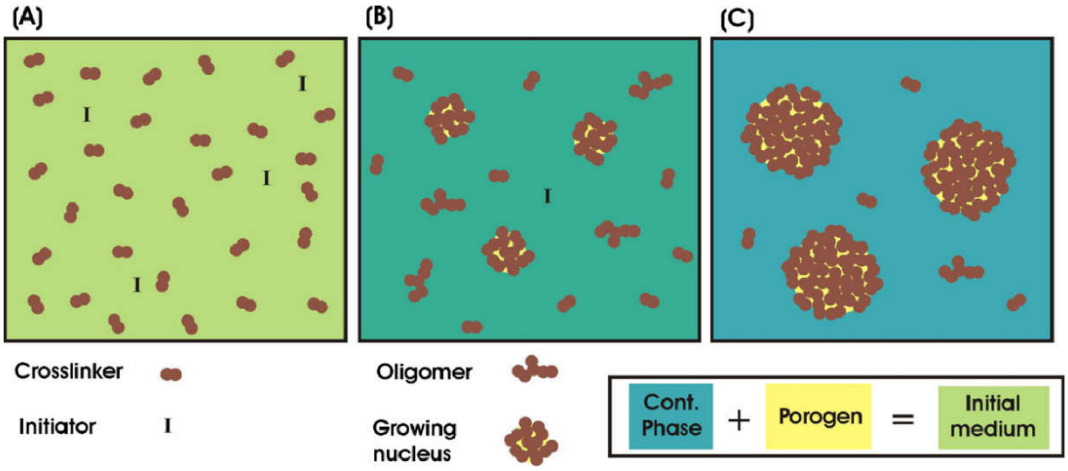

Figure 3. 10 Schematic of precipitation polymerization for porous particle production. (A) Initial stage with only crosslinker and initiator molecules; (B) Oligomers and nuclei formed because of radical polymerization; (C) Nuclei grow by adding monomers and oligomers from the medium. Reproduced with permission from [118].

Multistage heterogeneous polymerizations are very powerful techniques in terms of achieving polymer particles with any desired size, monodispersity, porosity, pore size distribution, hollowness and functionality by a careful selection and control of the different stages of the polymerization. An example is “supraballs” (seed assembly), spherical colloidal crystals obtained via assembly of monodisperse seeds (0.1–2 μm latex) into larger spheres as shown in Figure 3.11 [124, 125]. Another example is “cage-like” porous particles (hollow particles with huge pores) prepared with a combination of Pickering emulsion and γ-ray polymerization. The shrinkage of the new polymer phase via γ-ray polymerization resulted in the removal of the seeds and thus turned into huge pores of the final porous hollow particle [126].

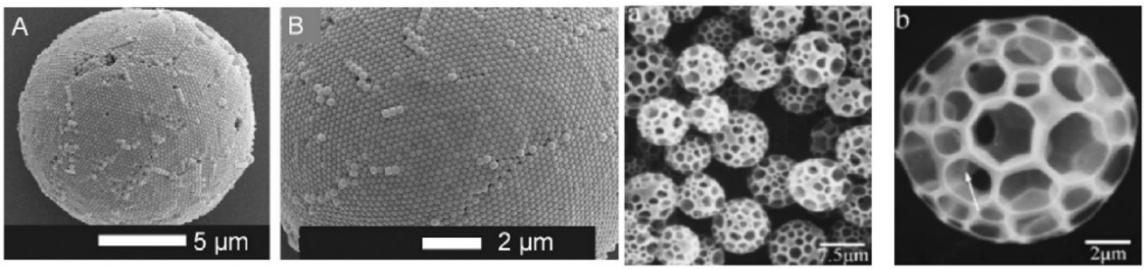

Figure 3. 11 SEM images of "supraballs" (left two) and "cage-like" (right two) porous particles. Reproduced with permission from [125, 126].

Membrane/microchannel emulsification has been developed to generate uniform emulsion droplets and thus monodisperse particles [118, 127]. The quality of the size monodispersity of emulsion droplets is related to the hydrophilicity/hydrophobicity of the membrane/microchannel. Emulsion prepared with the hydrophobic polymer via hydrophilic membrane is more uniform than the one prepared via hydrophobic membrane [128]. Figure 3.12 demonstrates the setup of membrane emulsification.

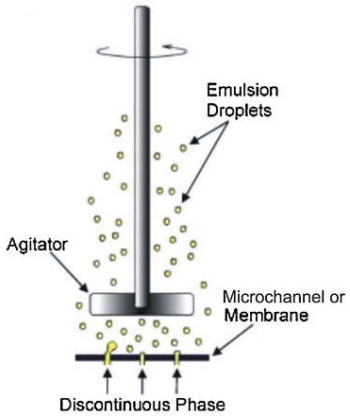

Figure 3. 12 Schematic of membrane/microchannel emulsification. Reproduced with permission from [129].

An ultimate control of droplet formation is achieved by microfluidics, the youngest particle production technique. The process of microfluidics was discussed in the *section 3.2.1.4*. The elaborate chip design allows not only the preparation of narrowly monodisperse spherical particles but also the non-spherical and even porous particles. There are several significant parameters such

as flow rates, polarity differences, viscosity, wettability and channel dimensions in the microfluidics process. For porous particles, the effect of polarity can be very prominent because it is the interfacial tension, hence the polarity difference between two phases, that allows droplet growth at the tip of the inner liquid orifice. An increase in polarity of the monomer phase will lead to smaller droplets and a smaller value of critical jetting velocity [118]. The first polymer porous particles prepared by the microfluidics method was reported in 2005 (porous particles of ~250 μm in diameter with a mean pore size of 0.90 μm) [130]. It was concluded that particles prepared by microfluidics have a finer porous structure. Microfluidics has also been utilized to form monodisperse supraballs, consisting of an assembly of smaller particles to form larger porous particles. An approach realized exclusively by microfluidics is using gas bubbles instead of any liquid or solid porogen, forming G/W/O double emulsion [131].

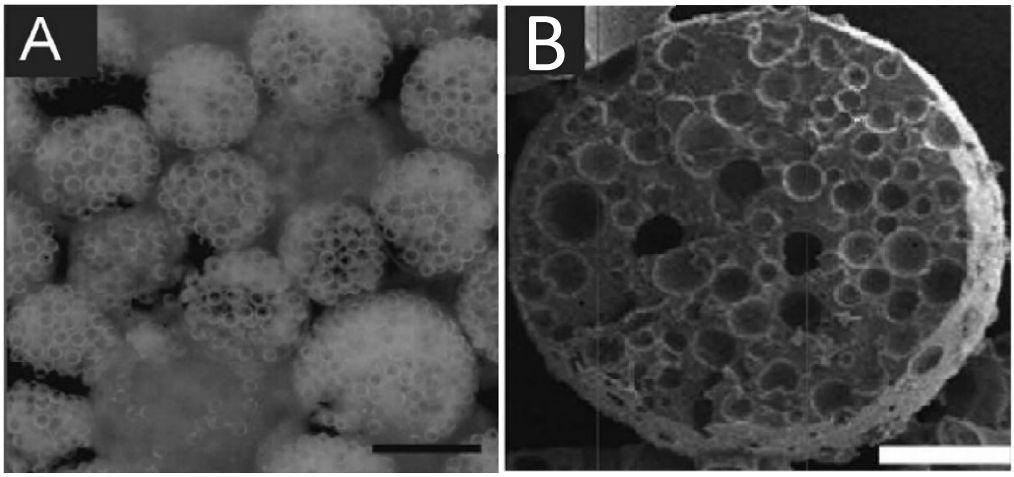

Figure 3. 13 Images of porous particles prepared via gas bubbles (G/W/O emulsion). Scale bars represent 50 μm. Reproduced with permission from [131, 132].

In addition, some other techniques have the potential to generate porous particles including selective withdrawal [133], flow lithography techniques [134], electrospray method [135], and aerosol polymerization [136].

3.3 EXPERIMENT

3.3.1 Materials

Poly(lactic acid) (PLA, Mw=50,000, Tg=51.2℃) was purchased from Lakeshore Biomaterials (Evonik Industries). Polystyrene (PS, Mw=50,000) was purchased from Polysciences, Inc. Polycaprolactone (PCL, Mw=45,000) was purchased from Sigma-Aldrich. Pluronic F68 (PF68) was purchased from Sigma-Aldrich. Ethyl acetate (EA) and glycerol were purchased from J.K. Baker. Diclofenac (DCF) was purchased from Sigma-Aldrich. All the chemicals used are analytical level and without any further purification. Deionized (DI) water used in all the process was supplied by a Barnstead nanopure Diamond-UV purification unit equipped with a UV source and final 0.2 μm filter at 18.2 MΩ purity. Nanomixer was purchased from the PRIMIX Corporation. Filter papers (0.1 μm and 0.03 μm) were purchased from Millipore.

3.3.2 Preparation of PLA-PS heterogeneous microparticles

Ethyl acetate (EA) and DI water were mixed and saturated before using for the emulsion. The mixing solution of PLA and PS were prepared by dissolving different PLA weight ratios among the total PLA and PS weight (100%, 66.7%, 50%, 33.3%, 0%) into the water-saturated EA. PF68 (15mg/ml) was dissolved in a mixer of EA-saturated DI water and glycerol (1:1 v/v). The volume ratio of the organic polymer solution (O-phase) to the aqueous solution (W-phase) was 1:3, regardless of the addition of polymers and PF68. The polymer solution and aqueous solution was then emulsified using a modified high-shear Taylor-Couette type of Nanomixer under a speed of 12500 s^{-1} for 2 min. The resulting emulsion was then gradually poured into 90 ml of pure DI water under stirring (280 rpm) in a flask to induce the diffusion of EA from emulsion droplets to the outside water phase for overnight diffusion. The emulsification temperature was controlled by a

circulating cooling water system around the outer tank wall. The resulting particle suspension was then stored in the refrigerator for future use or further characterizations.

For parallel experiments, toluene was used as the solvent of PLA-PS mixture instead of EA. All the other conditions were the same. PCL was used to prepare PLA-PCL composite microparticles with 50% wt% PLA. All the other conditions were the same. Pure PCL microparticles were also prepared to make a comparison.

3.3.3 Preparation of porous (cage-like) PLA microparticles

PLA porous particles were obtained through selective solvent extraction using cyclohexane, which only dissolves PS but not PLA. 2 ml of the PLA-PS particle suspension was mixed with 2 ml of cyclohexane under stirring for 24 hours. After extracting PS, the resulting suspension was filtered through a membrane to collect PLA porous particles.

3.3.4 Morphology characterizations

Scanning Electron Microscope (SEM) The particle suspension was filtered using a 0.1 or 0.03 μm pore size filter paper, after which was dried for the SEM test. The sample loaded filter paper was then coated by a platinum coating. The images were taken under a 3kv electron accelerating voltage, ~4.5 mm working distance.

Transmission Electron Microscopy (TEM) The particle suspension was placed into a dialysis membrane tube within a slow stirring water bath to gently remove the glycerol and excess surfactant. After 3 days of dialysis, the suspension was then diluted 1:10 with DI water. Several drops of the dilution were then dripped on the carbon coated copper grid and air dried for TEM.

Fluorescence or Optical Microscopy In order to observe the structure of the emulsion, a water soluble dye called Acridine Orange was added into the aqueous phase before the emulsion process. One drop of the resulting emulsion was dripped on the glass slide and covered by a cover glass. The sample was then put under an optical microscope with a blue excitation light source. A undyed sample was also carried on to see the transformation of droplet along time.

3.3.5 Thermal Analysis

Thermogravimetric analysis (TGA) The particles suspension was washed with DI water by centrifugation three times and then freeze dried. The TGA equipment is from TA Instruments, Q Series^{TM} Thermal Analysis (Q500). About 15 mg of the sample powder in the platinum crucible was heated from 10 to 500 °C at 10 °C/min under nitrogen flow.

Differential scanning calorimetry (DSC) The freeze-dried samples (~15 mg) were purged with dry nitrogen at a flow rate of 20 ml/min. The temperature was raised at 10 °C/min. The equipment used is from TA Instruments (Q2000).

3.3.6 Encapsulation of diclofenac (DCF) and Release Test

Diclofenac (DCF), which is hydrophilic and water-soluble, was dissolved in the water phase accordingly before the emulsion process. All the other procedures were the same as the particle preparation method as section 3.3.2. After obtaining the freeze-dried sample, 5 mg of DCF-loaded particles were suspended in 1 ml of 0.02 M phosphate buffer (pH 7.4). The suspension was stirred and sonicated for 2 min and maintained at 37 °C in an incubator under shaking. At predetermined interval time spots, the suspension was centrifuged at 12,000 *g for 10 min. The 1 ml supernatant

was withdrawn and 1 ml fresh butter was added for further release. The concentration of DCF was then measured by UV-Vis at the peak of 276 nm.

3.3.7 Encapsulation of hydrophilic iron oxide nanoparticles (IONPs)

Hydrophilic IONPs (~10 nm) were dispersed in the water phase before emulsion. All the other steps were the same with the PLA-PS particle preparation. The preparation of hydrophilic IONPs was described previously in section 2.3.2.

3.4 RESULTS AND DISCUSSION

3.4.1 Morphology of PLA-PS anisotropic microparticles

Figure 3.14 shows the morphology of microparticles prepared with PLA-PS (50:50 wt%) mixing solution under the emulsification temperature of 60 °C. Both open-hollow and closed microparticles were observed from the SEM results as shown in Figure 3.14 (a). As observed in Figure 3.14 (b-c), the outer and inner surfaces of the microparticle shell were embedded with smaller particle protrusions. This unique structure is defined as multicompartment particles of PLA-PS in this study. The smaller particle protrusion is PS while the microparticle shell is made of PLA. Figure 4.13 (d) is the higher magnification of the microparticle inner surface, which shows that the protrusion particles from the inner surface were less uniform than that of the outer surface.

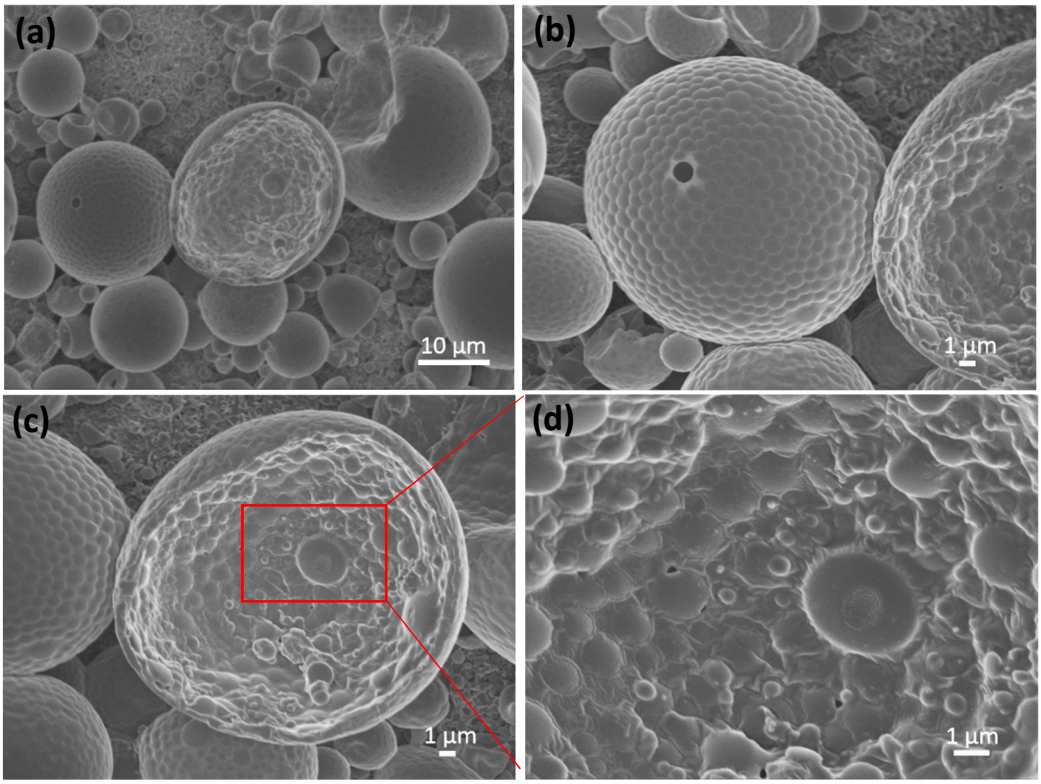

Figure 3. 14 SEM images of PLA-PS (50:50) multicompartment microparticles.

Figure 3.15 is the corresponding TEM results that demonstrate the internal structure of PLA-PS microparticles. The obvious contrast between the large light particle shell and the small black nanospheres in Figure 3.15 (a) confirmed that the obtained closed particles were hollow as well. Figure 3.15 (c) is a higher magnification image to show the waving edge of particle shell, which is the projection of the embedded nanoparticles on the side. The same is with Figure 3.15 (b), which shows the overlap of the protrusions coming from the projection of the top and the bottom of the particle. Figure 3.15 (d) is an example of the open hollow particle, which is corresponding to Figure 3.14 (c). Figure 3.16 demonstrates a set of SEM and TEM images of open-hollow multicompartment microparticles from a different angle compared to Figure 3.15 (d). It shows that the protrusions existed on the transition edge of the particle shell (red arrow).

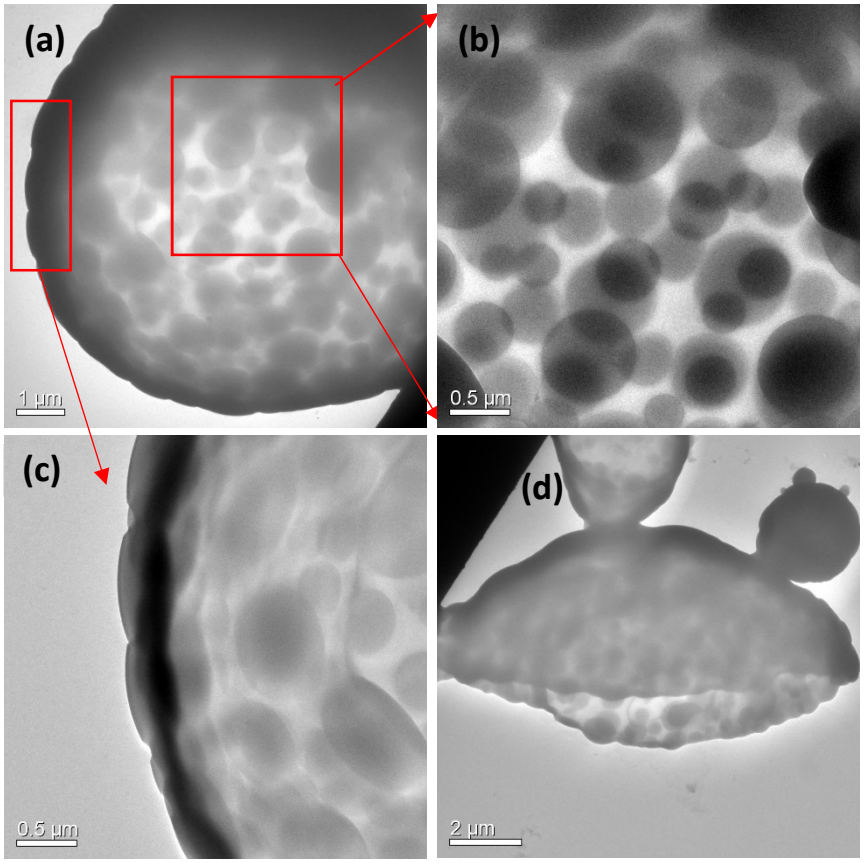

Figure 3. 15 TEM images of PLA-PS (50:50) multicompartment microparticles.

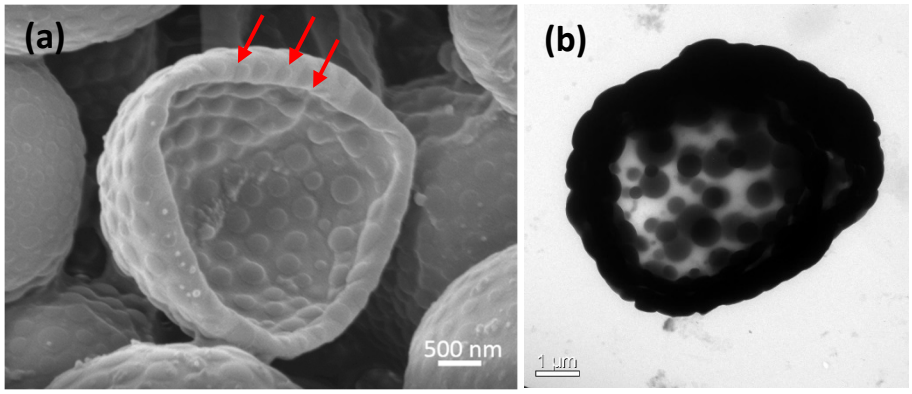

Figure 3. 16 SEM and TEM images of an open-hollow microparticle.

In order to study how the PLA/PS ratio affects the particle morphology, different PLA/PS ratio samples were prepared with the same other conditions. Figure 3.17 shows the overall particle morphology prepared with different PLA weight ratios, 100%, 66.7%, 50%, 33.3%, 0%,

respectively. As observed, the overall particle size decreased with the weight ratio of PLA decreasing. Statistically, the mean particle size of 66.7% PLA sample is 3.41 μm while the mean particle size of 33.3% PLA sample decreased to 1.78 μm. It is worthy of notice that pure PLA (Figure 3.17 (a)) mainly formed large, open-hollow microparticles with sizes around 6-7 μm, while pure PS particles were smaller (~3μm). This could possibly explain the overall size decrease with less PLA and more PS. It is also noticed that the addition of PS led to less open particles, but more closed hollow particles compared to pure PLA particles.

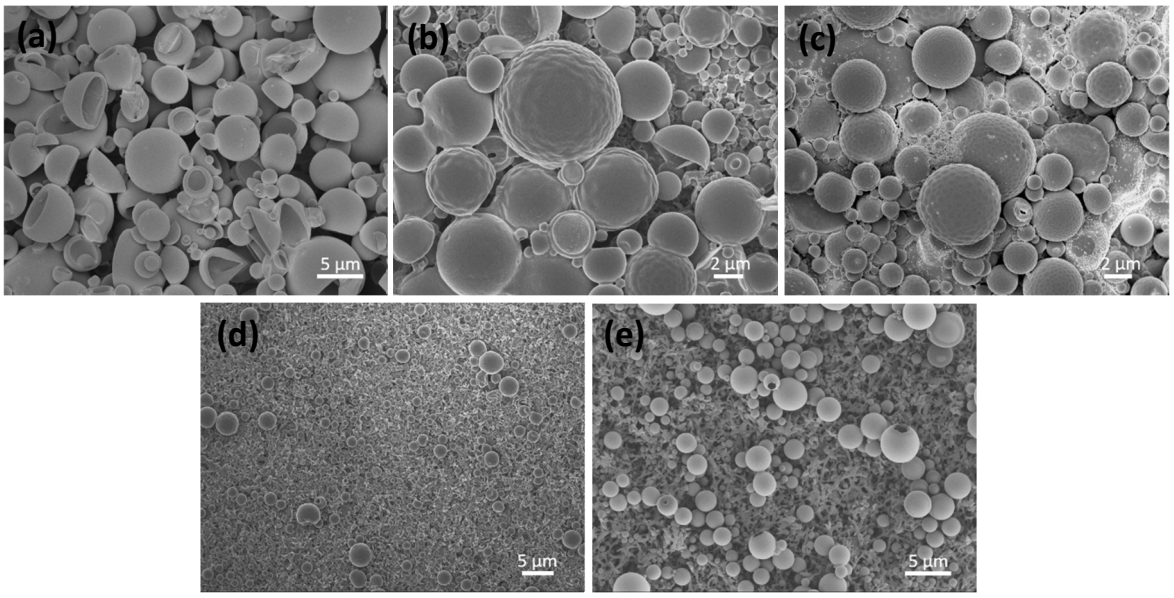

Figure 3. 17 SEM images of PLA-PS microparticles of different compositions. (a) 100% PLA; (b) 66.7% PLA; (c) 50% PLA; (d) 33.3% PLA; (e) 0% PLA.

The PLA/PS ratio not only affected the overall particle size, but also the relative size of the small particle protrusion as shown in Figure 3.18. The ratio of the large particle vs its protrusion is ~33 for PLA (66.7%, Figure 3.18 (a)) sample and ~8 for PLA (33.3%, Figure 3.18 (c)) sample. It is concluded that, with more PS, the relative size of the protrusion particle was larger due to more materials for PS to form a larger particle.

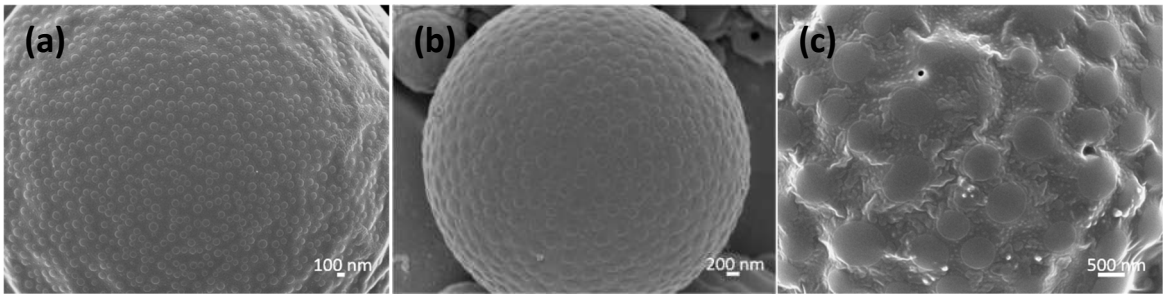

Figure 3. 18 SEM images of higher magnification to demonstrate the ratio between PLA large particle shell and PS protrusion. (a-c): 66.7%, 50%, 33.3% PLA, respectively.

TGA analysis of PLA-PS composite particle with different ratios is demonstrated in Figure 3.19. The weight loss vs temperature curves of PLA-PS composite particles all fell between the pure PLA and pure PS curves, which suggests a good compatibility between PLA and PS. From the current literature, PLA-PS composite is non-compatible or partially compatible due to the immiscibility between PLA and PS, which is always challenging for the composite production field. In comparison, our method is much more efficient to prepare composite with two immiscible polymers. The possible reason is that PS was held within PLA microparticles and reduced the extent of phase separation between them. This theory is compatible with the TGA analysis of PLA/PS 1:2 sample, where there are two decomposition steps compared to the other two composite samples, indicating the less compatibility between PLA and PS.

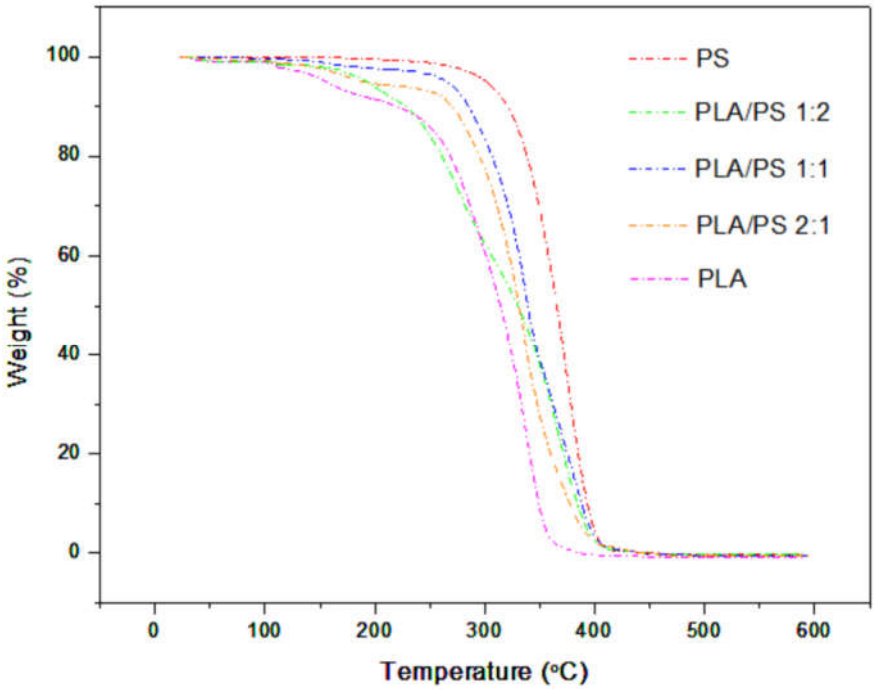

Figure 3. 19 TGA analysis of PLA-PS microparticles of different composition ratios.

3.4.3 Cage-like PLA porous particles

Porous PLA particles were obtained by the selective solvent extraction method using cyclohexane, which can only dissolve PS but not PLA. The resulting sample after solvent extraction was observed under SEM as shown in Figure 3.20. The porous particle is cage-like porous instead of the common interconnected porous structure because of the hollow structure of the PLA-PS microparticle. One point needs to be mentioned is that the larger the particle, the easier it cracks after cyclohexane extracting PS. This could possibly explain why the overall size of porous particles decreased compared to the original particles. The cage-like porous particle is better suitable for tissue engineering scaffolds since the hollow pores will allow the growth of the nerves and blood vessels.

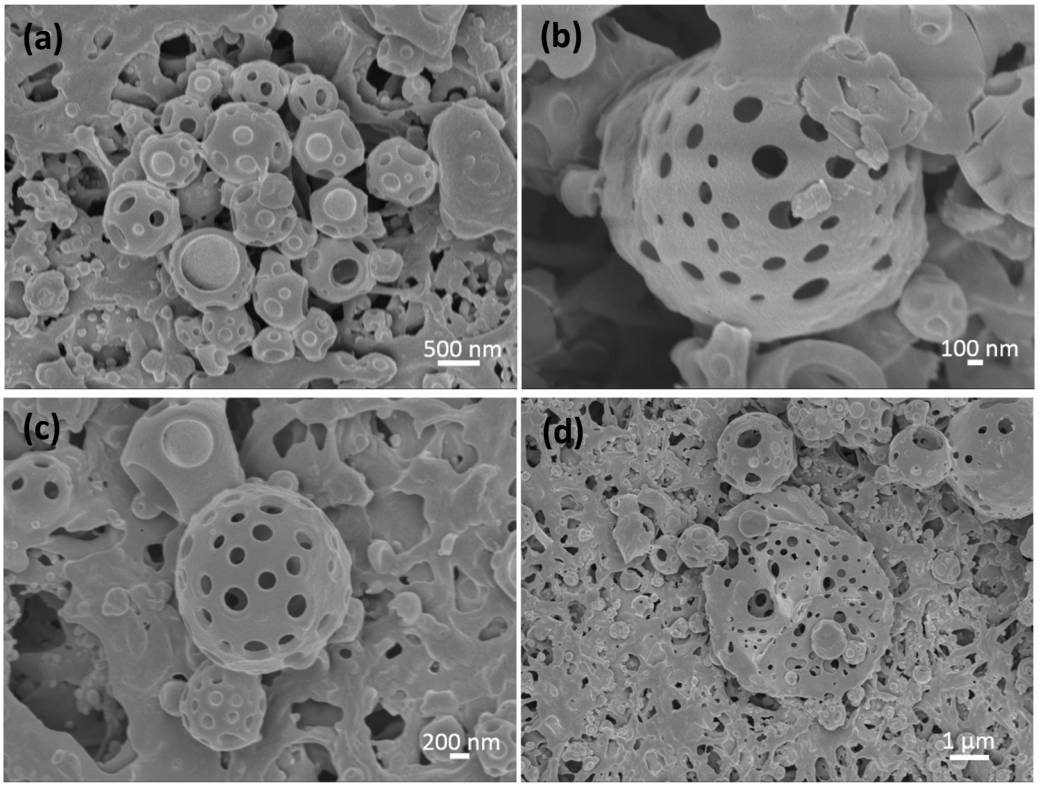

Figure 3. 20 SEM images of cage-like porous PLA microparticles.

In fact, the solvent extraction method helped confirm the composition of the microparticle shell and the small particle protrusion. Figure 3.21 compared the particles washed by cyclohexane or acetone (acetone can only dissolve PLA but not PS). While porous particles were observed in the samples washed by cyclohexane, the only solid sphere was found in the acetone washed samples which were PS particles released from the dissolved PLA big particle shell.

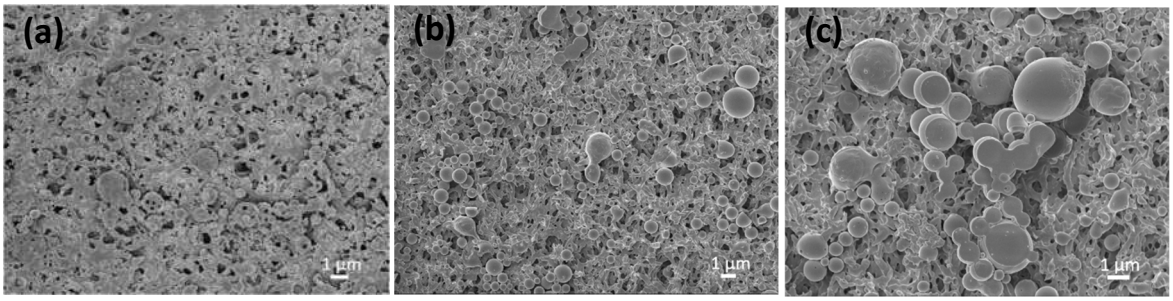

Figure 3. 21 SEM images of PLA-PS particles washed by cyclohexane (a) and acetone (b-c).

When compare the TGA analysis of solvent extraction samples with the pure PLA or PS particles (Figure 3.22), the result is corresponding with what observed from the SEM images. The weight loss vs temperature curve of "extract PLA" is closer to the PS curve, which suggests the leftover after solvent washing is mainly PS with minor PLA. Vice versa for the "extract PS" curve.

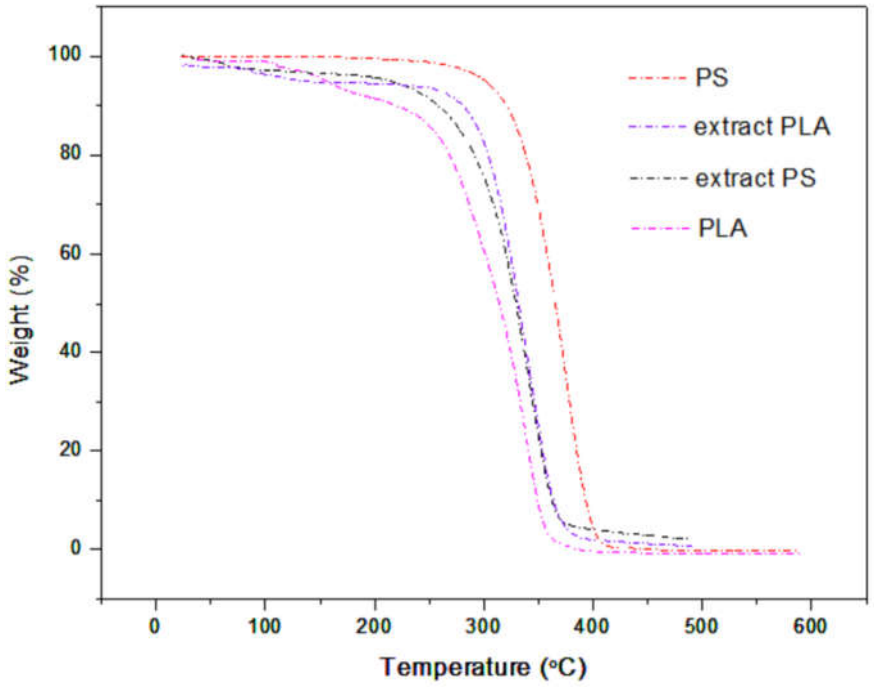

Figure 3. 22 TGA analysis of selective solvent extraction samples.

3.4.3 Mechanism of multicompartment particle via solvent-induced phase separation

The mechanism and preparation process of PLA-PS multicompartment particles are described in the schematic, Figure 3.23. The one-step W/O/W emulsion method developed in our group was employed to prepare PLA-PS composite particles by dissolving PLA and PS in the same solvent (ethyl acetate) successively. The polymer solution was preheated to 50 °C in order to fully dissolve PS due to its poor solubility in ethyl acetate at room temperature. Therefore, this method starts with a completely homogenous solution. Under high emulsification temperature (HT, 60°C)

condition, the transitional behavior between O/W emulsion and W/O/W emulsion were obtained by controlling the viscosity of the continuous phase [10].

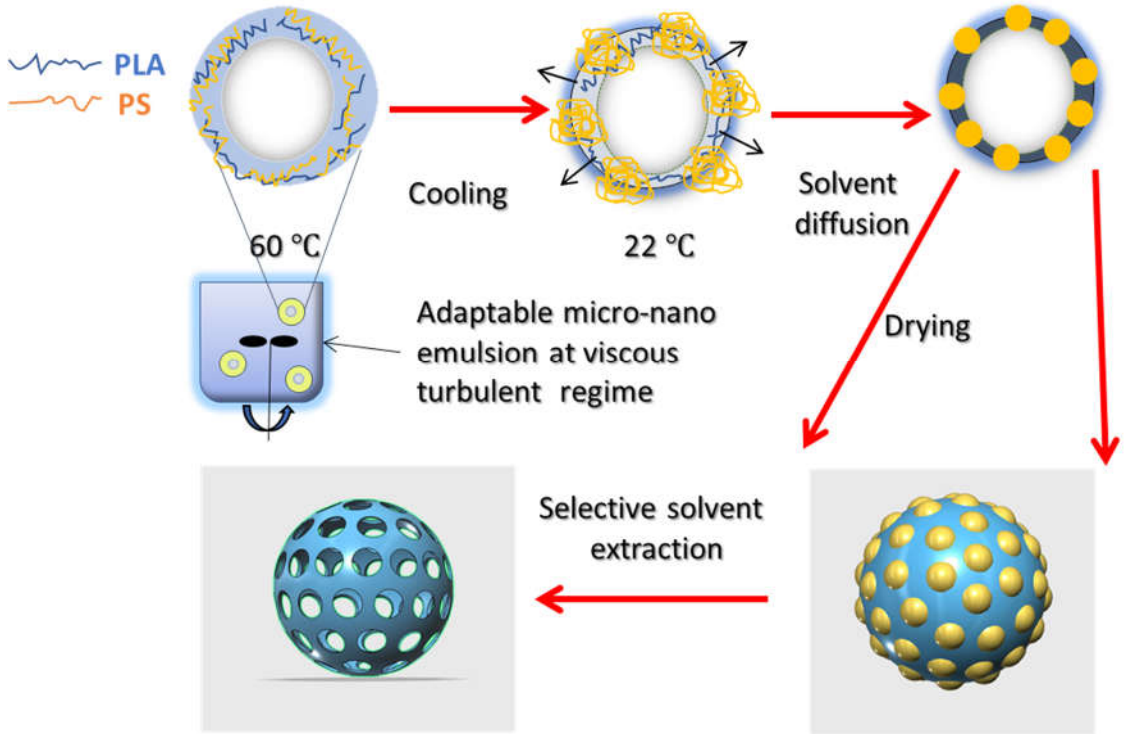

Figure 3. 23 Schematic of the mechanism of PLA-PS multicompartment microparticles and cage-like PLA porous particles.

The emulsion droplet with water-soluble dye was observed under a fluorescence microscope to confirm the W/O/W droplet as shown in Figure 3.24. The green region represents the water phase while the dark ring region represents the polymer solution, which suggests that the PLA-PS solution was still homogeneous at the stage of forming emulsion droplet.

When the W/O/W emulsion (60 °C) was poured into room temperature water (25 °C) to induce the solvent-diffusion process, a phase separation process was expected to happen during the formation of polymeric particles, due to the solubility of PS in ethyl acetate decreased when the overall temperature dropped suddenly [137]. Figure 3.25 reflects how solubility of PS along temperature. As observed, when the temperature is 50 °C, the PLA-PS mixing solution was

transparent. When the temperature dropped to 45 °C, it became cloudy, indicating the precipitation of PS out of the mixing solution. As the solvent diffuses out, PS nucleation domains were firstly formed in the emulsion droplet [82] and extended to solidified protrusions with hemispherical architecture both inside and outside of the particle shell because the existence of outer and inner water phase causing the hydrophobic effect as shown in SEM images. The porous PLA particles were then made by using selective solvent extraction method.

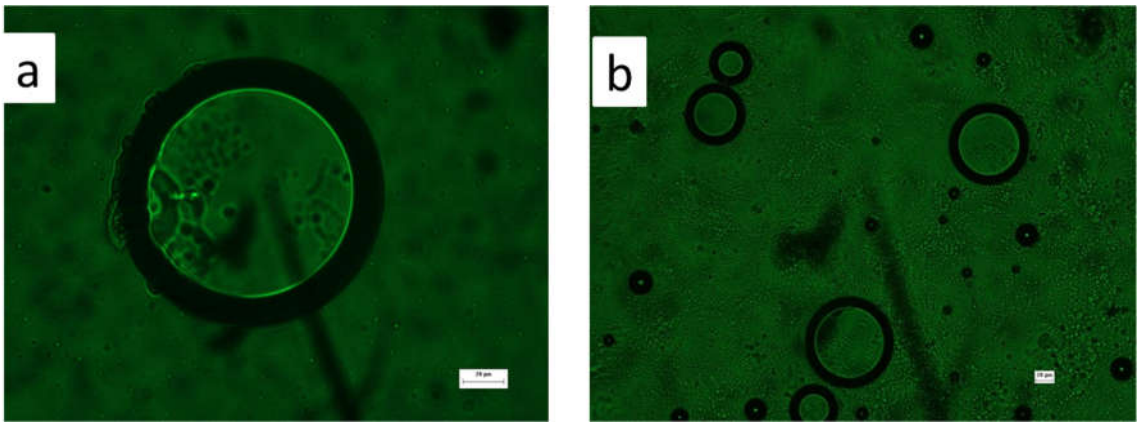

Figure 3. 24 Fluorescence microscopy images of emulsion droplets (a) PLA at 60 °C; (b) PLA/PS (1:1) at 60 °C. (Scale bars are 10 µm.)

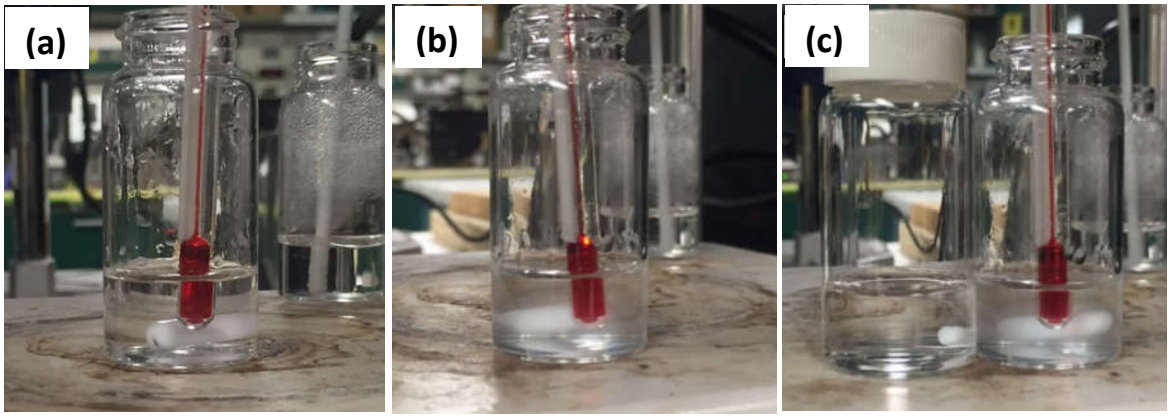

Figure 3. 25 Images of PLA-PS mixing solution along temperature drop.

Here, the phase separation is rapid because PS separate out from ethyl acetate once the diffusion process started. (Temperature drops below 45 °C). In order to confirm the key effect of non-solvent for PS, ethyl acetate, a parallel experiment using toluene as the solvent was carried. Toluene is a good solvent for both PLA and PS under the room temperature. The result shows that a solvent that can dissolve both PLA and PS under room temperature leads to a half-half Janus particle morphology, with one part is open hollow (as shown in Figure 3.26). Min N. et al. reported a similar approach to generate PLA-PS Janus particle [82]. However, the unique "liberty bell" shape was firstly developed with our method.

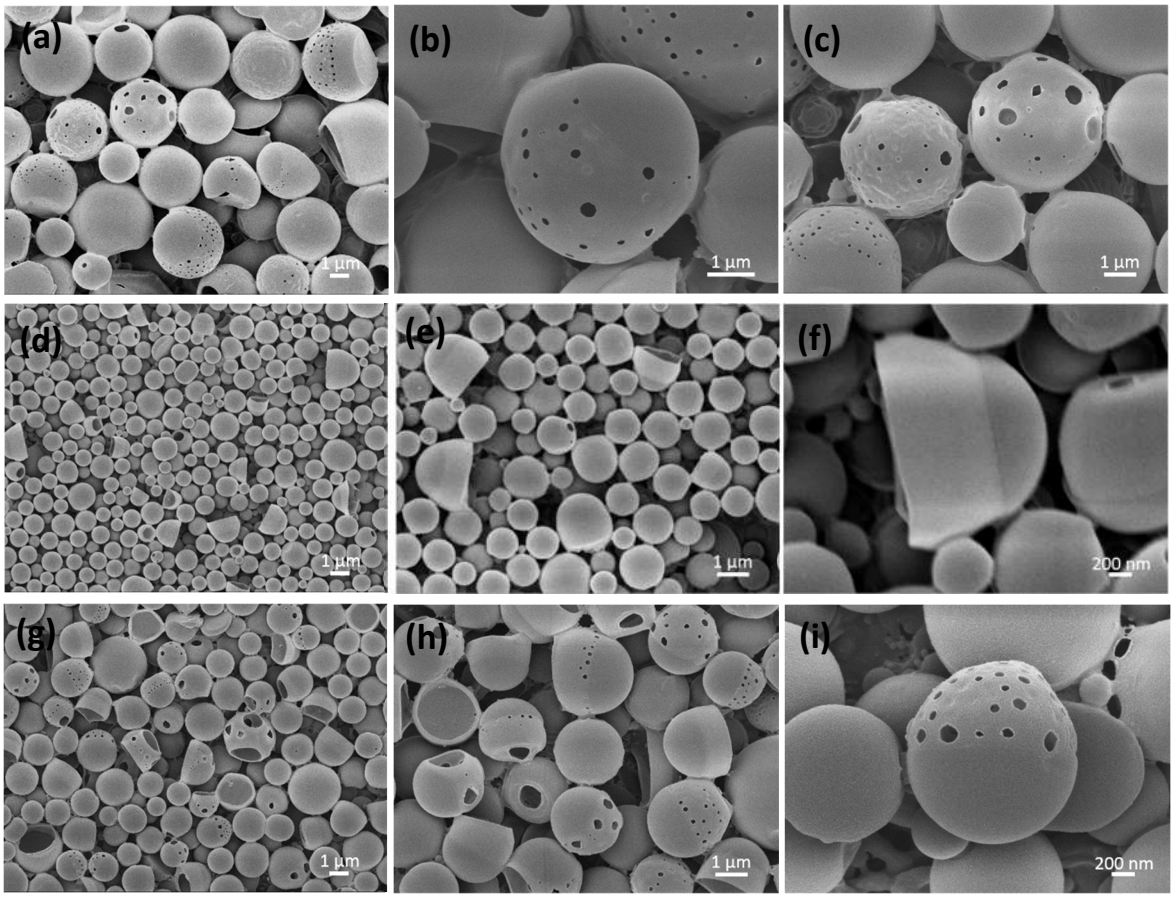

Figure 3. 26 SEM images of PLA-PS particles prepared with toluene as solvent. (a-c) 30% PLA; (d-f) 50% PLA; (g-i) 70% PLA.

3.4.3 Effect of Solvent and its extension

Figure 3.26 demonstrates PLA-PS Janus particles prepared with toluene as the oil phase solvent. Figure 3.26 (d-f) shows the particles prepared with PLA/PS (50:50 wt%) under 60 °C. As observed, instead of multicompartment, Janus particles formed with half PLA and half PS. Some of the particles had one side open, which is called a bell shape. Due to the fact that PLA particle will shrink under electron beam of SEM, the open side of the particle is most likely PLA (Figure 3.26-f). This is consistent with what concluded from Figure 3.17 that pure PLA generated mostly open hollow particles while the addition of PS led to closed hollow particles.

Figure 3.26 (a-c) is PLA-PS particles prepared via toluene solvent diffusion with PLA/PS (30:70 wt%) and Figure 3.26 (g-i) is particles prepared with PLA/PS (70:30 wt%). Both of them generated hollow porous particles and the porous structure only located on one-half of the particle while the other half is non-porous. As a comparison (Figure 3.27), the particle size of PLA/PS (30:70) was larger than that of PLA/PS (70:30). In addition, for PLA/PS (30:70), the pore size was relatively uniform and distributed mainly over half of the hollow particles. For PLA/PS (70:30), as shown in Figure 3.28, some of the particles were porous throughout the particle such as the cage-like particle and the ring porous particle. This might be because the porous structure came from the PLA composition. Therefore, when the PLA ratio was as high as 70%, the porous structure was then dominant.

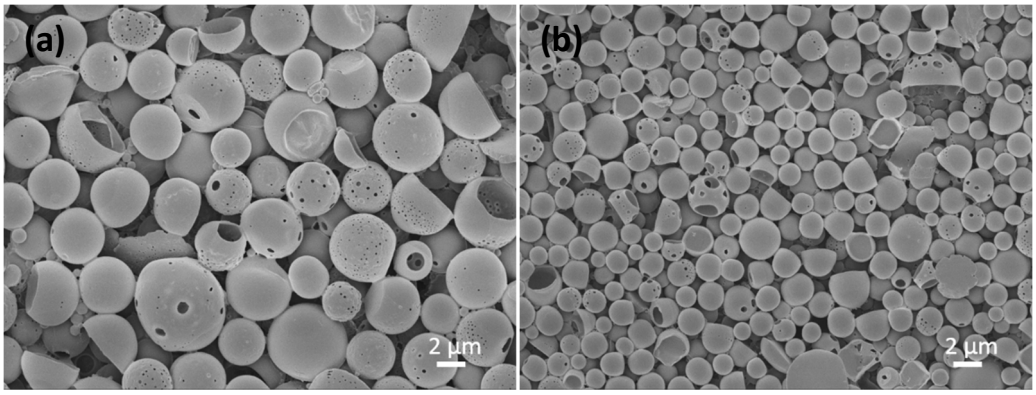

Figure 3. 27 SEM of porous PLA-PS particles of 30% PLA (a) and 70% PLA (b).

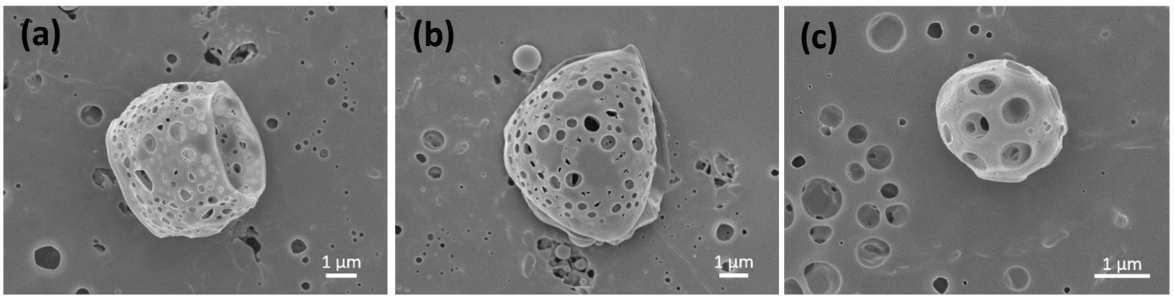

Figure 3. 28 SEM of one-step porous PLA-PS particles by toluene, 70% PLA.

3.4.4 Effect of diffusion rate and diffusion media temperature

Solvent-evaporation method is another type of solvent-removal process compared with solvent-diffusion. An emulsion-solvent evaporation (in air) experiment was carried out under the optical microscope. Figure 3.29 shows the images of droplet taken at different time points. As observed, a W/O/W droplet was formed and last from the beginning to 16 s. From 24 s, one spherical part started to separate out from the droplet and eventually formed a Janus particle in 80 s. The phase separation process was relatively slow compared to the emulsion-diffusion method since there was no dramatic temperature drop that would affect the solubility of PS in ethyl acetate. Therefore, it gave enough time for PLA and PS to separate to two parts.

In order to confirm the temperature drop fastened the solubility change of PS and thus fastened the phase separation process. A high-temperature diffusion water (50 ºC) was used to

induce the solvent removal as shown in Figure 3.30. As observed, the compartments within the particles are much larger, and even separated to two connected hemisphere particles. Therefore, the slower of the phase separation rate, the bigger the PS compartments can grow.

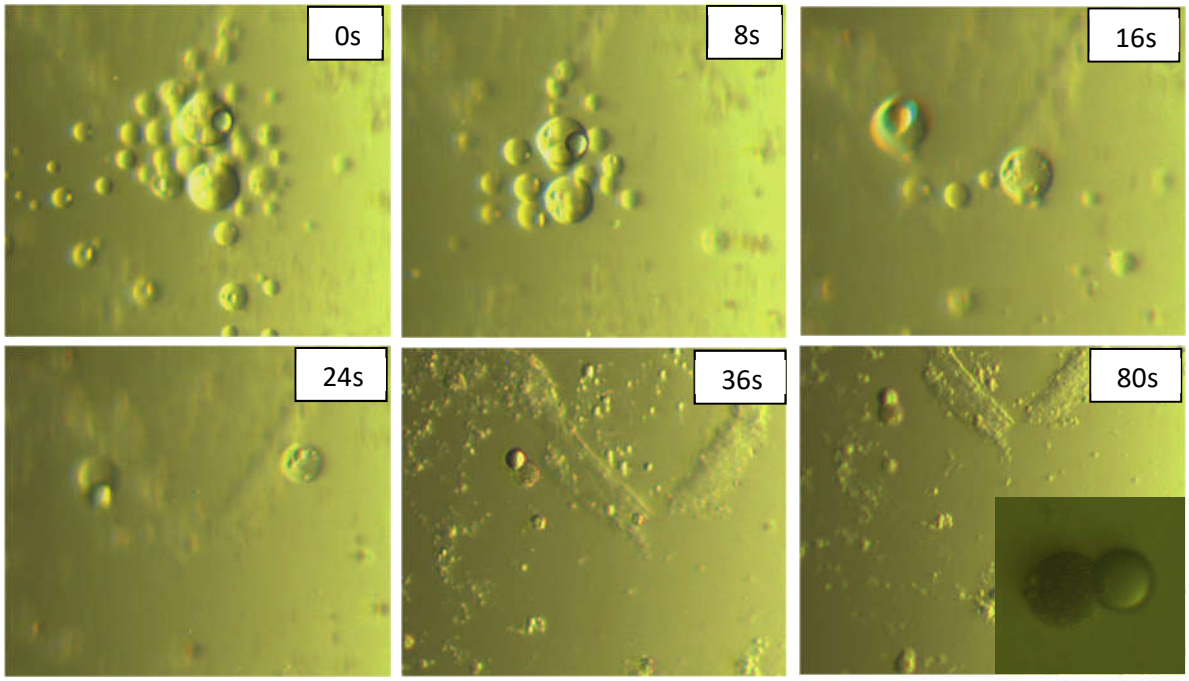

Figure 3. 29 Optical microscope images of an emulsion droplet transformation along time without the diffusion process.

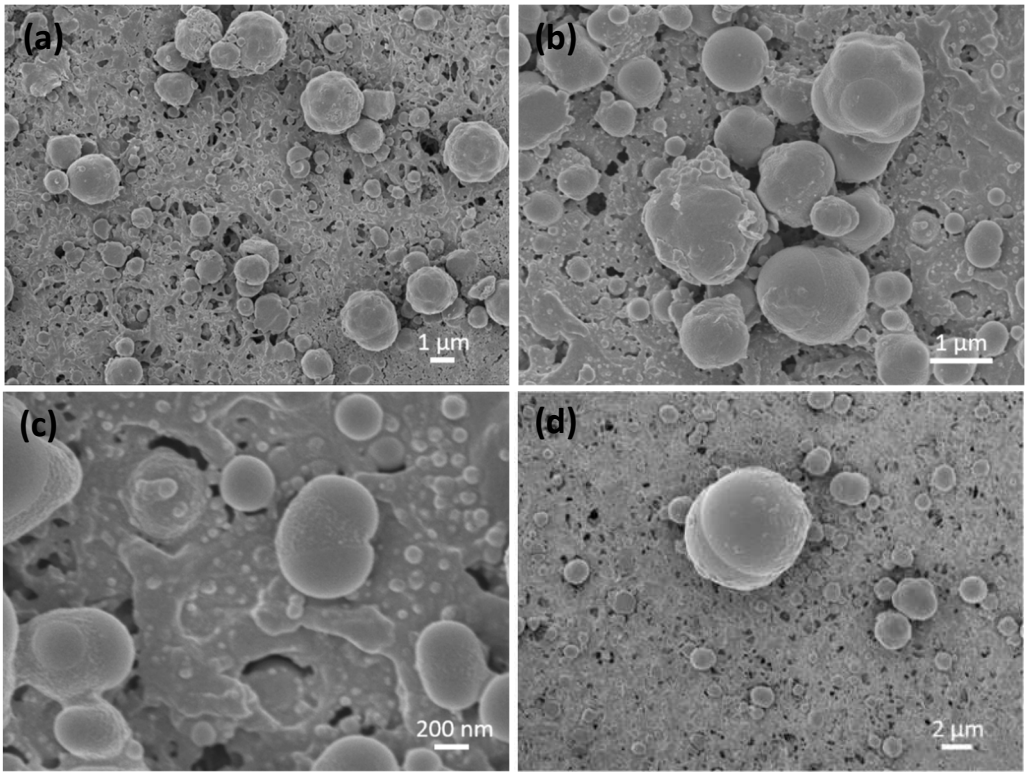

Figure 3. 30 SEM of PLA-PS microparticles prepared with 50 ºC diffusion water

3.4.5 Effect of emulsification temperature

As discussed in Chapter 2, the emulsification temperature is a key factor in designing the size of the polymer particles prepared by the one-step double emulsion method developed in our group. Figure 3.31 shows the PLA-PS particles prepared under different emulsification temperature. As shown in Figure 3.31 (b), nanospheres (200 nm) were obtained under room temperature emulsion.

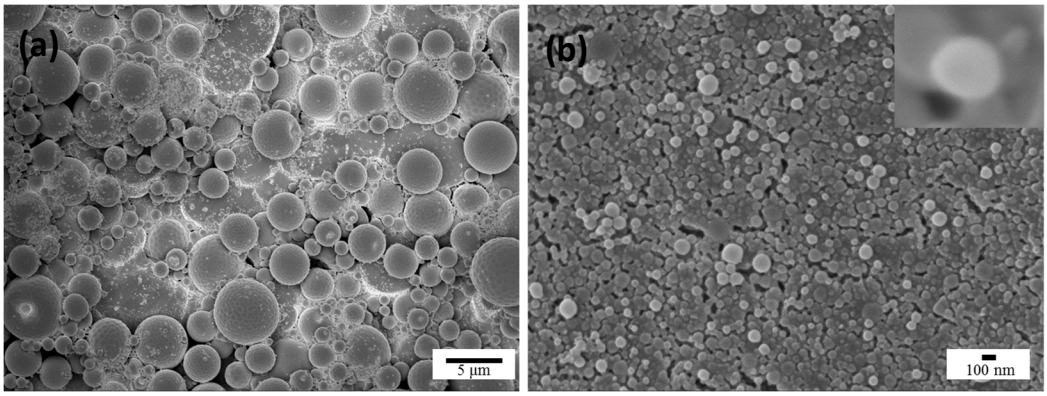

Figure 3. 31 PLA/PS (50:50) particles under different emulsion temperatures. (a) 60℃; (b) 25℃.

3.4.6 PLA-PCL composite microparticles

In order to test if the multicompartment structure is unique for the PLA and PS blend, PLA and PCL mixing solution was used instead of PLA and PS. Figure 3.32 shows the PLA-PCL (1:1) microparticles with a Janus particle morphology. As observed, the particle size of pure PCL particles is slightly larger than that of PLA-PCL Janus particles. The surface of the PCL half is rough with lines and small pebble.

Figure 3.33 shows the SEM results of PCL and PLA-PCL nanoparticles prepared under the room temperature. While pure PCL formed mostly spherical shape nanoparticles, the particle shape of PLA-PCL is non-spherical, which suggests the possibility of well-mixed PLA-PCL nanoparticles.

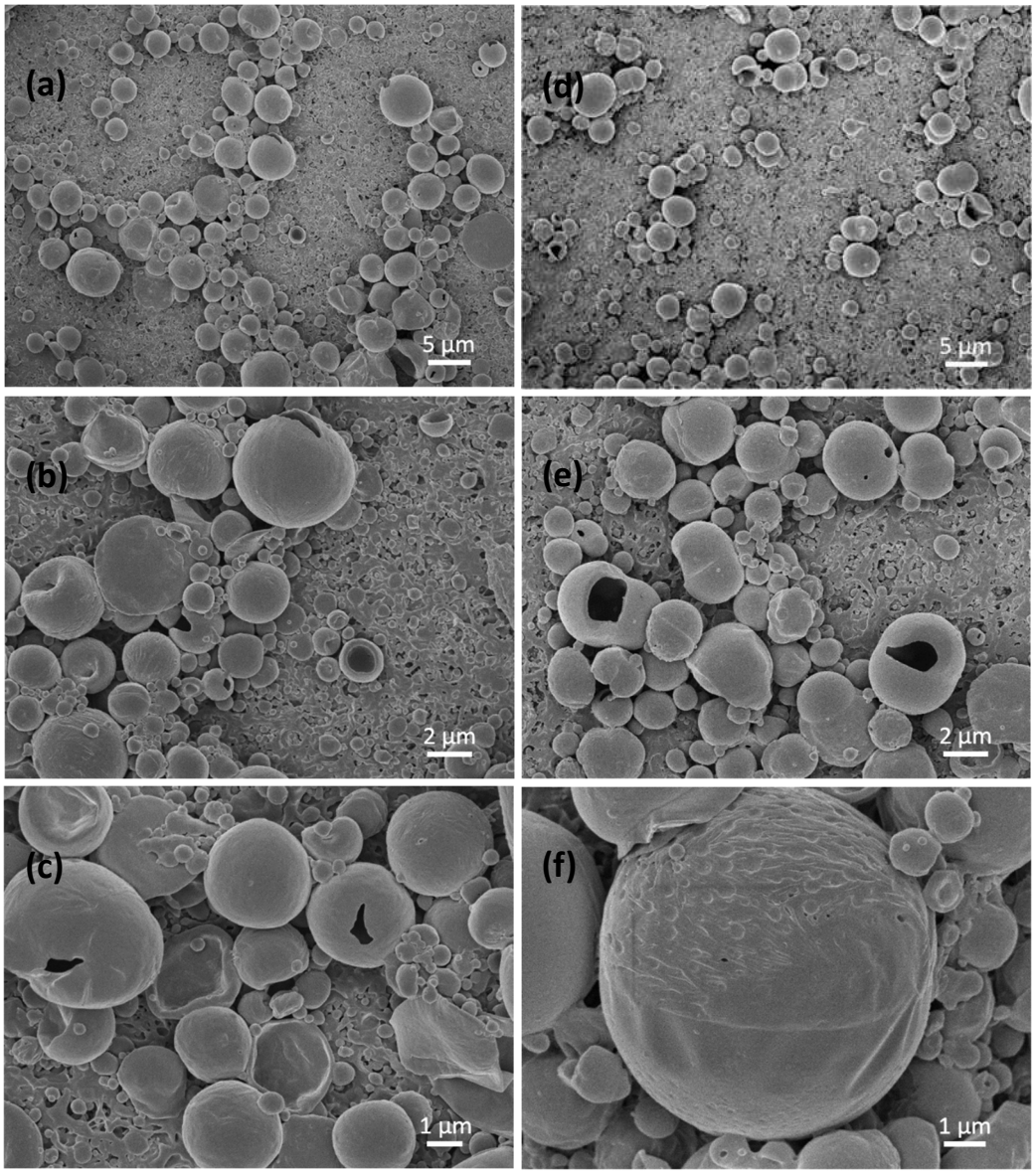

Figure 3. 32 SEM of PCL microparticles (a-c) and PLA-PCL microparticles (d-f) prepared under 60 ºC emulsification.

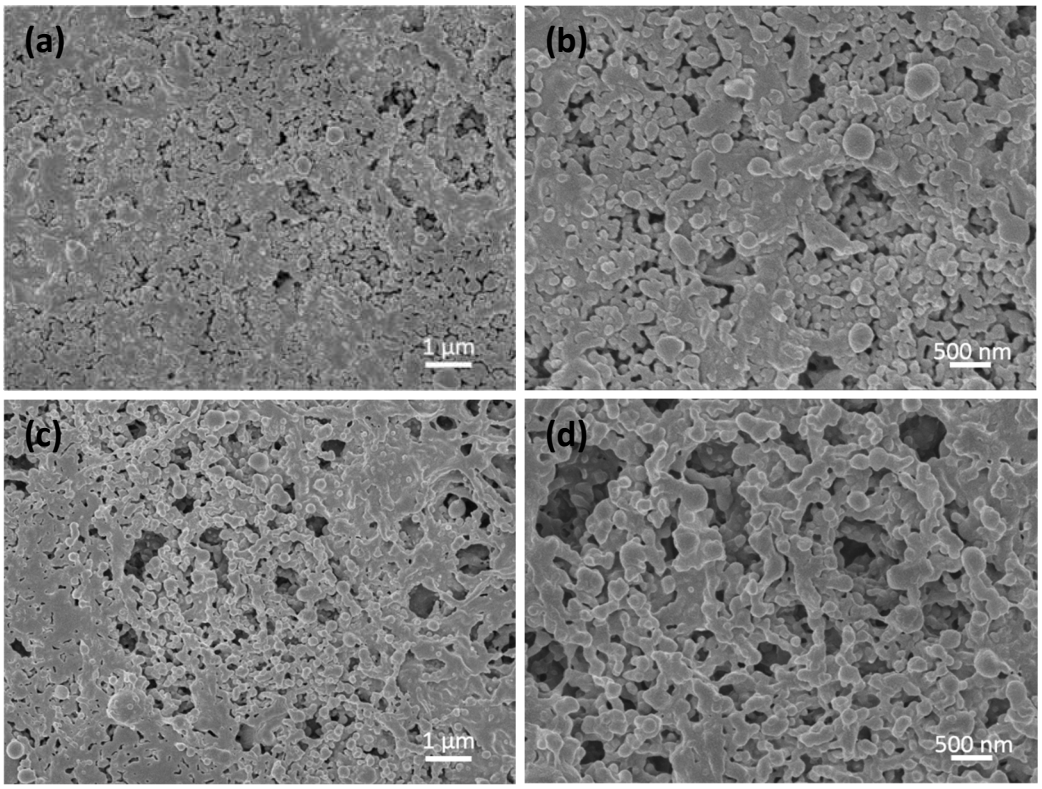

Figure 3. 33 SEM of PCL (a-b) and PLA-PCL (c-d) nanoparticles prepared under 25 ºC emulsification.

3.4.7 Release and Encapsulation behavior of PLA-PS multicompartment particles

Diclofenac (DCF) was used to test the release behavior of the novel PLA-PS multicompart particles. As shown in Figure 3.34, the initial release rate of PLA-PS particles was lower than that of the PLA particles, which was possibly caused by the slower degradation rate of PS (the effect of the composition). In addition, PLA-PS particles demonstrated two changes of release rate while PLA particles only had one. This is related to the structure of the PLA-PS particles.

Iron oxide nanoparticles (IONPs) were used to illustrate the encapsulation behavior of PLA-PS particles as shown in Figure 3.35. It is obvious that the IONPs distributed all over the particle surface without selection on PLA or PS. In addition, it is worthy of notice that the PS protrusion

became more uniform and flat after the addition of IONPs, which could be due to the effect of Pickering emulsion.

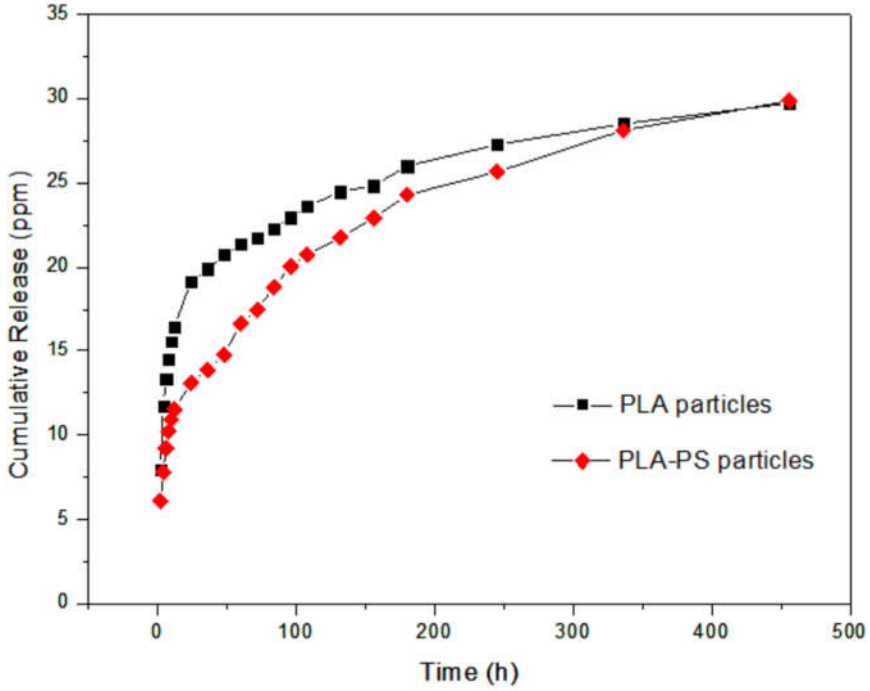

Figure 3. 34 Cumulative release profile of DCF from pure PLA and PLA-PS particles.

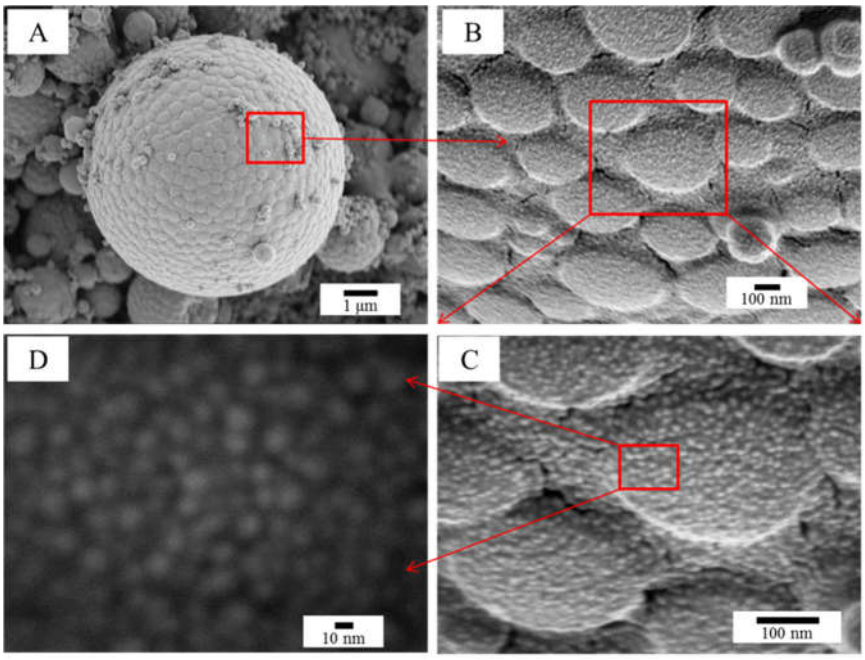

Figure 3. 35 SEM of hydrophilic IONPs encapsulated PLA-PS multicompartment microparticles.

3.5 CONCLUSIONS

In this study, a novel PLA-PS bioblend multicompartment hollow microparticles have been successfully developed via a one-step double emulsion method combined with solvent-induced phase separation. The overall microparticle size decreased with increasing amount of PS while the relative size of PS protrusion particle increased along with increasing PS. The TGA result suggests that there is good compatibility between PLA and PS, which is unusual for these two immiscible polymers. By selective solvent extraction process, cage-like porous PLA microparticles were obtained afterward.

The driven forces for this unique multicompartmental structure are the dramatic change of the solubility of PS in EA, the rapid solvent removal rate from the diffusion process, and the existence of the outer water phase. When replacing EA with toluene, which is a good solvent for PS at room temperature, Janus open-hollow microparticles (50% PLA), as well as half-porous microparticles (30% or 70% PLA), were obtained. When using solvent-evaporation (atmosphere condition) instead of solvent-diffusion, Janus droplets were observed under the optical microscope.

The PLA-PCL composite microparticles were also prepared to study if the multicompartment structure is unique for the PLA-PS blend. The resulting PLA-PCL (50:50) microparticles showed a Janus (two connected hemisphere) shape with linear texture on the PCL surface, which illustrates that the existence of PS is the key in forming the uniform multicompartment structure.

The release profile shows that PLA-PS microparticles had a slower initial burst release and two release rate changes. The encapsulation of IONPs was distributed uniformly within the PLA-PS particles. Therefore, both of the particle compositions and structure affect the release behavior while their effect on the encapsulation behavior is not that obvious.

4 POLY(LACTIC ACID)-NANOCLAY COMPOSITE MICRO-/NANO-PARTICLE FORMULATIONS FOR DRUG DELIVERY

4.1 MOTIVATION

Biodegradable polymer particulate drug delivery systems are often employed by pharmaceutical industry for protecting drug molecules from the chemical and enzymatic reactions (especially proteins, peptides and nucleic acids), targeting to the diseased organ/tissue, enhancing aqueous solubility of hydrophobic drugs, and delaying and extending the release of drugs [1, 138, 139]. However, some issues still exist including 1) initial burst release caused by polymer swelling, 2) non-bacteria inflammation caused by the acid degradation production of polymers, 3) low hydrophilicity and bioavailability of polymers, 4) low mechanical properties.

Recently, natural inorganic materials have attracted more and more attention due to their abundant natural resources and good biocompatibility [140-142]. Among these, clay minerals have been widely used as excipients in the pharmaceutical industry for a long history (Table 4.1) [143]. Not only as excipients, some of the natural clays are also considered medical clay (Table 4.2) [144]. Calcium montmorillonite has been widely used in the treatment of pain, open wounds, diarrhea, stomach ulcers, colitis, hemorrhoids, intestinal problems, acne, anemia and so on [145]. Due to their layered structure and high aspect ratio (1000:1) [145], nanoclays have shown strong antibacterial effect through physically absorbing bacteria [146, 147]. Besides, nanoclays can reduce the side effects caused by formulated drug [148]. For example, basic nanoclays can reduce the non-bacterial inflammation caused by FDA approved biodegradable polymers like poly(lactic acid) (PLA) and poly(lactic-co-glycolic acid) (PLGA) by neutralizing their acid degradation

products. Furthermore, the addition of nanoclay has been proved that can improve the mechanical property of polymers as well as the rheology properties [149, 150]. Currently, clay minerals have already been used for controlled release of drugs for both extended release and targeting release (Table 4.3).

Table 4. 1 Inactive clay/clay mineral ingredients in pharmaceutical dosage forms. Reproduced with permission from [151].

Inactive clay/clay mineral ingredients in pharmaceutical dosage forms (FDA, 2009).

Clay/clay mineral (USA pharmacopoeial name)	Route of administration	Dosage form
Talc	Oral	Solid (conventional and modified release capsules and tablets, chewable tablets, and granules) Liquid (drops, mucilage, solutions, elixir, suspensions, and syrup)
	Buccal	Chewing gums and tablets
	Sublingual	Tablets
	Topical	Lotions, ointments, and powders
	Rectal	Tablets
Activated Attapulgite	Oral	Powder
Bentonite	Oral	Solid (capsules and tablets) Liquid (suspensions)
	Topical	Lotions, powders, and suspensions
	Transdermal	Films and patches
	Rectal	Suspensions
	Vaginal	Ovules
Magnesium Aluminum Silicate (MAS)	Oral	Solid (conventional and modified tablets, granules, capsules, chewable tablets, and powders) Liquid (drops, suspensions, and syrups)
	Topical	Emulsions, creams, lotions, and suspensions
	Rectal	Suspensions
	Vaginal	Ointments
Magnesium trisilicate*	Oral	Conventional, modified and chewable tablets
Kaolin	Oral	Solid (conventional and modified tablets and capsules, powders) Liquid (syrups)
	Topical	Controlled release films

* Magnesium trisilicate is the pharmaceutical denomination of sepiolite.

Table 4. 2 Therapeutic uses of clays/clay minerals. Reproduced with permission from [151].

Clay/clay mineral (pharmaceutical names)	Kaolin	Bentonite and MAS	Talc	Attapulgite and magnesium Trisilicate*
Therapeutic use	Antidiarrhoeal Gastrointestinal protector Anti-inflammatory Antacid Homeopathic product	Antidiarrhoeal Gastrointestinal protector Antipruritic Antacid	Anti-haemorrhoids Anti-rubbing Pleurodesis	Antidiarrhoeal Antacid

* Magnesium trisilicate is the pharmaceutical denomination of sepiolite.

Table 4. 3 Controlled release systems based on clay minerals. Reproduced with permission from [150].

Delivery system	Function	Clay mineral
Extended release systems	Clay–drug interaction	Natural clays (smectites and fibrous silicates) Synthetic clays (Laponite, LDH, hidrotalcites) Acid/thermal activated clays (smectites and kaolinite) Pillared layered structures from smectites
	Clay swelling	Swelling clays (smectites)
Site specific systems	Enteric coated	Montmorillonite and anionic 'clays' (oral release)
	Bioadhesion	Smectite and halloysite (local release)
	Micro- and Nanoparticles	Porous hollow particles from halloysite

Therefore, developing a novel particulate delivery system of nanoclay-biodegradable polymer composites become essential to combine the benefits of these two types of materials and thus trigger a synergetic effect. Feng et al. developed a series of MMT/biodegradable polymeric nanoparticle formulations for controlled delivery of anticancer drugs via an emulsion-solvent evaporation method [148, 152, 153]. Their study shows that the PLA/MMT nanoparticle formulation reduced the side effects of docetaxel drug compared with the commercial Taxotere® by achieving ~26 times longer half-life as well as ~4 fold more effective [148]. In another study of paclitaxel drug, the addition of MMT into PLGA nanoparticles increased the cellular uptake (Caco-2 and HT-29 cells) of nanoparticles [153]. However, there are several limitations in this method for further drug carrier modification and application extension. First, the composite of polymers and MMT stays at the macroscopic level but not the microscopic level. PLGA nanoparticles dispersed in the bulk MMT matrix. No mix between individual PLGA nanoparticle and MMT could be observed. Second, only natural MMT, which is hydrophilic, was used and added to the water phase of emulsion while polymer was dissolved in the organic phase. Thus, the affiliation between the polymer and MMT is not strong. Finally, due to the type of emulsion they used, which is called oil-in-water emulsion (O/W), this method is limited to the encapsulation of hydrophobic drugs.

In this study, various types of nanoclays, including organically modified nanoclays, were used to prepare PLA/nanoclay composite microparticles with a high speed, shear force Nanomixer, which could result in better affiliation between polymer and nanoclay. The water-in-oil-in-water (W/O/W) emulsion process employed in our method lead to the flexibility of encapsulating either hydrophilic or hydrophobic drug. A model drug-nanoclay interaction was also investigated by encapsulation efficiency and release behavior.

4.2 INTRODUCTION

4.2.1 Properties of nanoclays

Nanoclays are naturally occurring inorganic layered silicate minerals with a high aspect ratio and with at least one dimension of the particle in the nanometer range [145]. Nanoclays are widely used in various applications including heavy metals and dust gas sorbent [154, 155], reinforced polymer composite [156], thermal resistance and fire-resistance, drug delivery [145, 148-151]. Based on chemical composition and structure, nanoclays are categorized as montmorillonite, bentonite, kaolinite, hectorite, and halloysite. Organically-modified nanoclays are also developed to make polymer composites [145].

4.2.1.1 Montmorillonite (MMT)

Montmorillonite (MMT) is a natural hydrophilic nanoclay with abundant resources. The chemical formulation of MMT is $(Na, Ca)_{0.33}(Al, Mg)_2(Si_4O_{10})$, resulting in a negative net charge of clay particles. As shown in Figure 4.1, MMT has two tetrahedral sheets of silica sandwiching a central octahedral sheet of alumina [157]. In the stacking of the silica-alumina-silica units, the bond between each unit is very weak, resulting in an excellent cleavage between the units. The advantage of this structure feature is that the MMT can incorporate water and other polar molecules enter between the layers. Thus, MMT shows a good absorbent and swelling capacity when exposed to water. In MMT, the adsorption can occur both at the edge sites and the internal sites. In addition, it has a very high cation exchange capacity (CEC, ~0.7 meq/g) [158]. Due to the negative charge, cation exchange of MMT is fast. Cations like Na^+ and Ca^{2+} lead to outer-sphere surface complexes, which is known as the Na^+ MMT and Ca^{2+} MMT, respectively [157].

4.2.1.2 Kaolinite

Kaolinite ($Al_2Si_2O_5(OH)_4$) is another commonly used nanoclay with a 1:1 layer structure of a tetrahedral silica sheet of SiO_4 and an octahedral alumina (Al^{3+}) sheet. Theoretically, kaolinite has zero net layer charge due to no substitution of Al^{3+} with other cations (e.g., Mg^{2+}, Zn^{2+}, Ca^{2+}, Na^{+}, K^{+}) and thus is the least reactive clay. In nature, kaolinite has a minor net negative charge arising from broken edges of the clay crystals [157]. Compared to MMT, kaolinite has a low cation-exchange capacity (CEC, ~0.035 meq/g) and a low shrink-swell capacity [158]. The CEC of kaolinite highly depends on the pH of the environment [157].

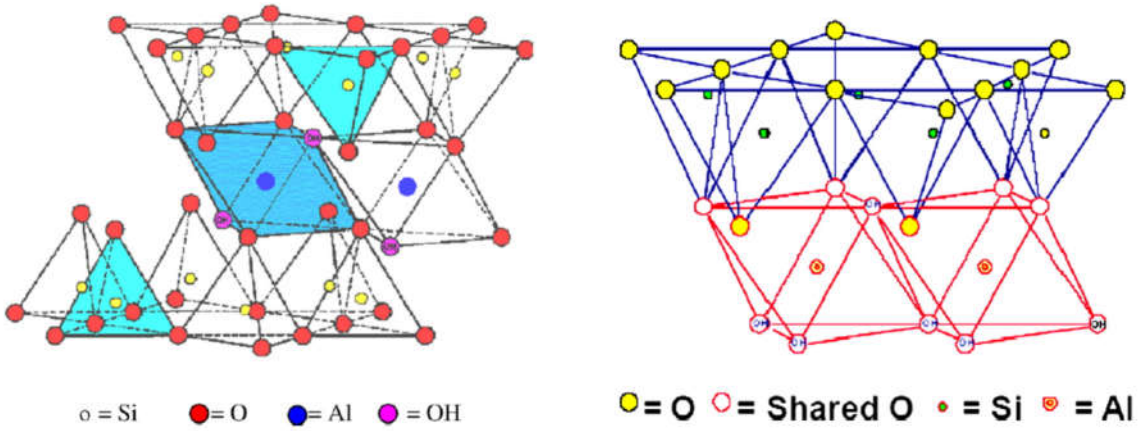

Figure 4. 1 Structure of Montmorillonite (left) and Kaolinite (right). Reproduced with permission from [157].

4.2.1.3 Organically-modified nanoclays

Organically-modified nanoclays, also called organo-nanoclay, are a class of hydrophobic nanoclays modified with organic molecules in order to improve the affinity between nanoclays and hydrophobic polymers [159]. As shown in Figure 4.2, an organophilic surface and interlayer are realized by replacing the naturally occurred inorganic cation exchange with various organic cations such as long chain alkylammonium ions [159-161]. The penetration of organic molecules into the interlayer space is called intercalation which results in swelling the clay galleries [159].

MMT is the most commonly used nanoclays to produce organo-nanoclays due to its high cation exchange capacity (CEC) and the 2:1 layered structure [161]. In addition, MMT has a high aspect ratio that can lead to better reinforcement effect. Most importantly, MMT is so abundant in nature and very inexpensive. Therefore, organo-nanoclays have a great potential in a wide range of applications such as polymer nanocomposites, the rheological modifier in inks, paints, and cosmetics, and drug delivery carriers [162].

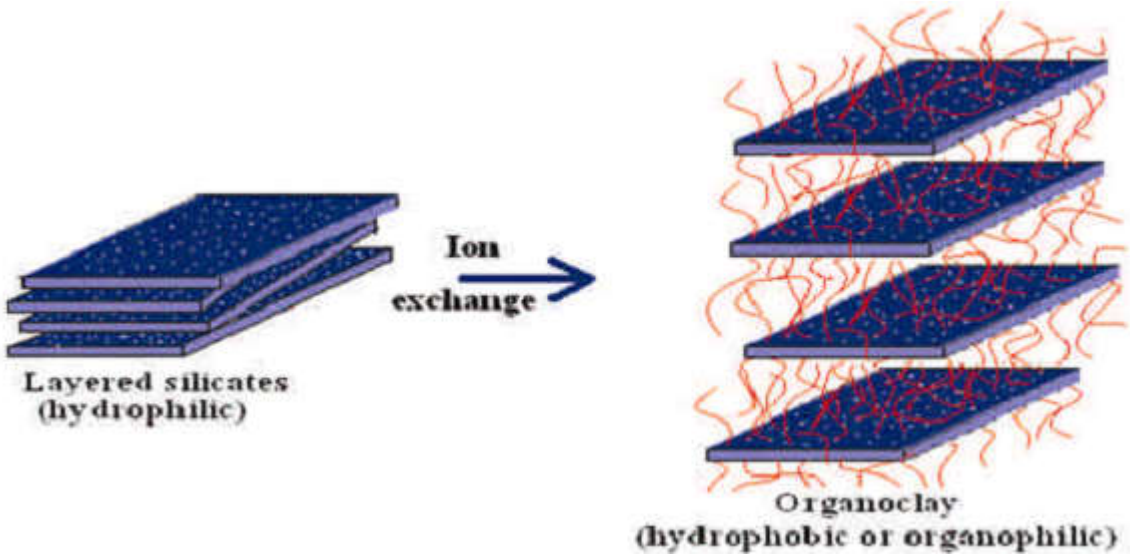

Figure 4. 2 Schematic of generation of organo-nanoclay via ion-exchange reaction. Reproduced with permission from [159].

4.2.2 Nanoclay-drug interaction

The interaction between nanoclay and drug molecules is one of the most important factors for drug loading efficiency and release behavior [150]. Nanoclays are naturally occurred ion exchanger and may undergo ion exchange with drug molecules in the solution. Due to the high ion-exchange capacity, MMT has been more commonly studied than other pharmaceutical clays such as kaolin. Because the surface charge of MMT is negative, the loading of cationic drug molecules is favorable compared to anionic and non-ionic drugs as shown in Figure 4.3. Anionic and non-ionic drugs

exhibit much weaker bonds and more rapid desorption compared with cationic compounds. Other than ionic interaction, there are several mechanisms that may exist between clay and organic molecules including hydrophobic interaction, hydrogen bonding, protonation, ligand exchange, pH dependent charge sites [145]. The layered structure can also lead to drug-intercalated nanoclay complex as the drug carrier [159].

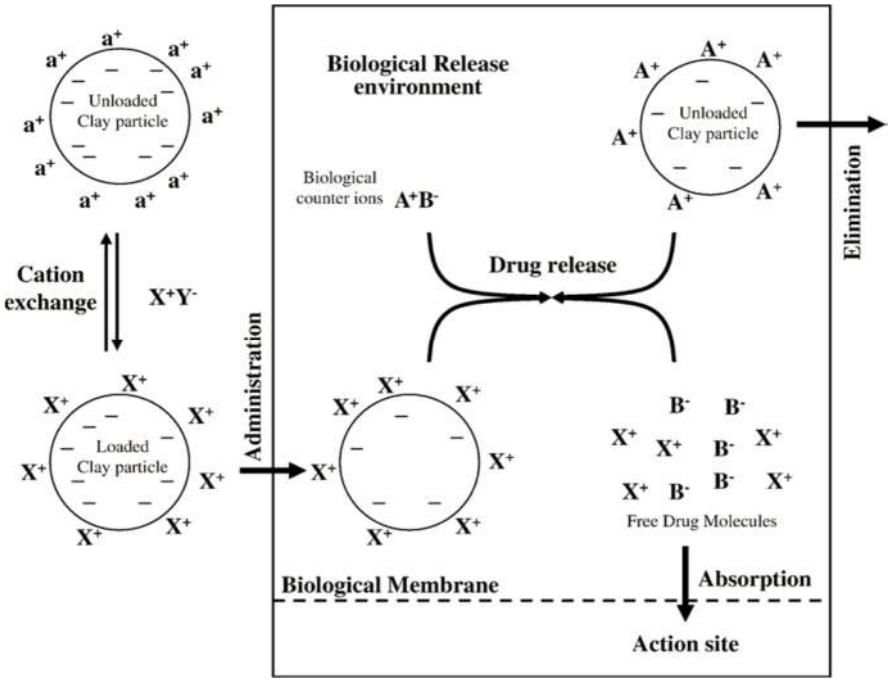

Figure 4. 3 Schematic mechanism of nanoclay-drug complexation and *in vivo* drug release. a^+ (compensating cations); X^+(cationic drug). Reproduced with permission from [145].

4.2.3 Polymer-nanoclay composites

Polymer-nanoclay nanocomposites have attracted great attention because they demonstrate remarkable property enhancement such as improved mechanical strength, reduced gaseous permeability, increased thermal stability and flame retardance, and decreased solvent uptake with a very low amount of clay content (3-6 wt%) [150, 159]. Due to the hydrophilicity of most natural nanoclays, organo-nanoclay, natural nanoclay modified with alkylammonium, is often applied as

fillers for polymer composites. The function groups of organo-nanoclay can improve the strength of the interface between polymer and fillers [159].

Based on the composition arrangement, polymer-nanoclay nanocomposites can be categorized as *Intercalated Nanocomposite* and *Exfoliated Nanocomposite*. As illustrated in Figure 4.4, the former one refers to composites that polymer chains are sandwiched in between the nanoclay layers; the latter one is that nanoclay layers are uniformly dispersed and exfoliated in the polymer matrix [150, 159, 163]. To determine the structure of polymer-nanoclay composite, wide angle X-ray diffraction (WXRD) and transmission electron microscopy (TEM) can be used. WXRD is the most commonly used method because of its easiness and availability. In an exfoliated nanocomposite, the disappearance of any coherent X-ray diffraction can be observed, resulting from the delamination of the original silicate layers and the extensive layer separation. While for intercalated nanocomposite, the layer expansion caused by polymer intercalation results in a new basal reflection peak [159, 164].

There are mainly three methods to prepare polymer-nanoclay nanocomposites: *in situ polymerization*, *solution-induced intercalation*, and *melt intercalation*. In *in situ* polymerization method, the layered nanoclay is swollen in the monomer solution or liquid monomer such that polymer can form between the nanoclay sheets. The solution-induced intercalation is based on a solvent system in which polymer dissolve and nanoclay disperse in the solvent. When the polymer chains spread into silicate sheet, the removal of the solvent results in the solidification of polymer intercalated within nanoclay. The melt intercalation method involves a mixture of the polymer and nanoclay above the melting point of the polymer. This method is more compatible with the current industrial setup like extrusion and injection molding as well as allowing the use of polymers which are not suitable for the other two methods [164].

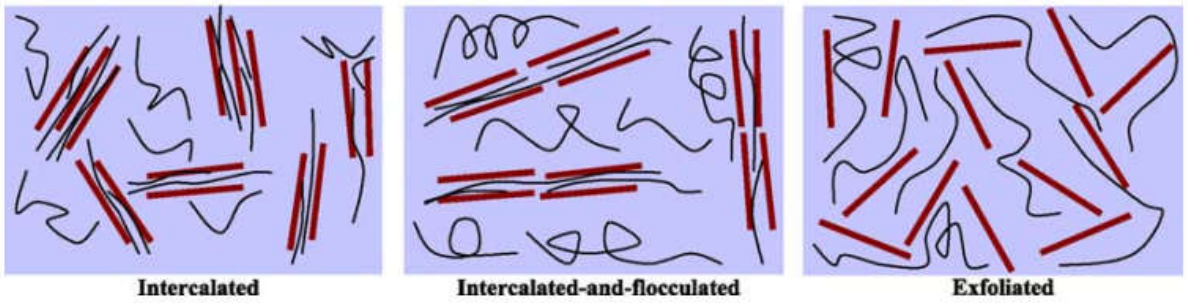

Figure 4. 4 Schematic of three types of polymer-nanoclay composite. Reproduced with permission from [164].

4.2.4 Biopolymer-nanoclay nanocomposites for pharmaceutical application

In pharmaceutical application, it is important to use therapeutic level of ingredients to realize the ideal controlled release of drugs such as site-specific release and extended release. Both nanoclays and biopolymers, including biodegradable synthetic polymers, have been widely used in the pharmaceutical products. Both of them show unique advantages as well as disadvantages.

On one hand, biopolymers have the benefits such as versatile dosage forms, stimulative target release and good biocompatibility and biodegradability. However, the mechanical property of biopolymers is not as good as that of inorganic materials like nanoclay. Drug vehicles must maintain suitable mechanical strength during the manufacturing process. For the pharmaceutical application, nanoclay is an ideal nanofiller for polymer because of its biological safe and low cost [150]. Initial burst release caused by swelling in the physiological condition is another common problem in biopolymer drug carriers. Research shows that the addition of nanoclay, especially the organo-nanoclay, can reduce the swelling behavior due to the barrier property of clay. With the increasing nanoclay/polymer ratio, the swelling ratio of polymer-nanoclay composite decreased [165, 166]. Incorporation of nanoclay can also change the rheological properties of polymers like increasing the polymer gel viscosity and tortuosity of the drug carrier matrix, resulting in slower drug diffusion through the polymer-nanoclay wall [167]. Other types of properties improvement

such as increased bioadhesion (adhesion of a polymer to a biological substance) [168]/cellular uptake [153], film coating [167] of drug pallet have been reported.

On the other hand, the addition of biopolymers can improve the properties of nanoclays as well. Dispersion stability is one of the important factors for drug carriers as it relates to absorption and bioavailability [150]. Clay dispersions are usually unstable under the physiological conditions due to the high salt concentration and the presence of polyelectrolytes, which leads to flocculation and precipitation [169, 170]. It is reported that a hybrid system of nanoclay and polyethylene glycol (PEG)/polyamine showed the increased stability of clay dispersion. The hypothesized mechanism behind is that the formation of non-ionic PEG layer on the clay surface provided a shielding of the negative charge of clay particles to reduce ionic interactions and thus enhanced the dispersion stability [170]. In addition, biopolymers can also improve the adsorption capacity of nanoclays on anionic and non-ionic drugs. An et al. reported that composite based on chitosan and montmorillonite showed higher anion exchange capacities than the clay alone [171]. Polyelectrolytic biopolymers have the potential for this purpose [150].

Several methods are available for loading drugs into polymer-nanoclay composites such as solution-based method, coating method, and built-in method. In the solution-based method, polymer-nanoclay composites are dispersed in aqueous drug solutions, allowing for some equilibrate time, and finally being the solid phase [165, 166, 171]. Coating method, as an example, is drug granule coated with a solution of polymer-nanoclay composite via a fluid bed equipment. Another example is to coat inert nanoparticles with a layer of drug and then a layer of composite [150]. The built-in method means that making the composite with the presence of drugs by mixing polymers matrix, clay particles and the active ingredient [149, 153, 172]. For example, Feng et al. utilized an emulsion-solvent evaporation method to prepare MMT-PLGA/PLA composite

nanoparticles with the hydrophobic anti-cancer drug dispersed into the oil phase before the emulsification process [148, 153].

4.3 EXPERIMENT

4.3.1 Materials

Poly(lactic acid) (PLA, MW=50,000) was purchased from Lakeshore Biomaterials, Evonik Industries. Nanoclays (Cloisite Ca++, Cloisite Na+, Cloisite 20, Cloisite 10A, Kaolin) were obtained from BYK Additives as samples. Pluronic F68 (PF68) was purchased from Sigma-Aldrich. Ethyl Acetate (EA) and glycerol were purchased from J.K. Baker. Nisin Z was purchased from Handary (Belgium). Diclofenac sodium salt (DCF) was purchased from Sigma-Aldrich. All the chemicals used are analytical level and without any further purification. Deionized (DI) water used in the whole process was supplied by a Barnstead NANOpure^{TM} Diamond-UV purification unit equipped with a UV source and final 0.2 μm filter at 18.2 MΩ purity. Nanomixer was purchased from the PRIMIX Corporation to mix two immiscible liquid phases. Filter papers (0.03 μm 0.1 μm, 0.45 μm) were purchased from EMD Millipore.

4.3.2 Preparation of PLA-Nanoclay composite particles

PLA (15 mg/ml) was dissolved in EA as the oil phase (O-phase) of the emulsion process. Water phase (W-phase) was prepared by dissolving PF68 (15 mg/ml) into a mixture of DI water and glycerol (1:1 v/v). Nanoclays were dispersed into O-phase or W-phase respectively based on the study. Hydrophobic nanoclays were dispersed into O-phase. Hydrophilic nanoclays were tried in both O-phase and W-phase. All the nanoclays were vacuum dried at 80 °C and stored in a desiccator. The volume ratio of O-phase to W-phase to make emulsions was 1:3, regardless of the addition of polymer, nanoclays, and PF68. Nanomixer was used as the homogenizer under a speed

of 12500 s^{-1} for 2 min with alternative temperatures. The temperature of mixing was controlled by a circulating cooling water system around the outer vessel wall of Nanomixer. The resulting emulsion was then poured into 90 ml of DI water under stirring (~220 rpm) in a flask to induce the diffusion of EA into the water and then the solidification of composite particles. The particles suspension was then stored in the freezer for future use.

4.3.3 Encapsulation of drug molecules into particles

Diclofenac and Nisin Z, both hydrophilic and water-soluble, were dissolved in the W-phase accordingly before the emulsion process. All the other procedures were the same as the particle preparation method (see section 4.2.2).

4.3.4 Characterizations of PLA-nanoclay composite particles

Scanning Electron Microscope (SEM) was used to observe the particles morphology. The particles suspension was filtered through a 0.1 μm pore size filter paper and washed with 10 times of DI water, after which was dried in a desiccator overnight. The sample loaded filter paper was sputter coated with platinum. SEM images were taken under 3kv electron accelerating voltage, ~4.5 mm working distance. Particle size distribution was then analyzed from SEM images using ImageJ with a minimum of 100 particles collected randomly.

The thermogravimetric analysis (TGA) was conducted by Mettler Toledo TGA/DSC 1 STAR^e system. The frozen sample was freeze-dried in order to get dry powder. About 10 mg of samples (freeze-dried samples and pure nanoclays) in the alumina crucible was heated from 50 to 670 °C at 20 °C/min under nitrogen flow (20 ml/min). The weight percentage of the sample was plotted against temperature to determine the nanoclay content.

4.3.5 Drug encapsulation efficiency

Encapsulation efficiency was obtained by measuring the amount of drug that was not encapsulated, with knowing the total amount of drug used. The concentration of DCF was measured by Mass Spectrometry. Nisin concentration was determined by a reverse phase HPLC system with a C-18 column. The column temperature is 30 °C. The flow rate is 1 ml/min. The mobile phases consisted of 0.05% (v/v) TFA/water (eluent A) and 0.05% (v/v) TFA/acetonitrile. The sample was eluted by 20% eluent B for 5 min, followed by a gradient elution for 20 min from 20% eluent B to 60% eluent B. The UV detector was set at 215 nm. The Nisin came out at 17-18 min.

4.3.6 In *vitro* drug release

5 or 10 mg of drug-loaded particles were suspended in 1 ml of 0.02 M phosphate buffer with 0.05 M NaCl (pH 4.5 or 6.8). The suspension was stirred and sonicated for 2 min and maintained at 37 °C in an incubator under shaking. At predetermined interval time spots, the suspension was centrifuged at 12,000 *g for 10 min. The 1 ml supernatant was withdrawn and 1 ml fresh butter was added for further release. The Nisin concentration was determined by HPLC as described above. The concentration of DCF was measured by UV-Vis at the peak of 276 nm.

4.4 RESULTS AND DISCUSSION

4.4.1 Hydrophobicity and alkalinity of nanoclays

As shown in Table 4.4, five types of nanoclays were selected to make PLA-nanoclay composite particles as drug delivery carrier. MMT-Na^{+} and MMT-Ca^{++} are natural montmorillonite clay. In this study, OMT represents MMT organically modified with amines as simplified. OMT-10A is designed as fillers for polar matrix while OMT-20 is more compatible with the nonpolar system.

Table 4. 4 Nanoclays used in this study

Type of Nanoclay	Hydrophobicity	Affinity with polymer
MMT-Na+	Hydrophilic	---
MMT-Ca++	Hydrophilic	---
OMT-10A	Hydrophobic	polar
OMT-20	Hydrophobic	non-polar
Kaolin	Hydrophilic /Hydrophobic	---

Figure 4.5 shows the dispersibility of different nanoclays in ethyl acetate (EA), which was the organic solvent used in the particle preparation process. The transparency of the suspension indicates that OMT-10A and Kaolin are the most stable in EA, followed by OMT-20, and then MMT Na^{+} and MMT Ca^{++}. Natural MMT is hydrophilic and thus not well dispersed in the organic solvent. OMT-10A is more stable in EA than OMT-20 since EA is a polar solvent [173]. It is worthy of notice that Kaolin has good dispersibility in both organic solvent and water.

Table 4. 5 pH values of Nanoclay aqueous suspension

Nanoclay	MMT-Na+			MMT-Ca++			OMT-20			OMT-10A			Kaolin		
Conc. (mg/ml)	0.5	1.0	2.0	0.5	1.0	2.0	0.5	1.0	2.0	0.5	1.0	2.0	0.5	1.0	2.0
pH	8.87	9.31	9.53	8.67	8.59	8.47	8.72	9.05	9.10	8.78	8.90	9.13	8.88	8.26	8.21

The alkalinity of nanoclays in aqueous solution was tested along different concentrations under continuous stirring condition. The results are demonstrated in Table 4.5 and Figure 4.6. MMT-Na^{+}, OMT-10A, and OMT-20 showed increased pH values with increasing concentration. Meanwhile, the other two nanoclays had an opposite trend when increased concentration. All the nanoclays are basic, which can be helpful to reduce the side effects caused by acid degradation products of PLA (lactic acid) [148].

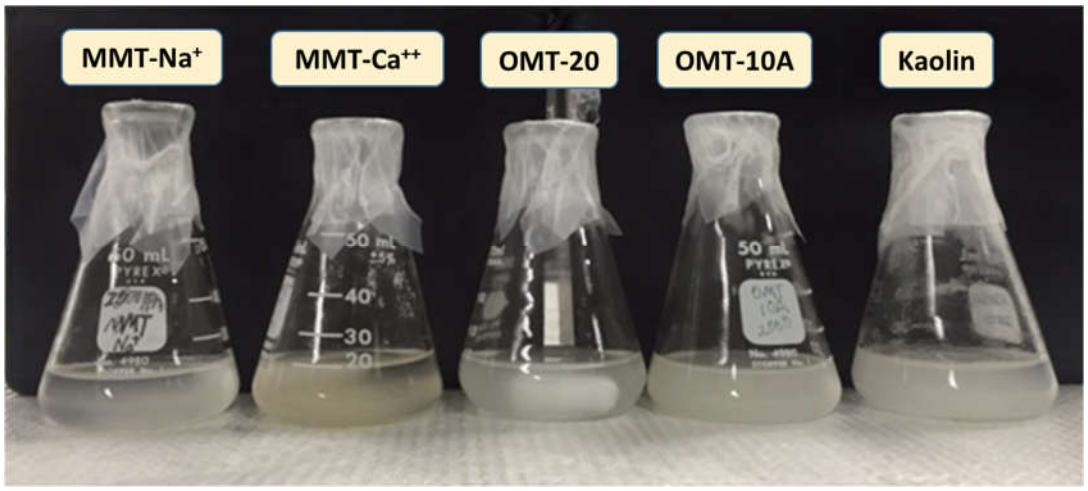

Figure 4. 5 Image of ethyl acetate suspensions of different nanoclays

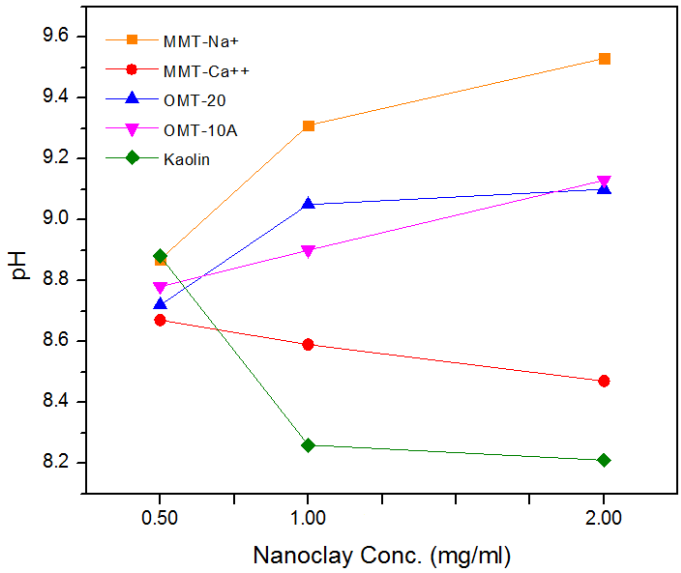

Figure 4. 6 pH of nanoclay aqueous suspensions vs. concentration

4.4.2 Morphology study of PLA-nanoclay composite particles

4.4.2.1 Effect of surfactant concentration

As discussed in the previous chapters, a unique W/O/W emulsion method was developed in our group based on an established protocol, in which the surfactant concentration was fixed at 15 mg/ml [174]. However, nanoclays are often used as stabilizers for emulsions [175, 176]. For example, OMT-20 (commercially known as Cloisite 20) was used to stabilize an inverse Pickering

emulsion polymerization without surfactant [175]. Therefore, adding nanoclay into the system will dis equilibrate the original interfacial balance of the emulsion. With the same amount of OMT-20 (16.7% wt%), the sample of the original surfactant concentration (15 mg/ml) showed solvent (Ophase) separated from the colloid after Nanomixer process (Figure 4.7 (a)) and subsequently formed big clusters in the particle suspension. On the other hand, the one with 10 times less surfactant (1.5 mg/ml) formed a uniform, stable emulsion (Figure 4.7 (b)). Figure 4.7 (c) and (d) are the SEM results of (a) and (b), respectively, filtered with the same volume of particle suspension. As observed, the particle concentration of sample (a) is much less than that of the sample (b), which was the consequence of forming particles aggregation clusters. In addition, open-hollow microparticles were formed in sample (a) while in sample (b) only spherical particles were observed. The higher surfactant concentration (15 mg/ml) led to a wider size distribution of particles. It was also noticed that the affiliation between PLA and OMT-20 in sample (a) was not as good as sample (b) since the existence of bulk clay-PLA clusters and less texture on particle surfaces in Figure 4.7 (c). In comparison, particles prepared with 10 times less surfactant (1.5 mg/ml) demonstrated a relatively even size distribution and successful mixing between PLA and OMT-20.

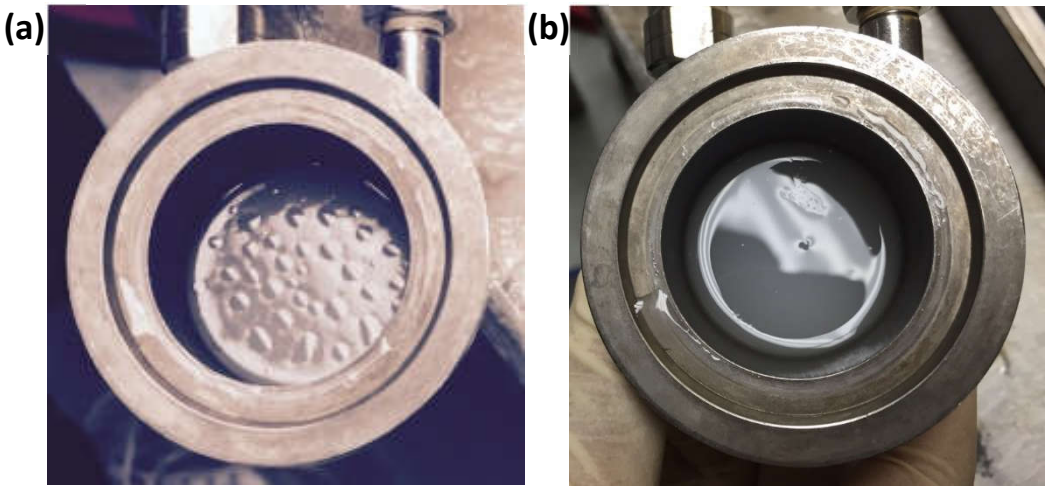

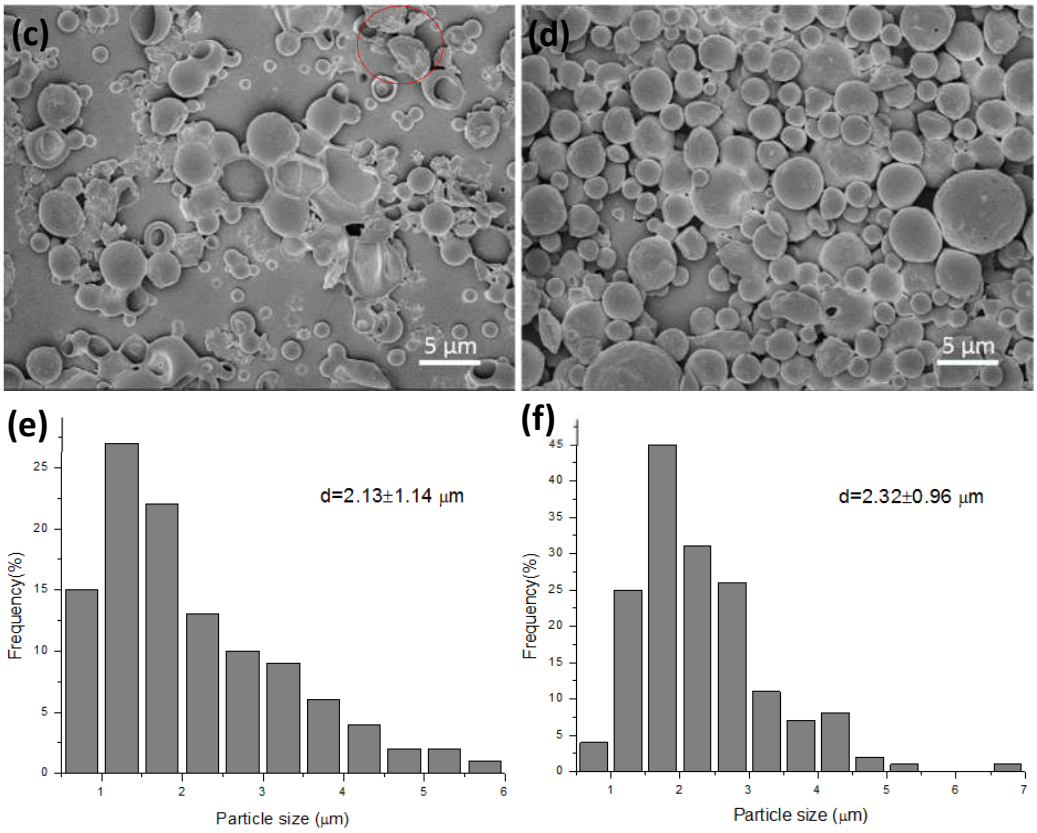

Figure 4. 7 PLA/OMT-20 (16.7% wt%) particles with different surfactant (PF68) concentration. (a, c, e): 15 mg/ml surfactant; (b, d, f): 1.5 mg/ml surfactant.

When switched to a lower OMT-20 weight ratio (6.25%), the same trend was observed regarding the size distribution, as shown in Figure 4.8. Higher concentration led to a wider size distribution (from 0.6 to 9 µm) compared to lower concentration sample as observed from Figure 4.8 (c-d). It is worth of noting that, in Figure 4.8 (c), 87% of particles fell into the 1-2 µm size range as a single peak while Figure 4.8 (d) showed a more spread-out distribution.

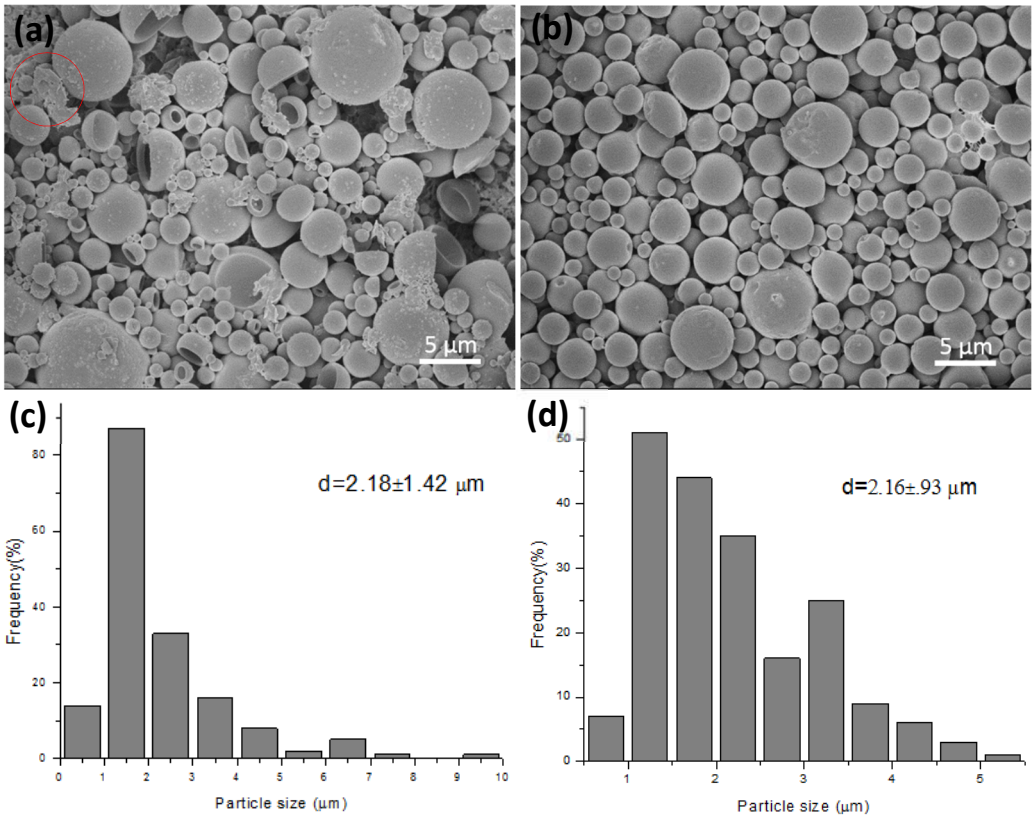

Figure 4. 8 PLA/OMT-20 (6.25% wt%) particles with different surfactant (PF68) concentrations. (a, c): 15 mg/ml surfactant; (b, d): 1.5 mg/ml surfactant.

The usage of synthesized surfactant in the preparation of biodegradable polymer particles has always been questioned due to the potential harmfulness and the compatibility issue inside the human body. In addition, synthesized surfactants have a higher cost than natural nanoclay. Therefore, making nanoclay/biodegradable polymer composite particles has the biocompatible and economic benefits. The addition of MMT can reduce the use of commercial surfactant and thus reduce the cost of such drug delivery particles, which is considered as one of the multifunctional effects of nanoclay.

4.4.2.2 Effect of nanoclay/PLA weight ratio

Figure 4.9 demonstrates the SEM results of different OMT-20/PLA ratio particles (6.67 wt%, 13.3 wt%, 20 wt%) under the same surfactant concentration condition (1.5 mg/ml) and the same magnification (*5,000). It is obvious that increasing the OMT-20 concentration did not change the bimodal size distribution pattern as well as the overall particle size, with a slightly increased particle size of 20 wt% sample. However, a higher concentration of OMT-20 changed the surface morphology and the particle shape. The rough texture on the particle surface indicates the successful entrapment of OMT-20 into PLA particles. In Figure 4.9 (c), some of the larger particles did not hold the spherical shape, possibly caused by the nanoclay coating around the spherical particles.

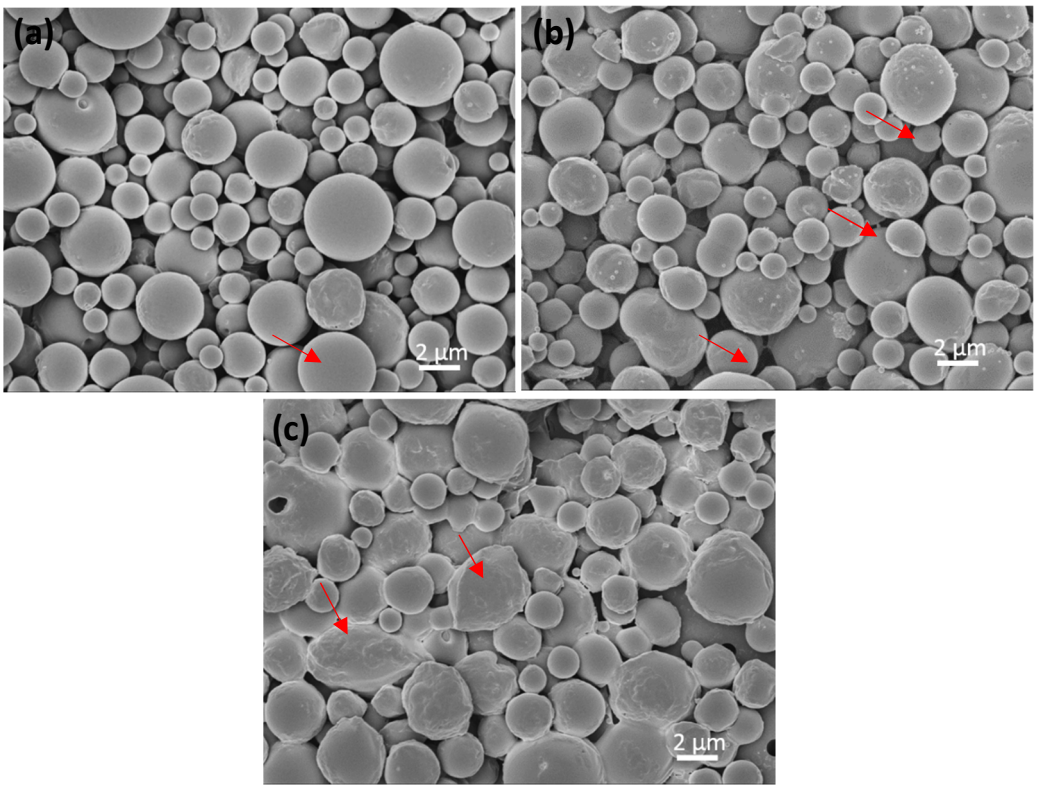

Figure 4. 9 SEM images of PLA/OMT-20 composite particles with different PLA/OMT ratios: (a) 6.67%; (b) 13.3%; (c) 20%. (Surfactant: 1.5 mg/ml)

In samples prepared with higher surfactant concentration (15 mg/ml, Figure 4.10), the increasing amount of OMT-20 did not change the overall particles morphology. As observed, increasing nanoclay resulted in decreased thickness of particle shell shown in the insets of Figure 4.10 ((a): 600 nm; (b): 90 nm), which looks opposite with the pattern in Figure 4.9. However, both can be explained by the same mechanism. Adding nanoclay changed the rheology of the fluid flow and then increased the droplet diameter. Therefore, with the same amount of PLA, when it comes to hollow particles, larger W/O/W droplets would form a thinner particle shell. The detailed mechanism behind this was described in the previous study [177].

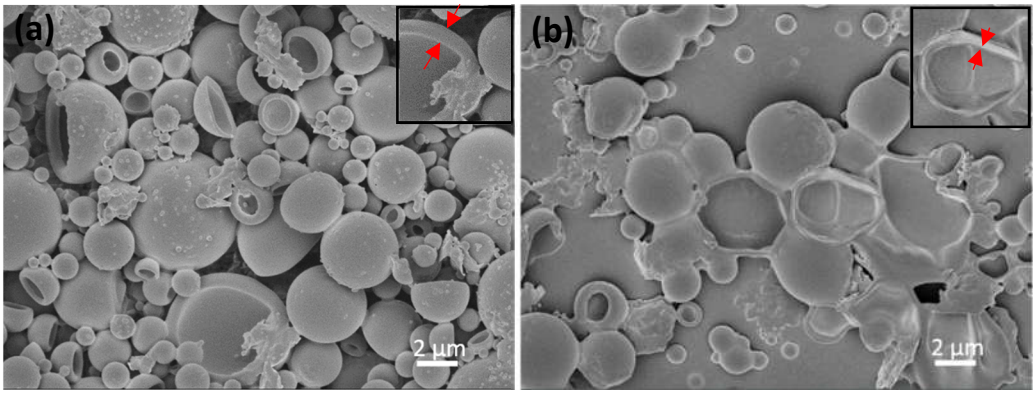

Figure 4. 10 SEM images of PLA/OMT-20 composite particles with different PLA/OMT ratios: (a) 6.67%, inset shows 600 nm in thickness; (b) 20%, inset shows 90 nm thickness. (Surfactant: 15 mg/ml)

4.4.2.3 Effect of emulsification duration

Figure 4.11 and 4.12 exhibit the morphology and size distribution of PLA/OMT-20 composite particles prepared with different emulsification duration time: 2 min, 3 min, 4 min, 6 min. As shown in Figure 4.11, from 2 min to 4 min, the mean particle size increased slightly with relatively narrow size distribution. This is opposite with the previous study on pure PLA particles that the particle size decreased along with longer emulsification time within a certain range. The possible

reason caused this might be the surfactant used in this batch of samples is 10 times less, reducing from 15 mg/ml to 1.5 mg/ml.

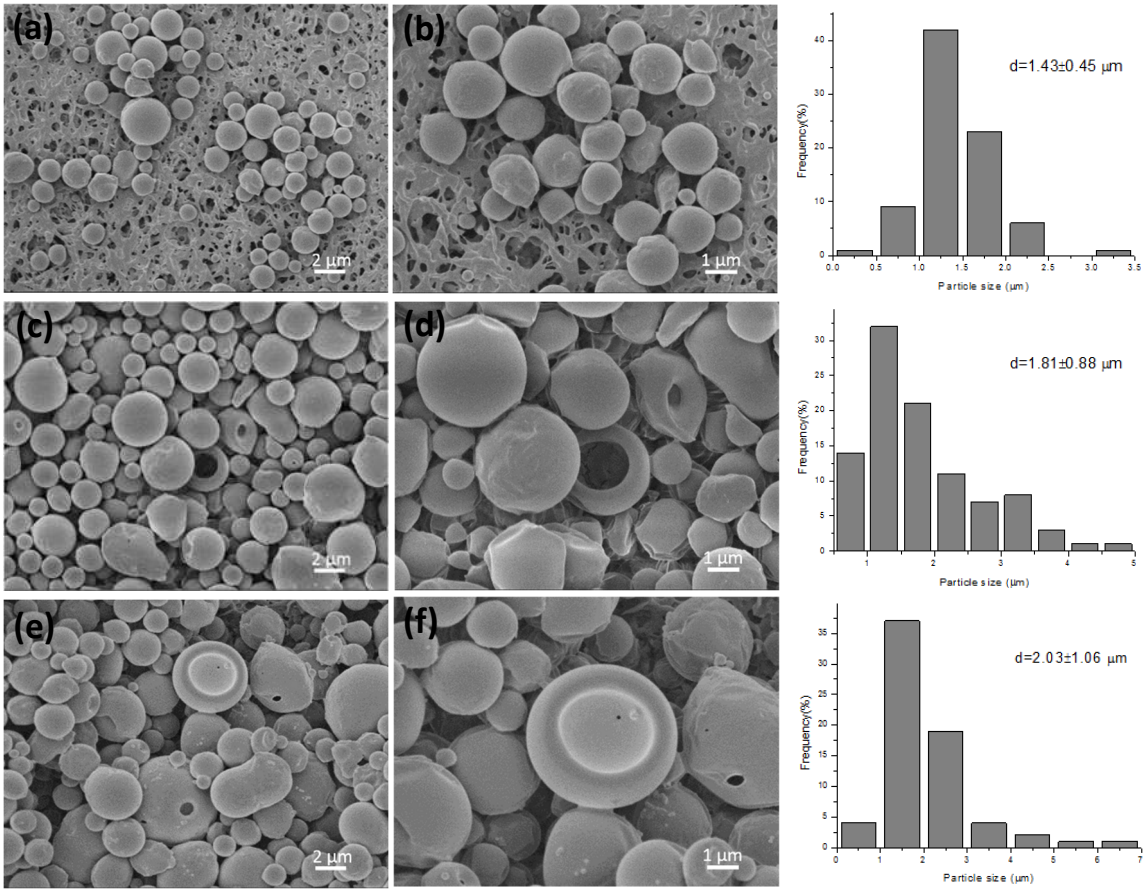

Figure 4. 11 SEM images of PLA/OMT-20 composite particles prepared with different emulsification duration: (a-b) 2 min, (c-d) 3 min, (e-f) 4 min. Right column is the corresponding particle size histogram.

When the emulsification extended to 6 min (Figure 4.12 (a-c)), the particle size distribution changed dramatically with the higher end at ~15 µm and the lower end at ~100 nm. For the 6 min sample, O-phase partially separated from emulsion after the emulsification process and formed big clusters in the particle suspension, which suggests the break of the emulsion equilibrium. Figure 4.12 (d-f) shows the sample prepared with 15 mg/ml surfactant with 6 min. As observed, this sample also showed a very wide distribution from ~8 µm to ~100 nm. Compared to sample made

with 1.5 mg/ml surfactant, the size of the larger particles is smaller because the surfactant can keep droplets from coalescing to the bigger droplet.

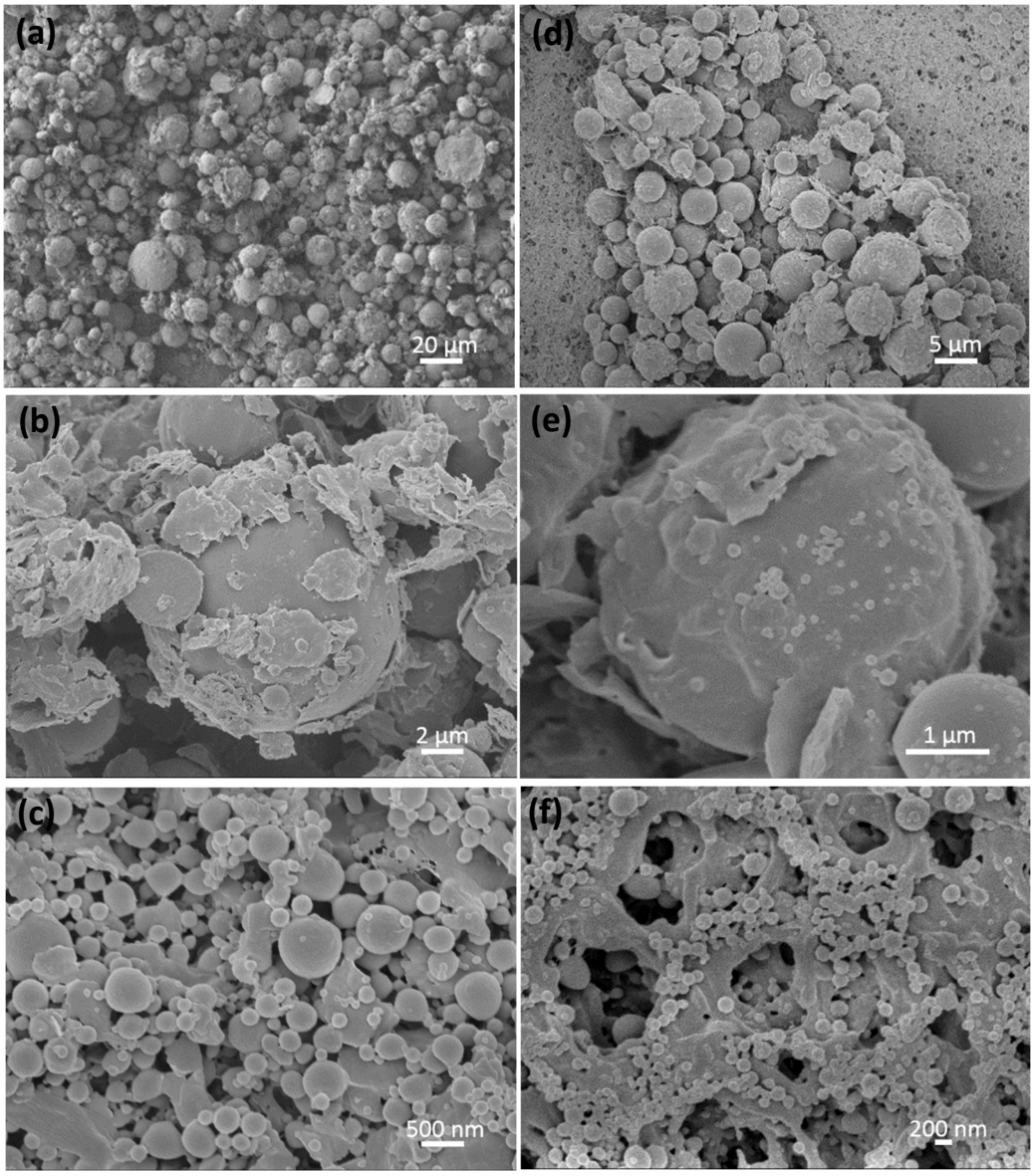

Figure 4. 12 SEM images of PLA/OMT-20 composite particles prepared by 6 min emulsification duration with different surfactant concentration: (a-c) 1.5 mg/ml, (d-f) 15 mg/ml.

4.4.2.4 Effect of glycerol

Adding glycerol to the water phase of the emulsion is a key step to enlarge the eddy size and thus form hollow microparticles of pure PLA. This is due to the relation between the viscosity and

turbulent eddy size [174, 177]. Since nanoclay can affect the fluid viscosity, Laponite was added into the water phase to study how glycerol affected on the particle morphology with the existence of Laponite. Figure 4.13 shows the SEM results of PLA particles prepared with Laponite (1 mg/ml) in the water phase. The 40% glycerol sample (Figure 4.13 (a-b)) showed larger particle size (~ 4 μm) compared to the one with 60% glycerol (~ 1.5 μm). However, without Laponite, adding 50% or more glycerol will lead to larger particles with a hollow structure [174].

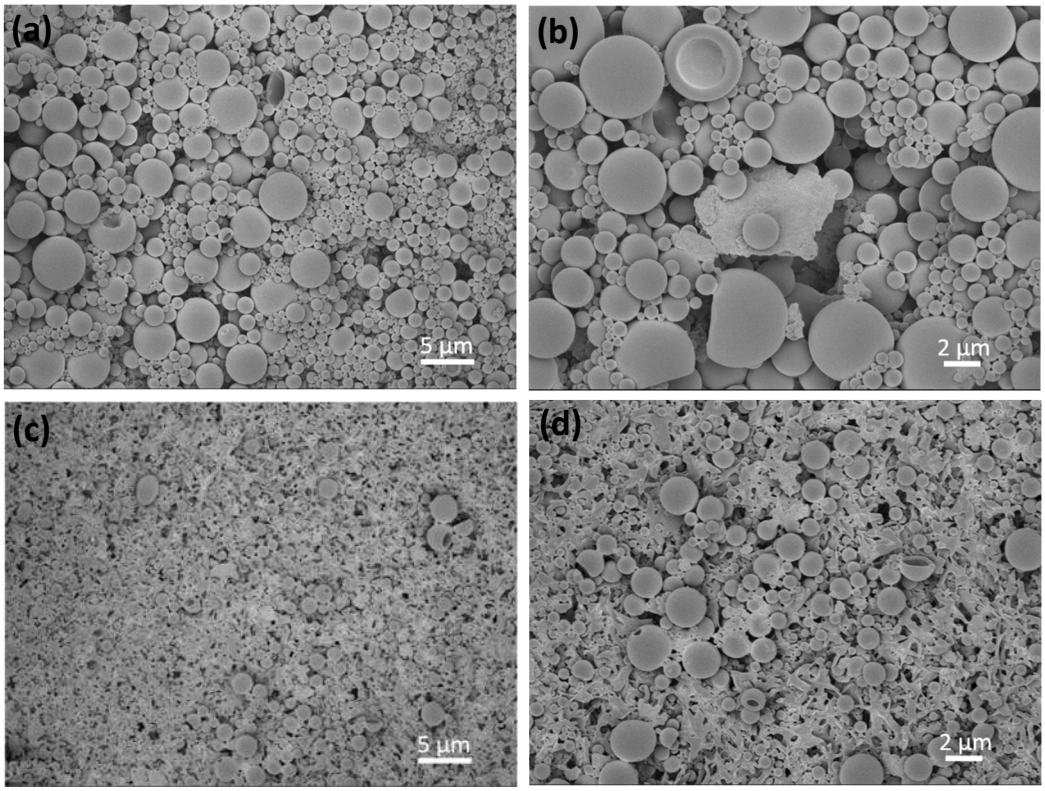

Figure 4. 13 SEM images of PLA particles prepared with Laponite (1 mg/ml) in W-phase and 15 mg/ml surfactant. (a-b): 40% (v/v) glycerol; (c-d): 60% glycerol.

4.4.2.5 Overall screening of different factors by DOE

In order to decide the critical factors and an optimized recipe for particle generation, a Design of Experiment (DOE) screening with III resolution was employed to create a factorial design as shown in Table 4.6. The nanoclay type was fixed as OMT-10A as a model since it has a good

affinity with the polar system among all the nanoclays that are available for our study. The utility of screening DOE minimized the number of experiment runs. In our study, seven factors were considered and eight runs of experiments were generated by Minitab software. The SEM and particle sizes results are shown in Figure 4.14. No 2 and 8 experiments led to big clusters and thus not tested for SEM. Figure 4.15 demonstrated the Standardized effects of important factors regarding particle size by the factorial analysis function in Minitab.

Table 4. 6 DOE screening recipes of OMT-10A with a fixed concentration of 2 mg/ml

	pH of Wphase	Nisin (mg/ml)	Glycerol (v/v)	PLA (mg/ml)	PF68 (mg/ml)	Time (min)	Speed (m/s)
1	5.5	1	50%	15	15	5	20
2	5.5	0.25	50%	5	1.5	5	30
3	2	1	50%	5	1.5	2	20
4	2	0.25	50%	15	15	2	30
5	5.5	1	10%	15	1.5	2	20
6	2	1	10%	5	15	5	20
7	5.5	0.25	10%	5	15	2	30
8	2	0.25	10%	15	1.5	5	30

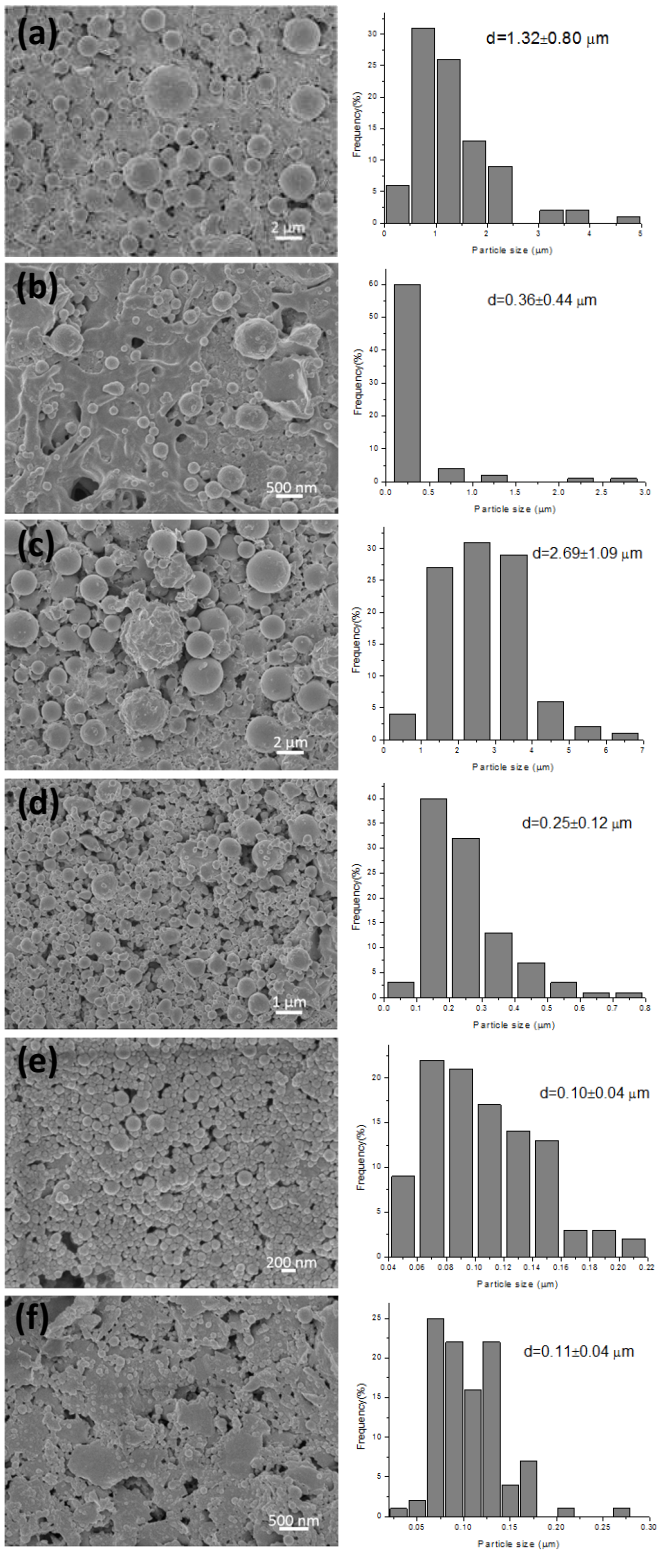

Figure 4. 14 SEM images of PLA/OMT-10A composite particles based on DOE screening recipes (Table 4.6).

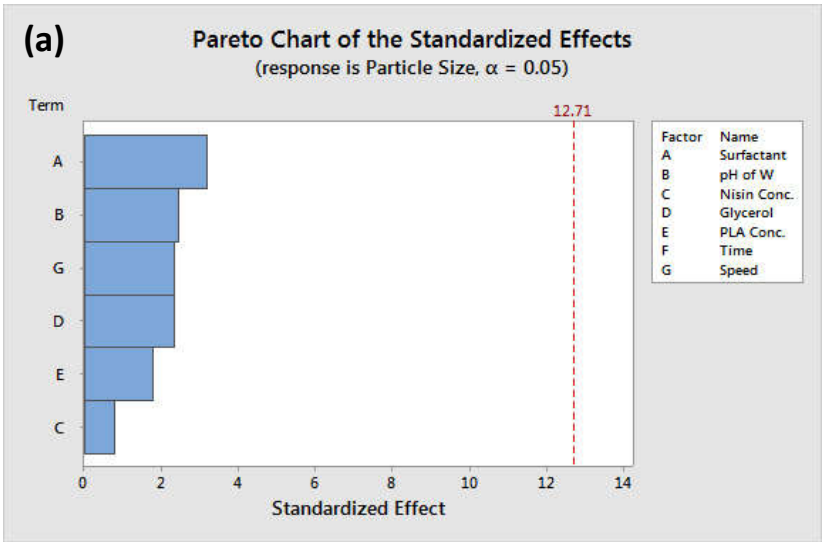

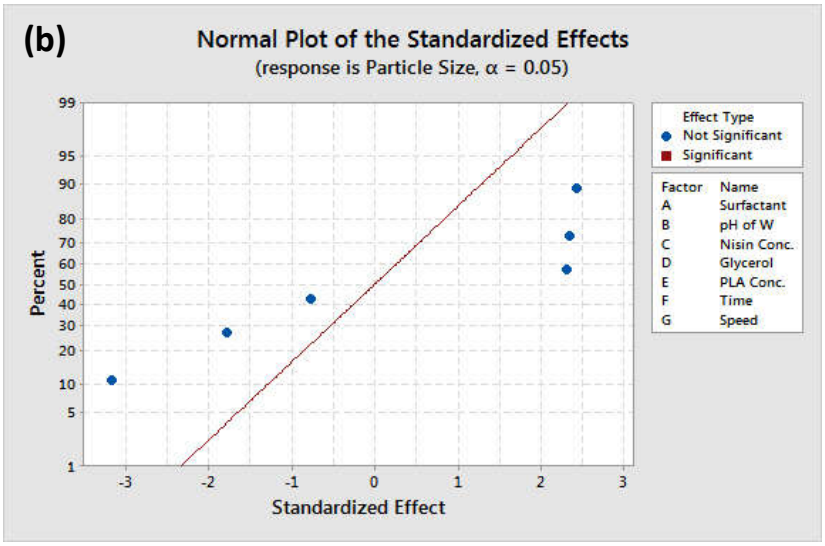

Figure 4. 15 (a) Pareto chart from analyzing particle size as a response from DOE factorial analysis; (b) Normal plot of standardized effects.

As shown in Figure 4.15 (a), the surfactant concentration is the most sensitive factor among all the others, which is corresponding to the results discussed in section 4.4.2.1 previously. Emulsion duration time, represented by F here, is listed in the Pareto chart, suggesting that it affects the average particle size slightly. This is consistent with Figure 4.11 in section 4.4.2.3. One thing worth of knowing is that the second most sensitive factor is the pH value of the water phase. Figure

4.16 shows a brief illustration on how the pH of water phase affects the particle morphology. As observed, higher pH condition led to much smaller particle size.

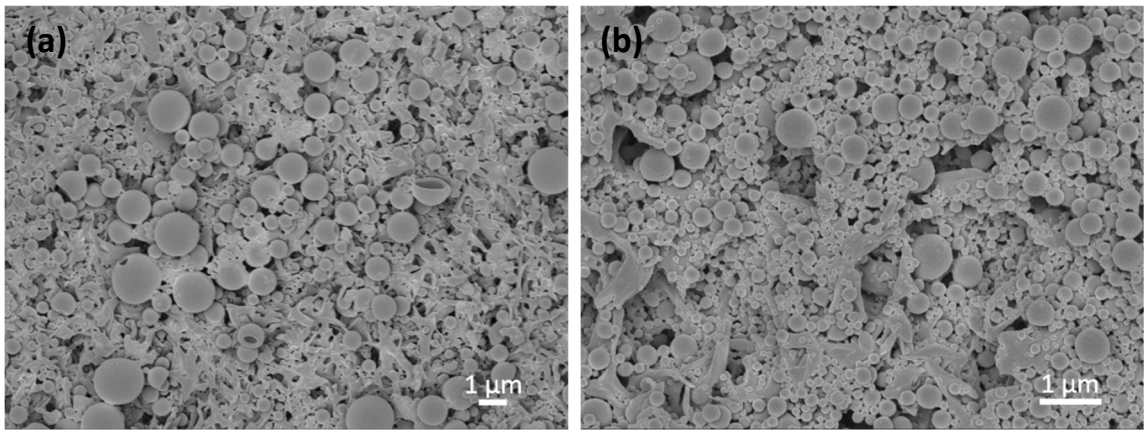

Figure 4. 16 SEM of PLA-laponite particles prepared with different pH values of the water phase. (a) lower pH; (b) higher pH.

4.4.2.6 Effect of the hydrophilic nanoclay position

As discussed in section 4.4.1, MMT-Na^+ and MMT-Ca^{++} are hydrophilic and the dispersibility in ethyl acetate is much lower than other nanoclays. Typically, hydrophilic MMT has been added into the water phase before the emulsification process. Feng et al. dispersed MMT-Na^+ in the water phase, which was a different phase with the polymer. Therefore, the modification of polymer particles was limited and stayed at a bulk material level. Herein we added MMT into both the water phase and the oil phase separately. Figure 4.17 compared the morphology of microparticles prepared under the same condition except for the position of MMT-Na^+. When MMT was dispersed in the water phase, most MMT flakes were not well mixed within PLA particles and formed a massive layer as shown in Figure 4.17 (a). When MMT was added in the oil phase, however, PLA-MMT microparticles were observed, along with a few MMT clusters (Figure 4.17 (d)). Comparing the particle surface texture in Figure 4.17 (b) and (e), (e) had continuous roughness while (b) had some plain surface. Figure 4.17 (c) and (f) show the open hollow particles.

The thickness of MMT-in-water particle (~500 nm) was much less than that of MMT-in-oil sample (~2 μm). The shell thickness to particle radius ratio also increased when MMT was added into the oil phase. Making polymer composite with hydrophilic filler has always been a challenge. Here, with a proper fluid flow condition and the employment of Nanomixer, we successfully generated a polymer-hydrophilic MMT composite system with 2 min. This indicates a promising way to make polymer composites by fluid flow as well as the strong mixing capability of Nanomixer.

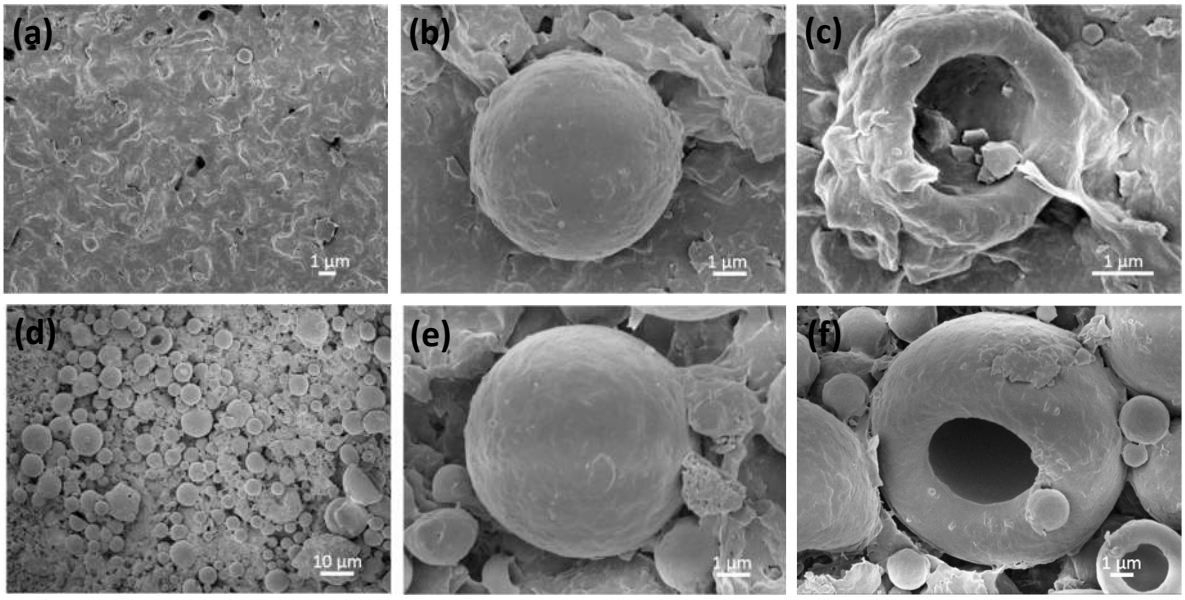

Figure 4. 17 SEM images of PLA/MMT-Na^+ composite particles. (a-c): MMT-Na^+ dispersed in water phase; (d-f) MMT-Na^+ dispersed in oil phase.

4.4.3 Encapsulation of diclofenac (nanoclay-drug interaction)

Diclofenac (DCF), a prevalent anti-inflammatory drug, was employed as a model drug in this study to test the encapsulation capability and release behavior of nanoclay-modified PLA composite micro-/nano-particles. DCF was dissolved in the water phase because it is hydrophilic. Figure 4.14 compared the SEM results between plain PLA/OMT-20 microparticles and DCF-loaded PLA/OMT-20 microparticles. As observed, the addition of DCF dramatically increased the overall particle size (from ~ 2 μm to ~ 8 μm) as well as widen the particle size distribution. Figure 4.14

(b) and (d), the higher magnification images, demonstrate different particle surface textures. In Figure 4.14 (b), nanoclay was embedded within PLA particles while in Figure 4.14 (d), nanoclay formed a layer that covered on top of PLA particles. Besides, free crystallized DCF and nanoclay flakes were found in Figure 4.14 (c-d). This suggests that the addition of DCF decreased the affinity extent between PLA and OMT-20. DCF is negatively charged due to the presence of carboxyl group (COO^-) [178]. As mentioned previously, MMT including OMT is anionic and a natural cation exchanger. Therefore, a repelling force between DCF and OMT-20 could lead to the break of the emulsion equilibrium as well as low encapsulation efficiency of DCF in PLA/OMT-20 microparticles.

The encapsulation efficiency (Figure 4.19) and in vitro release profile (Figure 4.20) of DCF were correspondence with the proposed DCF/OMT-20 (drug/nanoclay) interaction. The encapsulation efficiency of DCF was slightly lower in PLA/OMT-20 particles (81.08%) than that of pure PLA particles (84.05%). The initial burst release of PLA and PLA/OMT-20 are 29% and 34%, respectively. In the following two weeks, about 50% DCF was accumulatively released from pure PLA particles while 62% DCF was released from PLA/OMT-20 microparticles. Both of the release rate and the amount released from PLA/OMT-20 microparticles are higher compared to pure PLA microparticles. Some literature reported that the addition of nanoclay slowed down the initial burst release and delayed the release because nanoclay reduces the extension of polymer swelling as well as the permeability for diffusion [148, 153]. In this study, nanoclay (OMT-20) speeded the release because of the static electric repulsion between it and the drug. Therefore, the drug-nanoclay interaction is significant for the design of biodegradable polymer and nanoclay composite drug carrier compared with other types of polymer composite drug vehicles.

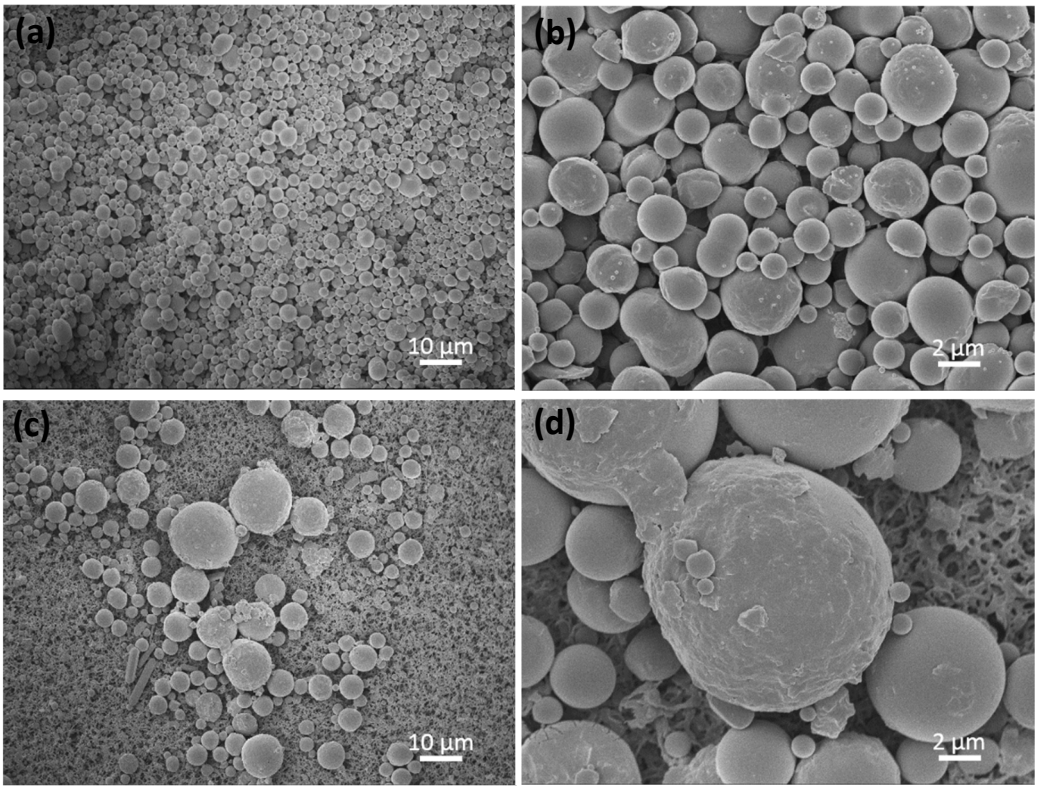

Figure 4. 18 SEM images of plain PLA/OMT-20 particles (a-b) and DCF-loaded PLA/OMT-20 particles (c-d).

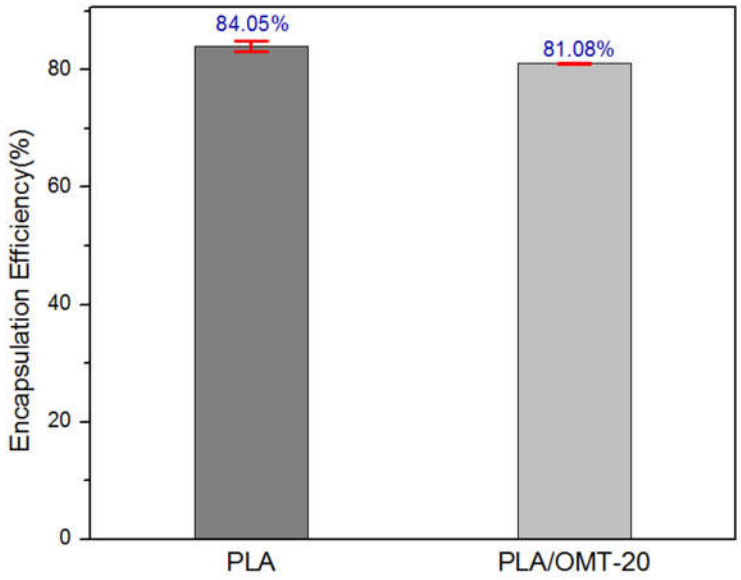

Figure 4. 19 Encapsulation Efficiency of Diclofenac in PLA microparticles and PLA/OMT-20 microparticles prepared under the same condition.

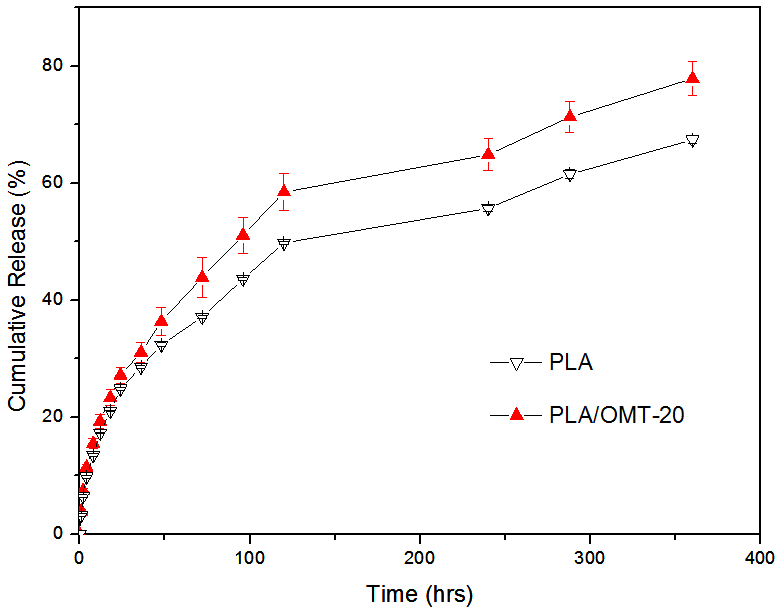

Figure 4. 20 Accumulative release profile of Diclofenac from PLA microparticles and PLA/OMT-20 microparticles.

4.4.4 Encapsulation of polypeptide drug (Nisin)

Nisin, a water-soluble antimicrobial, was encapsulated into PLA/nanoclay particles to reach synergetic antimicrobial effects. Figure 4.21 shows the fluorescent microscopy image of Nisin-loaded PLA/OMT-10A composite microparticles. As observed from Figure 4.21 (a), Nisin was distributed throughout the particles. In the higher magnification image, Figure 4.21 (b), individual Nisin clusters were clearly seen, which indicates the hollow structure of the particles. MMT-Ca^{2+} was also tried to prepare the composite PLA particles as Nisin vehicle due to its well-known medical benefit. As shown in Figure 4.22, Nisin was successfully encapsulated into the PLA/MMT-Ca^{2+} composite particles.

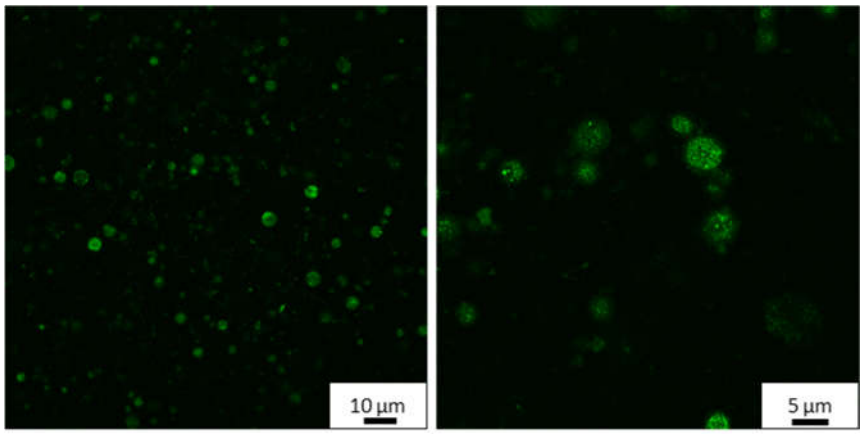

Figure 4. 21 Confocal images of Nisin-loaded PLA/OMT-10A particles.

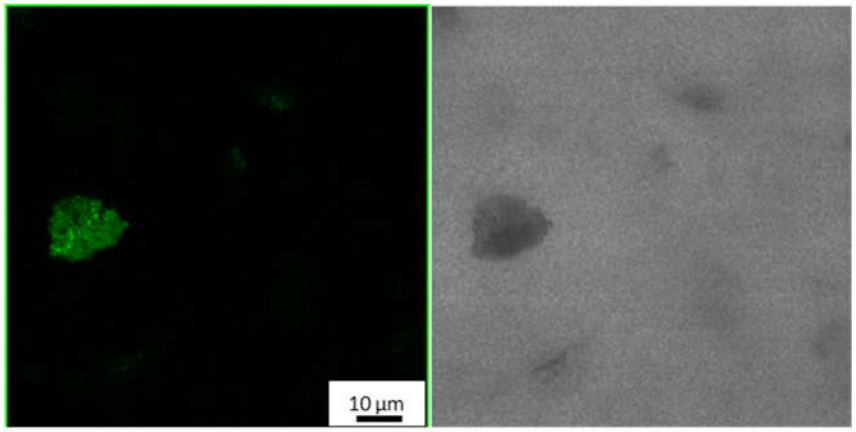

Figure 4. 22 Confocal images of Nisin-loaded PLA/MMT-Ca^{2+} particles.

4.4.5 TGA analysis of PLA/nanoclay composite microparticles

The content of nanoclay in the composite particles was obtained from the TGA data by neglecting the encapsulated drug because of its minor fraction. Figure 4.23 shows the TGA plots of freeze-dried pure PLA particles, composite particles, and pure nanoclays. As an example, from 200 to 670 °C, the pure PLA sample exhibited about 97.4% weight loss. In comparison, 2.4% weight loss was observed from freeze-dried pure MMT-Na^+. Therefore, the weight loss of PLA/ MMT-Na^+ composite particles (64.14%) can be attributed to PLA and MMT-Na^+ respectively. Assuming the MMT-Na^+ content is X, the calculation is as follows:

$$64.14\% = x * 2.4\% + (1 - x) * 97.4\%$$

The root solved from this equation is about 35%, which is the content of MMT-Na^{+}. Similarly, the nanoclay content was calculated and listed in Table 4.7. From the data, PLA/MMT-Ca^{2+} exhibited the highest clay content as 42.7%, followed by MMT-Na+ (35%), OMT-10A (22.2%), Kaolin (15.9%), and OMT-20 (15%). It is worth noting that, during the preparation process, aggregation clusters were observed from the PLA/Kaolin, PLA/OMT-10A, and PLA/OMT-20 samples, which suggests the emulsion equilibrium break happened. This was discussed in detail in section 4.4.2.1. Briefly speaking, the amount of surfactant (15 mg/ml) was over the required amount for the new equilibrium system with these nanoclays. This might be the reason of the lower nanoclay content in PLA/organic nanoclay composites.

Table 4. 7 Nanoclay content of different PLA/nanoclay composite particles.

Type of Nanoclay composite particle	Nanoclay Content
PLA/MMT-Na+	35%
PLA/MMT-Ca++	42.7%
PLA/OMT-10A	22.2%
PLA/OMT-20	15%
PLA/Kaolin	15.9%

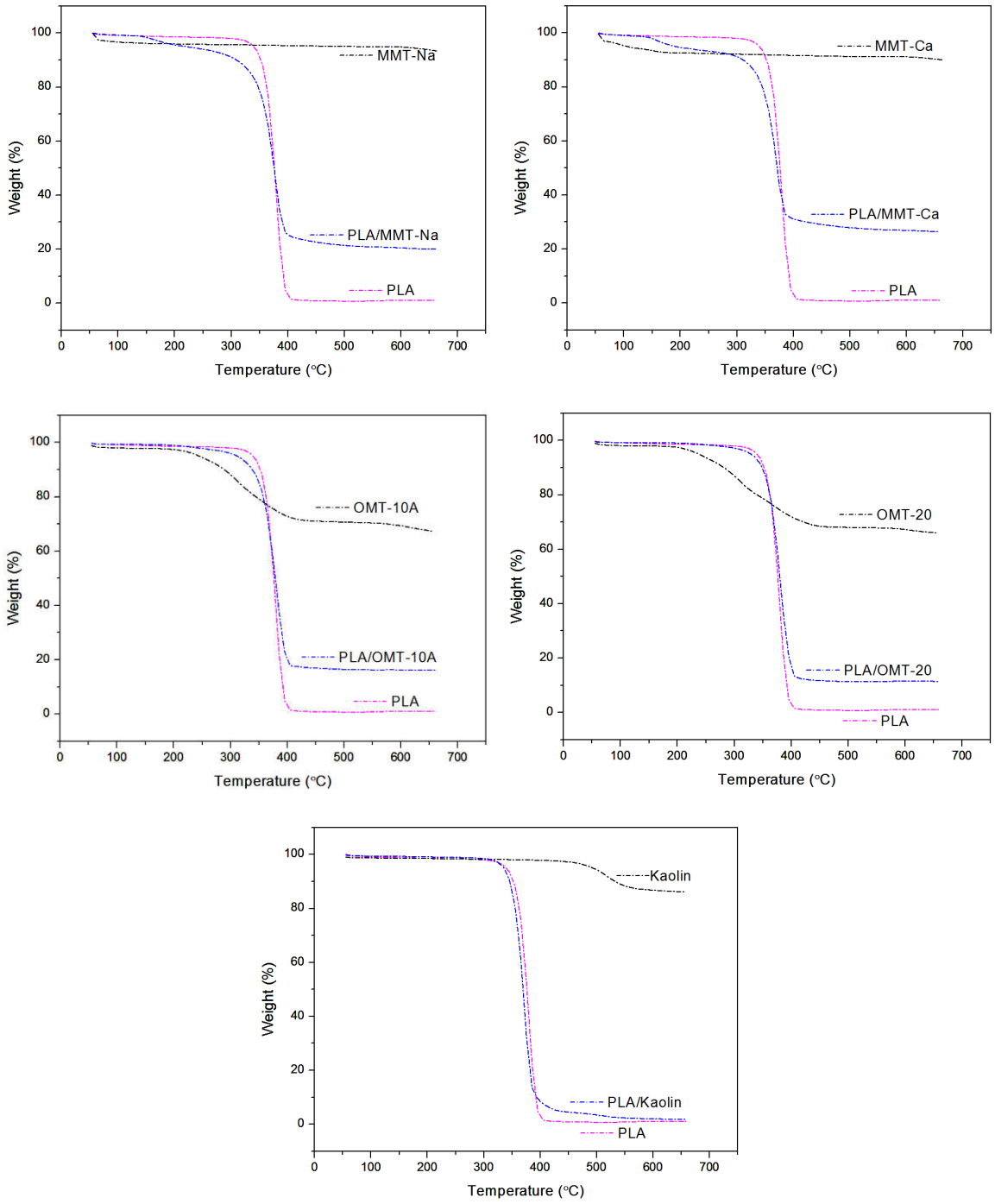

Figure 4. 23 TGA analysis of PLA, nanoclays and PLA/nanoclay composite particles.

4.4.6 XRD analysis of PLA/nanoclay composite microparticles

As discussed in the introduction part, the polymer-nanoclay composite can be categorized as *Intercalated Nanocomposite* and *Exfoliated Nanocomposite* (Figure 4.4). For intercalated nanocomposite, new basal reflection peaks would be observed on the XRD graph because of expansion of layer space caused by intercalation. On the other hand, exfoliated nanocomposites would lead to the disappearance of some reflection peaks due to the breakdown of the layered structure. As shown in Figure 4.24, the XRD graph of PLA/MMT-Ca^{2+} microparticles did not show the peak near 30° compared to the pure MMT-Ca^{2+} sample, which indicates the composite microparticles prepared in our method are exfoliated rather than intercalated. In this study, a modified Taylor-Couette Nanomixer was employed to carry out the mixing function for emulsion formation. The strong shear force from the fluid flow likely break down the layer structure of nanoclays, which is consistent with the XRD result in Figure 4.24.

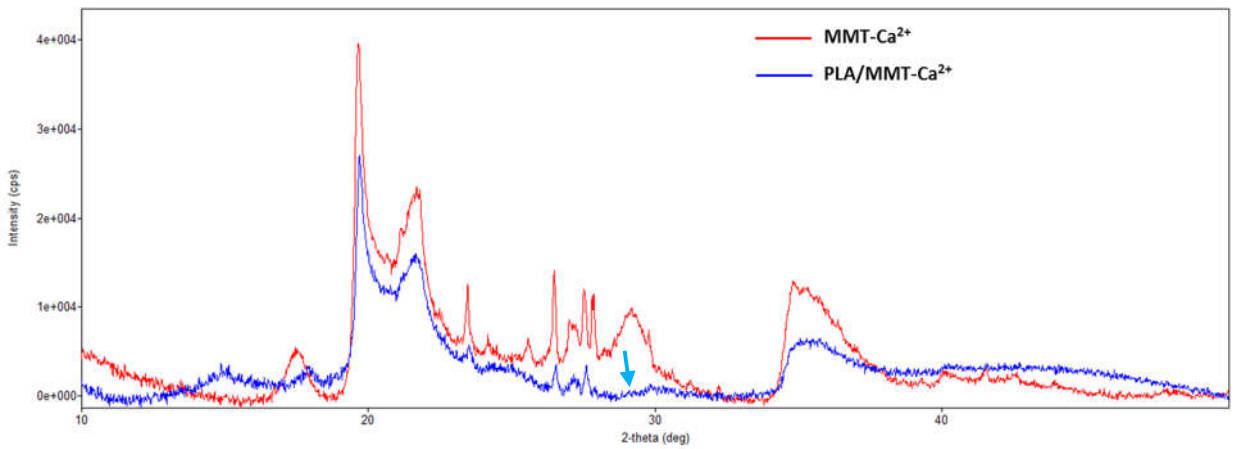

Figure 4. 24 XRD analysis of the freeze-dried pure MMT-Ca2+ sample and PLA/MMT-Ca2+ microparticles.

4.4.7 PLA/nanoclay particles under HT-RT emulsion

As mentioned earlier, emulsification temperature is important to design the size and morphology of PLA particles [174]. Briefly speaking, when the emulsification temperature was above the glass transition temperature (HT) of PLA, hollow microparticles were obtained, while nanospheres were generated under the room temperature (RT) emulsion condition. With a dynamic emulsion (HT-RT) [177], nanospheres were generated but with more interaction with the molecules disturbed in the water phase. The dimension of one nanoclay layer is about 15 * 1000 nm. Thus, microparticles are more suitable to generate successful composite particles between PLA and nanoclays, which has mainly been discussed in the above sections. Figure 4.25 shows the PLA/OMT-20 particles prepared with the dynamic HT-RT emulsification with different surfactant and OMT-20 concentrations. Under 10,000* magnification, shrunk PLA particles were observed (Pure PLA particles will deform and shrink under electron beam). Compared to the similar size particles made from HT condition (eg, Figure 4.11 (b)), most of PLA particles demonstrated shrink, which suggests that few composite particles were prepared. Still, individual PLA/OMT-20 composite particle was observed in the SEM images.

Figure 4.26 compares the particle size of PLA/OMT-20 with the same surfactant concentration (15 mg/ml) but different OMT-20 concentration. It is obvious that higher OMT-20 concentration led to smaller particle size (1000 ppm: ~100 nm; 300 ppm: >100 nm). In addition, the particle size distribution was wider for the lower OMT-20 concentration. The effect of OMT-20 on the particle size and distribution on HT-RT emulsion is consistent with the HT emulsion. However, when the surfactant concentration was 10 times lower (1.5 mg/ml, Figure 4.25 (a,c)), the effect was not obvious, which is consistent with our previous conclusion that surfactant is the most effective factor.

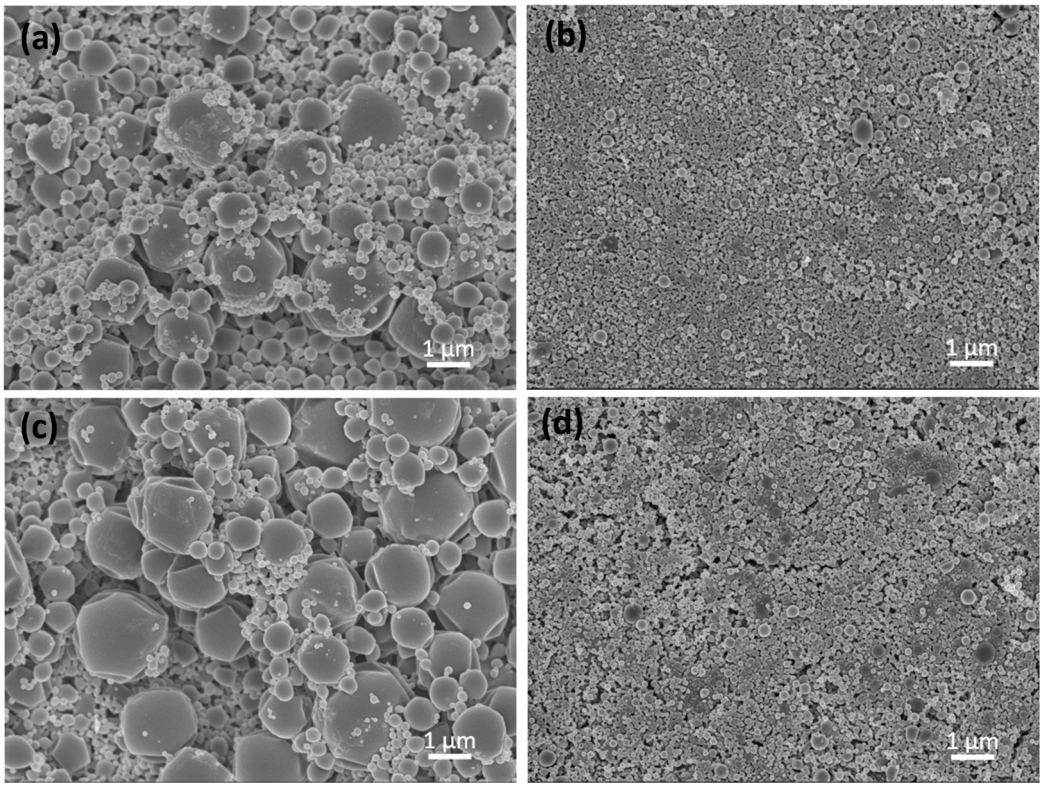

Figure 4. 25 SEM of PLA/OMT-20 particles prepared under HT-RT condition. (a) 1.5 mg/ml surfactant, 300 ppm OMT; (b) 15 mg/ml surfactant, 300 ppm OMT; (c) 1.5 mg/ml surfactant, 1000 ppm OMT; (d) 15 mg/ml surfactant, 1000 ppm OMT.

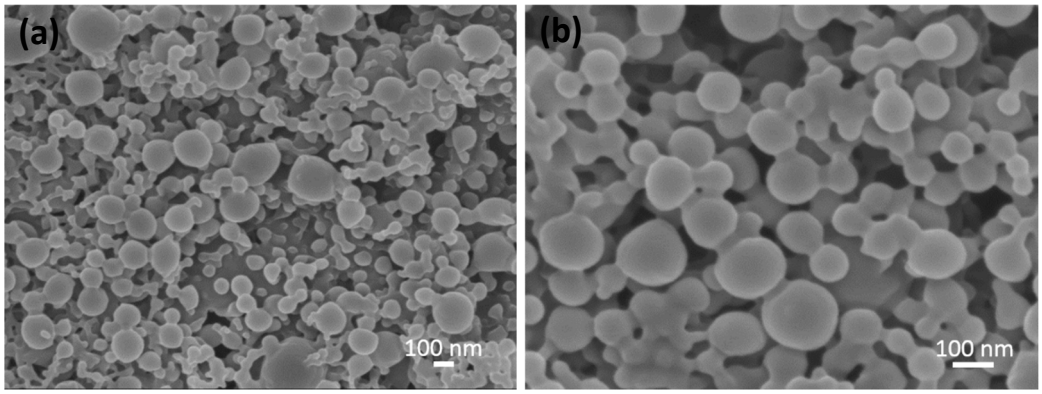

Figure 4. 26 SEM of PLA/OMT-20 particles prepared under HT-RT condition (higher magnification). (a) 15 mg/ml surfactant, 300 ppm OMT; (b) 15 mg/ml surfactant, 1000 ppm OMT.

4.5 CONCLUSION

PLA/nanoclay (various types) composite microparticles were successfully developed by the one-step double emulsion method either under the HT condition or the HT-RT condition. The particle morphology, in terms of particle size and size distribution, is highly related to the surfactant concentration, PLA/nanoclay weight ratio, emulsification duration, glycerol ratio, and pH value of the water phase. A DOE screening (resolution III) was employed to minimize the number of experiments for identifying the key parameters in the preparation process. Its factorial analysis regarding particle size concluded the same key factors as mentioned above. Among these, surfactant concentration was identified as the most effective parameter, which is consistent with our observation in both HT condition and RT condition.

The TGA analysis shows that the content of hydrophilic nanoclay (MMT) was as high as 42.7%, which demonstrates a great potential to make PLA-hydrophilic nanoclay composite in general. The reason for the lower content of organo-nanoclay in PLA composite particle might be that the excess amount of surfactant (15 mg/ml) break the emulsion equilibrium and thus affect the mixing between PLA and OMT. The XRD analysis suggests that the PLA/nanoclay composite is the *Exfoliated* nanoclay composite, caused by the high shear force of Nanomixer.

The model drug, DCF, was encapsulated to study the nanoclay-drug interaction due to the high cation exchange capacity of MMT. Repelling force was expected to form between DCF and MMT because they both negatively charged. The resulting encapsulation efficiency and release profile also confirmed this interaction since a lower encapsulation efficiency in PLA/MMT and a faster and higher amount of release was observed. Nisin, a natural antimicrobial, was successfully encapsulated within the PLA/nanoclay composite particles as proven by the fluorescence microscope.

5 FUTURE WORK

5.1 EXTENSION OF ANISOTROPIC PARTICLES

Anisotropic micro-/nano-particles have a great potential in drug delivery and other fields. Our development of the unique PLA-PS multicompartment hollow microparticle via simple, fast emulsion process is definitely an industry-suitable, cost effective approach to generate anisotropic micro-/nano-particles. By changing the polymer blend recipe as well as the solvent, various types of functional polymer blend composite particles should be able to develop.

"Liberty Bell" PLA-PS open-hollow microparticle. When toluene was used to dissolve PLA and PS at 50:50 ratio, Janus, closed/open-hollow microparticles were generated. Based on the fact that PLA normally shrinks under the electron beam of SEM, the open part was identified as PLA. However, further study is needed to confirm the composition of each part of the Janus particles.

One-step preparation of cage-like porous particle. Cage-like PLA-PS porous particles were obtained when adjusting the PLA weight ratio to 30% or 70% in the toluene experiment. Compared to the PLA cage-like porous particle via solvent extraction, this PLA-PS porous particle was made of two parts: one continuous particle shell and one cage-like porous particle. This structure holds two polymer composition in one unit while maintaining the porous structure. The hypothesis here is that the porous part came from PLA because these pores were generated as broken holes based on the observation of the pore edges in SEM images. But further research is needed to decide the composition of the pore structure. In addition, the relation between the PLA/PS ratio and the final pore features is worthy of study.

PLA-PS particle preparation with toluene should also be carried on under room temperature emulsification and compared to the one prepared with EA.

PLA-PCL biodegradable Janus particles. Both of PLA and PCL are FDA approved biodegradable and biocompatible polymers for biomedical applications. Thus, the PLA-PCL bioblend particles are even more promising in the field of biomedical application. Here, only 50:50 PLA/PS ratio was tried to make composite particles. Various ratios of PLA and PS should be tested in the future.

The mechanism of how the polymer blend recipe would lead to the multicompartment particles is still not clear. It is certain that the crystalline structure is not the key factor, or at least not the only factor to form the PLA-PS multicompartment microparticles. My hypothesis, hereby, is that the fact that PS is very hydrophobic is the reason why uniform PS protrusion particles were formed. In the future, another super hydrophobic polymer should be blended with PLA to verify this hypothesis.

Finally, since both of the particle structure and composition affect the function of polymer particles in general. In order to find out the suitable application for different anisotropic particles, the encapsulation and release tests should be carried on with different types of drugs in the future. Furthermore, modeling and simulation approaches can be used to predict the particle morphology based on the condition given.

5.2 EXTENSION OF PLA/NANOCLAY PARTICLES

The negatively charged nanoclay suspension is not ideal for anionic or neutral drugs. As discussed in chapter 4, the encapsulation of DCF in PLA/nanoclay composite particle is lower than that of pure PLA particle. However, in some other research, nanoclay (MMT) increased the encapsulation

efficiency of drugs. In the future, cationic drugs should be tested in our double emulsion system together with nanoclay, expecting an improved drug loading efficiency. In addition, polyelectrolytic biopolymers, such as chitosan, have been proposed to improve the binding between nanoclay and anionic drugs. Chitosan is also widely studied for biomedical applications such as drug delivery carrier and tissue engineering scaffolds. Therefore, a triple blend, PLA-nanoclay-chitosan, should be a good direction in the future to explore more drug encapsulation possibilities.

Nanoclay system can also be combined with PLA-PS anisotropic system to generate medically synergetic anisotropic particles. The challenge here would be the effect of nanoclay on the interfacial tension as well as the fluid viscosity. Since both of them are important parameters that related to particle morphology, further research needs to be applied to figure out how to design the particle by controlling different parameters. Previously, the addition of IONPs did not change the morphology of PLA-PS particle. In the case of nanoclay, it might change the PLA-PS particle morphology dramatically.

In order to further develop the PLA/nanoclay system for pharmaceutical application, more dissolution test and *in vitro* drug test need to be done if applicable in our lab. For dissolution test, two parameters are subject to change to mimic different *in vivo* drug release: pH and NaCl concentration. Different biodegradable polymers react differently to the pH change. For example, PLA showed faster release when the pH is basic while PLGA had a faster release in acid solution.

Another different extension direction of the PLA/nanoclay system is to develop PLA and hydrophilic nanoclay composite, and the exfoliation of nanoclay. For the first one, our TGA results showed that about 40% of hydrophilic MMT existed in the PLA/MMT composite particles. This confirmed the advantage of our one-step double emulsion in the area of encapsulation of

hydrophilic materials/molecules in the hydrophobic polymer system. Out of the scope of biomedical application, other industry level polymers can also be tried in this system in order to get mechanically reinforced polymer-nanoclay composites.

The exfoliation of nanoclay is important to utilize nanoclay as a nanofiller for fabricating composite materials. Our TGA analysis suggested a *Exfoliated* nanoclay composite was obtained from the PLA/nanoclay particle. Hereby, our Nanomixer with high shear force, providing efficient mixing, can be proposed for simple and fast exfoliation of nanoclays. The possible challenge here would be the thermodynamic stability of exfoliated nanoclay layers and thus surfactants might be needed to maintain the nanoclay layers separated.

5.3 OTHER DIRECTIONS

Research shows that graphene has some antimicrobial effects. Therefore, PLA/graphene composite particle is another good topic to develop for drug delivery application. Graphene can also improve the mechanical property of PLA particles.

REFERENCES

REFERENCES

1. Soppimath, K.S., et al., *Biodegradable polymeric nanoparticles as drug delivery devices.* Journal of controlled release, 2001. **70**(1): p. 1-20.

2. Martins, I.M., et al., *Microencapsulation of essential oils with biodegradable polymeric carriers for cosmetic applications.* Chemical Engineering Journal, 2014. **245**: p. 191-200.

3. Kumari, A., S.K. Yadav, and S.C. Yadav, *Biodegradable polymeric nanoparticles based drug delivery systems.* Colloids and Surfaces B: Biointerfaces, 2010. **75**(1): p. 1-18.

4. Musyanovych, A., et al., *Preparation of biodegradable polymer nanoparticles by miniemulsion technique and their cell interactions.* Macromolecular bioscience, 2008. **8**(2): p. 127-139.

5. Pisani, E., et al., *Polymeric nano/microcapsules of liquid perfluorocarbons for ultrasonic imaging: Physical characterization.* Langmuir, 2006. **22**(9): p. 4397-4402.

6. Quintanar-Guerrero, D., et al., *Preparation and characterization of nanocapsules from preformed polymers by a new process based on emulsification-diffusion technique.* Pharmaceutical research, 1998. **15**(7): p. 1056-1062.

7. Quintanar-Guerrero, D., et al., *Preparation and characterization of nanocapsules from preformed polymers by a new process based on emulsification-diffusion technique.* Pharmaceutical Research, 1998. **15**(7): p. 1056-1062.

8. Allemann, E., R. Gurny, and E. Doelker, *Preparation of aqueous polymeric nanodispersions by a reversible salting-out process - influence of process parameters on particle-size.* International Journal of Pharmaceutics, 1992. **87**(1-3): p. 247-253.

9. Zambaux, M.F., et al., *Influence of experimental parameters on the characteristics of poly(lactic acid) nanoparticles prepared by a double emulsion method.* Journal of Controlled Release, 1998. **50**(1-3): p. 31-40.

10. Ji, S., et al., *Transitional behavior of polymeric hollow microsphere formation in turbulent shear flow by emulsion diffusion method.* Polymer, 2012. **53**(1): p. 205-212.

11. McClements, D.J., E.A. Decker, and J. Weiss, *Emulsion-based delivery systems for lipophilioc bioactive components.* Journal of Food Science, 2007. **72**(8): p. R109-R124.

12. Fessi H, D.J., Puisieux F, Thies C, *Process for the preparation of dispersible colloidal systems of a substance in the form of nanocapsules.*, 1991: US.

13. Fessi H, P.F., Devissaguet JP, Ammoury N, Benita S, *Nanocapsules formation by interfacial polymer deposition following solvent displacement.* Int J Pharm, 1989. **55**: p. R1-R4.

14. Sundar, S., J. Kundu, and S.C. Kundu, *Biopolymeric nanoparticles.* Science and Technology of Advanced Materials, 2010. **11**(1).

15. Calvo, P., et al., *Novel hydrophilic chitosan-polyethylene oxide nanoparticles as protein carriers.* Journal of Applied Polymer Science, 1997. **63**(1): p. 125-132.

16. Tokumitsu, H., H. Ichikawa, and Y. Fukumori, *Chitosan-gadopentetic acid complex nanoparticles for gadolinium neutron-capture therapy of cancer: Preparation by novel emulsion-droplet coalescence technique and characterization.* Pharmaceutical Research, 1999. **16**(12): p. 1830-1835.

17. Smith, W.V. and R.H. Ewart, *Kinetics of emulsion polymerization.* The journal of chemical physics, 1948. **16**(6): p. 592-599.

18. Floury, J., A. Desrumaux, and J. Lardieres, *Effect of high-pressure homogenization on droplet size distributions and rheological properties of model oil-in-water emulsions.* Innovative Food Science & Emerging Technologies, 2000. **1**(2): p. 127-134.

19. Hinze, J.O., *Fundamentals of the Hydrodynamic Mechanism of Splitting in Dispersion Processes.* Aiche Journal, 1955. **1**(3): p. 289-295.

20. Sleicher, C.A., *Maximum Stable Drop Size in Turbulent Flow.* Aiche Journal, 1962. **8**(4): p. 471-477.

21. R. N. Brogden, R.C.H., G. E. Pakes, T. M. Speight, G. S. Avery, *Diclofenac sodium: a review of its pharmacological properties and therapeutic use in rheumatic diseases and pain of varying origin.* Drugs, 1980. **20**(1): p. 24-48.

22. Vasilios A. Skoutakis, C.A.C., Timothy R. Mickle, Valorie H. Smith, Charles R. Arkin, Jane Alissandratos, Daniel E. Petty, *Review of Diclofenac and Evaluation of its Place in Therapy as a Nonsteroidal Antiinflammatory Agent.* Annals of Pharmacotherapy, 1988. **22**(11).

23. Cha, D.S. and M.S. Chinnan, *Emerging role of nisin in food and packaging systems.* Food Science and Biotechnology, 2003. **12**(2): p. 206-212.

24. Luc De Vuyst, E.V., *Nisin, a Lantibiotic produced by Lactococcus lactis subsp. lactic: Properties, Biosynthesis, Fermentation and Applications.* Bacteriocins of Lactic Acid Bacteria: Microbiology, Genetics and Applications, 1994: p. 151-221.

25. Delvesbroughton, J., *NISIN AND ITS USES AS A FOOD PRESERVATIVE.* Food Technology, 1990. **44**(11): p. 100-&.

26. Eefjan Breukink, B.d.K., *The Lantibiotic nisin, a special case or not?* Biochimica et Biophysica Acta (BBA) - Biomembranes, 1999. **1462**(1-2): p. 223-234.

27. de Arauz, L.J., et al., *Nisin biotechnological production and application: a review.* Trends in Food Science & Technology, 2009. **20**(3-4): p. 146-154.

28. Karam, L., et al., *Study of surface interactions between peptides, materials and bacteria for setting up antimicrobial surfaces and active food packaging.* Journal of Materials and Environmental Science, 2013. **4**(5): p. 798-821.

29. Gross, E. and J.L. Morell, *The structure of nisin.* Journal of the American Chemical Society, 1971. **93**: p. 4634-4635.

30. Layal Karam, C.J., Pascal Dhulster, Nour-Eddine Chihib, *Study of surface interactions between peptides, materials and bacteria for setting up antimicrobial surfaces and active food packaging.* J. Mater. Environ. Sci. , 2013. **4**(5): p. 798-821.

31. Delves-Broughton, J., *Nisin as a food preservative.* Food Australia, 2005. **57**(12): p. 525-527.

32. Kuwano, K., et al., *Dual antibacterial mechanisms of nisin Z against Gram-positive and Gram-negative bacteria.* International journal of antimicrobial agents, 2005. **26**(5): p. 396-402.

33. Galvez, A., et al., *Bacteriocin-based strategies for food biopreservation.* International Journal of Food Microbiology, 2007. **120**(1-2): p. 51-70.

34. Imran, M., et al., *Microstructure and physico-chemical evaluation of nano-emulsion-based antimicrobial peptides embedded in bioactive packaging films.* Food Hydrocolloids, 2012. **29**(2): p. 407-419.

35. Lee, C.H., et al., *A coating for use as an antimicrobial and antioxidative packaging material incorporating nisin and alpha-tocopherol.* Journal of Food Engineering, 2004. **62**(4): p. 323-329.

36. Quezada-Gallo, J.A., *Delivery of Food Additives and Antimicrobials Using Edible Films and Coatings*. Edible Films and Coatings for Food Applications, ed. M.E. Embuscado and K.C. Huber2009. 315-333.

37. Gupta, A.K. and M. Gupta, *Synthesis and surface engineering of iron oxide nanoparticles for biomedical applications.* Biomaterials, 2005. **26**(18): p. 3995-4021.

38. Mornet, S.p., et al., *Magnetic nanoparticle design for medical diagnosis and therapy.* Journal of Materials Chemistry, 2004. **14**(14): p. 2161.

39. Susamu Taketomi, M.U., Masaki Mizukami, Hideki Miyajima and Soshin Chikazumi, *Magnetooptical Effects of magnetic Fluid.* Journal of the Physical Society of Japan, 1987. **56**(9): p. 3362-3374.

40. Tsang, S.C., et al., *Magnetically Separable, Carbon-Supported Nanocatalysts for the Manufacture of Fine Chemicals.* Angewandte Chemie, 2004. **116**(42): p. 5763-5767.

41. Makoto Takafuji, S.I., Hirotaka Ihara and Zhenghe Xu, *Preparation of Poly(1-vinylimidazole)-Grafted Magnetic Nanoparticles and Their Application for Removal of Metal Ions.* Chem. Mater, 2004. **16**(10): p. 1977-1983.

42. Daniel W. Elliott, W.X.Z., *Field Assessment of Nanoscale Bimetallic Particles for Groundwater Treatment.* Environmental Science & Technology, 2001. **35**(24): p. 4922-4926.

43. Arruebo, M., et al., *Magnetic nanoparticles for drug delivery.* Nano Today, 2007. **2**(3): p. 22-32.

44. Kenneth J. Widder, A.E.S., Dante G. Scarpelli, *Magnetic microspheres: a model system for site specific drug delivery in vivo.* Experimental Biology and Medicine, 1978. **58**(141).

45. Shapiro, E.M., *Biodegradable, Polymer Encapsulated, Metal Oxide Particles for MRI-Based Cell Tracking.* Magnetic Resonance in Medicine, 2015. **73**(1): p. 376-389.

46. Lu, A.H., E.L. Salabas, and F. Schuth, *Magnetic nanoparticles: Synthesis, protection, functionalization, and application.* Angewandte Chemie-International Edition, 2007. **46**(8): p. 1222-1244.

47. Yu Lu, Y.Y., Brian T. Mayers, Younan Xia, *Modifying the Surface Properties of Superparamagnetic Iron Oxide Nanoparticles through A Sol-Gel Approach.* Nano Letters, 2002. **2(3)**: p. 4.

48. Bulte, J.W.M. and D.L. Kraitchman, *Iron oxide MR contrast agents for molecular and cellular imaging.* Nmr in Biomedicine, 2004. **17**(7): p. 484-499.

49. Arbab, A.S.B., Lindsey A.; Miller, Bradley R.; Jordan, Elaine K.; Bulte, Jeff W. M.; Frank, Joseph A., *Intracytoplasmic tagging of cells with ferumoxides and transfection agent for cellular magnetic resonance imaging after cell transplantation: methods and techniques.* Transplantation, 2003. **76**(7): p. 8.

50. Hinds, K.A., et al., *Highly efficient endosomal labeling of progenitor and stem cells with large magnetic particles allows magnetic resonance imaging of single cells.* Blood, 2003. **102**(3): p. 867-872.

51. Shapiro, E.M., S. Skrtic, and A.P. Koretsky, *Sizing it up: Cellular MRI using micron-sized iron oxide particles.* Magnetic Resonance in Medicine, 2005. **53**(2): p. 329-338.

52. Michael K. Nkansah, D.T., Erik M. Shapiro, *Magnetic Poly(lactide-co-glycolide) and Cellulose Particles for MRI-Based Cell Tracking.* Magnetic Resonance in Medicine, 2011. **65**: p. 10.

53. Bertorelle, F., et al., *Fluorescence-modified superparamagnetic nanoparticles: Intracellular uptake and use in cellular imaging.* Langmuir, 2006. **22**(12): p. 5385-5391.

54. Sun Sheng-Nan, W.C., Zhu Zan-Zan,Hou Yang-Long, Subbu S Venkatraman, Xu Zhi-Chuan, *Magnetic iron oxide nanoparticles: Synthesis and surface coating techniques for biomedical applications.* Chin. Phys. B, 2014. **23**(3).

55. Hong Zhao, J.G.a.U.O.H., *Process and formulation variables in the preparation of injectable and biodegradable magnetic microspheres.* Biomagnetic Research and Technology, 2007. **5**(2).

56. Khoee, S. and M. Yaghoobian, *An investigation into the role of surfactants in controlling particle size of polymeric nanocapsules containing penicillin-G in double emulsion.* European Journal of Medicinal Chemistry, 2009. **44**(6): p. 2392-2399.

57. Rosca, I.D., F. Watari, and M. Uo, *Microparticle formation and its mechanism in single and double emulsion solvent evaporation.* Journal of Controlled Release, 2004. **99**(2): p. 271-280.

58. Lee, J.W., T. Isobe, and M. Senna, *Magnetic properties of ultrafine magnetite particles and their slurries prepared via in-situ precipitation.* Colloids and Surfaces a-Physicochemical and Engineering Aspects, 1996. **109**: p. 121-127.

59. Willis, A.L., N.J. Turro, and S. O'Brien, *Spectroscopic characterization of the surface of iron oxide nanocrystals.* Chemistry of Materials, 2005. **17**(24): p. 5970-5975.

60. Park, J., et al., *One-nanometer-scale size-controlled synthesis of monodisperse magnetic iron oxide nanoparticles.* Angewandte Chemie-International Edition, 2005. **44**(19): p. 2872-2877.

61. Butter, K., A.P. Philipse, and G.J. Vroege, *Synthesis and properties of iron ferrofluids.* Journal of Magnetism and Magnetic Materials, 2002. **252**(1-3): p. 1-3.

62. Carpenter, E.E., C.T. Seip, and C.J. O'Connor, *Magnetism of nanophase metal and metal alloy particles formed in ordered phases.* Journal of Applied Physics, 1999. **85**(8): p. 5184-5186.

63. Wang, X., et al., *A general strategy for nanocrystal synthesis.* Nature, 2005. **437**(7055): p. 121.

64. Liu, Z.L., et al., *Synthesis and characterization of ultrafine well-dispersed magnetic nanoparticles.* Journal of Magnetism and Magnetic Materials, 2004. **283**(2-3): p. 258-262.

65. Gokhale, A.A., J. Lu, and I. Lee, *Immobilization of cellulase on magnetoresponsive graphene nano-supports.* Journal of Molecular Catalysis B: Enzymatic, 2013. **90**: p. 76-86.

66. Cohen-Sela, E., et al., *A new double emulsion solvent diffusion technique for encapsulating hydrophilic molecules in PLGA nanoparticles.* Journal of Controlled Release, 2009. **133**(2): p. 90-95.

67. Ji, S.W., et al., *Dynamic encapsulation of hydrophilic nisin in hydrophobic poly (lactic acid) particles with controlled morphology by a single emulsion process.* Journal of Colloid and Interface Science, 2014. **423**: p. 85-93.

68. Boxall, J.A., et al., *Droplet Size Scaling of Water-in-Oil Emulsions under Turbulent Flow.* Langmuir, 2012. **28**(1): p. 104-110.

69. Stroeve, P. and P.P. Varanasi, *An Experimental-Study on Double Emulsion Drop Breakup in Uniform Shear-Flow.* Journal of Colloid and Interface Science, 1984. **99**(2): p. 360-373.

70. Wang, J. and S.P. Schwendeman, *Mechanisms of solvent evaporation encapsulation processes: Prediction of solvent evaporation rate.* Journal of Pharmaceutical Sciences, 1999. **88**(10): p. 1090-1099.

71. Liu, B., J.W.J. de Folter, and H. Möhwald, *Magnetic nanoparticles-induced anisotropic shrinkage of polymer emulsion droplets.* Soft Matter, 2011. **7**(8): p. 3744.

72. Vilos, C., et al., *Superparamagnetic Poly (3-hydroxybutyrate-co-3 hydroxyvalerate) (PHBV) nanoparticles for biomedical applications.* Electronic Journal of Biotechnology, 2013. **16**(5).

73. Zhao, H., K. Saatchi, and U.O. Hafeli, *Preparation of biodegradable magnetic microspheres with poly(lactic acid)-coated magnetite.* Journal of Magnetism and Magnetic Materials, 2009. **321**(10): p. 1356-1363.

74. Xiao, Q., et al., *Preparation and characterization of polyaniline/nano-Fe3O4 composites via a novel Pickering emulsion route.* Synthetic Metals, 2007. **157**(18-20): p. 784-791.

75. Du, J. and R.K. O'Reilly, *Anisotropic particles with patchy, multicompartment and Janus architectures: preparation and application.* Chemical Society Reviews, 2011. **40**(5): p. 2402-2416.

76. Lee, K.J., J. Yoon, and J. Lahann, *Recent advances with anisotropic particles.* Current Opinion in Colloid & Interface Science, 2011. **16**(3): p. 195-202.

77. Nisisako, T., *Recent advances in microfluidic production of Janus droplets and particles.* Current Opinion in Colloid & Interface Science, 2016. **25**: p. 1-12.

78. Champion, J.A., Y.K. Katare, and S. Mitragotri, *Particle shape: a new design parameter for micro-and nanoscale drug delivery carriers.* Journal of Controlled Release, 2007. **121**(1): p. 3-9.

79. Huang, X., Q. Qian, and Y. Wang, *Anisotropic Particles from a One-Pot Double Emulsion Induced by Partial Wetting and Their Triggered Release.* Small, 2014. **10**(7): p. 1412-1420.

80. Mao, J., et al., *Macroporous and nanofibrous poly (lactide-co-glycolide)(50/50) scaffolds via phase separation combined with particle-leaching.* Materials Science and Engineering: C, 2012. **32**(6): p. 1407-1414.

81. Edwards, D.A., et al., *Large porous particles for pulmonary drug delivery.* Science, 1997. **276**(5320): p. 1868-1872.

82. Min, N.G., et al., *Anisotropic Microparticles Created by Phase Separation of Polymer Blends Confined in Monodisperse Emulsion Drops.* Langmuir, 2015. **31**(3): p. 937-943.

83. Zhang, Z.L. and S.C. Glotzer, *Self-assembly of patchy particles.* Nano Letters, 2004. **4**(8): p. 1407-1413.

84. Pawar, A.B. and I. Kretzschmar, *Fabrication, Assembly, and Application of Patchy Particles.* Macromolecular Rapid Communications, 2010. **31**(2): p. 150-168.

85. Kraft, D.J., et al., *Self-Assembly of Colloids with Liquid Protrusions.* Journal of the American Chemical Society, 2009. **131**(3): p. 1182-1186.

86. Snyder, C.E., et al., *Nanoscale functionalization and site-specific assembly of colloids by particle lithography.* Langmuir, 2005. **21**(11): p. 4813-4815.

87. Du, J.Z. and Y.M. Chen, *Organic-inorganic hybrid nanoparticles with a complex hollow structure.* Angewandte Chemie-International Edition, 2004. **43**(38): p. 5084-5087.

88. Srinivas, G. and J.W. Pitera, *Soft patchy nanoparticles from solution-phase self-assembly of binary diblock copolymers.* Nano Letters, 2008. **8**(2): p. 611-618.

89. Walther, A., C. Barner-Kowollik, and A.H.E. Muller, *Mixed, Multicompartment, or Janus Micelles? A Systematic Study of Thermoresponsive Bis-Hydrophilic Block Terpolymers.* Langmuir, 2010. **26**(14): p. 12237-12246.

90. Li, Z.B., et al., *Multicompartment micelles from ABC miktoarm stars in water.* Science, 2004. **306**(5693): p. 98-101.

91. Liu, C., M.A. Hillmyer, and T.P. Lodge, *Multicompartment Micelles from pH-Responsive Miktoarm Star Block Terpolymers.* Langmuir, 2009. **25**(24): p. 13718-13725.

92. Saito, N., et al., *Multicompartment Micelles from Polyester-Containing ABC Miktoarm Star Terpolymers.* Macromolecules, 2008. **41**(22): p. 8815-8822.

93. Li, Z.B., M.A. Hillmyer, and T.P. Lodge, *Morphologies of multicompartment micelles formed by ABC miktoarm star terpolymers.* Langmuir, 2006. **22**(22): p. 9409-9417.

94. Walther, A. and A.H.E. Muller, *Formation of hydrophobic bridges between multicompartment micelles of miktoarm star terpolymers in water.* Chemical Communications, 2009(9): p. 1127-1129.

95. Schacher, F., et al., *Interpolyelectrolyte Complexes of Dynamic Multicompartment Micelles.* Acs Nano, 2009. **3**(8): p. 2095-2102.

96. Schacher, F., et al., *Multicompartment Core Micelles of Triblock Terpolymers in Organic Media.* Macromolecules, 2009. **42**(10): p. 3540-3548.

97. Skrabania, K., et al., *Synthesis of Ternary, Hydrophilic-Lipophilic-Fluorophilic Block Copolymers by Consecutive RAFT Polymerizations and Their Self-Assembly into Multicompartment Micelles.* Macromolecules, 2010. **43**(1): p. 271-281.

98. Walther, A., C. Barner-Kowollik, and A.H. Müller, *Mixed, multicompartment, or Janus micelles? A systematic study of thermoresponsive bis-hydrophilic block terpolymers.* Langmuir, 2010. **26**(14): p. 12237-12246.

99. Tanaka, T., et al., *Preparation of "mushroom-like" Janus particles by site-selective surface-initiated atom transfer radical polymerization in aqueous dispersed systems.* Langmuir, 2010. **26**(11): p. 7843-7847.

100. Kim, S.W., et al., *Microfluidic fabrication of microparticles with multiple structures from a biodegradable polymer blend.* Rsc Advances, 2014. **4**(87): p. 46536-46540.

101. Dendukuri, D. and P.S. Doyle, *The synthesis and assembly of polymeric microparticles using microfluidics.* Advanced Materials, 2009. **21**(41): p. 4071-4086.

102. Lahann, J., *Recent Progress in Nano-biotechnology: Compartmentalized Micro- and Nanoparticles via Electrohydrodynamic Co-jetting.* Small, 2011. **7**(9): p. 1149-1156.

103. Wang, J.Y., et al., *Tuning Multiphase Amphiphilic Rods to Direct Self-Assembly.* Journal of the American Chemical Society, 2012. **134**(13): p. 5801-5806.

104. Roh, K.-H., D.C. Martin, and J. Lahann, *Biphasic Janus particles with nanoscale anisotropy.* Nature materials, 2005. **4**(10): p. 759-763.

105. Roh, K.-H., D.C. Martin, and J. Lahann, *Triphasic nanocolloids.* Journal of the American Chemical Society, 2006. **128**(21): p. 6796-6797.

106. Kim, B.-S. and T.A. Taton, *Multicomponent nanoparticles via self-assembly with cross-linked block copolymer surfactants.* Langmuir, 2007. **23**(4): p. 2198-2202.

107. Yang, Y., et al., *Development of highly porous large PLGA microparticles for pulmonary drug delivery.* Biomaterials, 2009. **30**(10): p. 1947-1953.

108. Klose, D., et al., *How porosity and size affect the drug release mechanisms from PLGA-based microparticles.* International journal of pharmaceutics, 2006. **314**(2): p. 198-206.

109. Sahoo, S.K., A.K. Panda, and V. Labhasetwar, *Characterization of porous PLGA/PLA microparticles as a scaffold for three dimensional growth of breast cancer cells.* Biomacromolecules, 2005. **6**(2): p. 1132-1139.

110. Salinas-Castillo, A., M. Camprubí-Robles, and R. Mallavia, *Synthesis of a new fluorescent conjugated polymer microsphere for chemical sensing in aqueous media.* Chemical Communications, 2010. **46**(8): p. 1263-1265.

111. Zhong, Z., et al., *Preparation of mesoscale hollow spheres of TiO 2 and SnO 2 by templating against crystalline arrays of polystyrene beads.* Advanced Materials, 2000. **12**(3): p. 206-209.

112. Wang, D. and F. Caruso, *Polyelectrolyte-coated colloid spheres as templates for sol− gel reactions.* Chemistry of materials, 2002. **14**(5): p. 1909-1913.

113. Chen, J.S., et al., *Top-down fabrication of α-Fe2O3 single-crystal nanodiscs and microparticles with tunable porosity for largely improved lithium storage properties.* Journal of the American Chemical Society, 2010. **132**(38): p. 13162-13164.

114. Eberle, U., M. Felderhoff, and F. Schueth, *Chemical and physical solutions for hydrogen storage.* Angewandte Chemie International Edition, 2009. **48**(36): p. 6608-6630.

115. Nikulshina, V., C. Gebald, and A. Steinfeld, *CO 2 capture from atmospheric air via consecutive CaO-carbonation and CaCO 3-calcination cycles in a fluidized-bed solar reactor.* Chemical Engineering Journal, 2009. **146**(2): p. 244-248.

116. Rao, T.P., R. Praveen, and S. Daniel, *Styrene–divinyl benzene copolymers: synthesis, characterization, and their role in inorganic trace analysis.* Critical Reviews in Analytical Chemistry, 2004. **34**(3-4): p. 177-193.

117. Rastogi, V., K.P. Velikov, and O.D. Velev, *Microfluidic characterization of sustained solute release from porous supraparticles.* Physical Chemistry Chemical Physics, 2010. **12**(38): p. 11975-11983.

118. Gokmen, M.T. and F.E. Du Prez, *Porous polymer particles—A comprehensive guide to synthesis, characterization, functionalization and applications.* Progress in polymer science, 2012. **37**(3): p. 365-405.

119. Beneš, M.J., D. Horák, and F. Svec, *Methacrylate-based chromatographic media.* Journal of separation science, 2005. **28**(15): p. 1855-1875.

120. Horák, D., et al., *The effect of polymeric porogen on the properties of macroporous poly (glycidyl methacrylate-co-ethylene dimethacrylate).* Polymer, 1993. **34**(16): p. 3481-3489.

121. Kanamori, K., et al., *Facile synthesis of macroporous cross-linked methacrylate gels by atom transfer radical polymerization.* Macromolecules, 2008. **41**(19): p. 7186-7193.

122. Zhou, W.-Q., et al., *Synthesis of macroporous poly (styrene-divinyl benzene) microspheres by surfactant reverse micelles swelling method.* Polymer, 2007. **48**(7): p. 1981-1988.

123. Wu, L., S. Bai, and Y. Sun, *Development of Rigid Bidisperse Porous Microspheres for High-Speed Protein Chromatography.* Biotechnology progress, 2003. **19**(4): p. 1300-1306.

124. Velev, O.D. and S. Gupta, *Materials Fabricated by Micro-and Nanoparticle Assembly–The Challenging Path from Science to Engineering.* Advanced Materials, 2009. **21**(19): p. 1897-1905.

125. Cho, Y.-S., et al., *Self-organization of colloidal nanospheres inside emulsion droplets: Higher-order clusters, supraparticles, and supraballs.* Colloids and Surfaces A: Physicochemical and Engineering Aspects, 2009. **345**(1): p. 237-245.

126. He, X., et al., *Synthesis of cagelike polymer microspheres with hollow core/porous shell structures by self-assembly of latex particles at the emulsion droplet interface.* Chemistry of materials, 2005. **17**(24): p. 5891-5892.

127. Nakashima, T., *Membrane emulsification by microporous glass.* Key Eng. Mater., 1991. **61**: p. 513-516.

128. Vladisavljević, G.T. and R.A. Williams, *Recent developments in manufacturing emulsions and particulate products using membranes.* Advances in colloid and interface science, 2005. **113**(1): p. 1-20.

129. Malik, D.J., et al., *Synthesis and characterization of size-selective nanoporous polymeric adsorbents for blood purification.* Separation and purification technology, 2009. **66**(3): p. 578-585.

130. Xu, S., et al., *Generation of monodisperse particles by using microfluidics: control over size, shape, and composition.* Angewandte Chemie, 2005. **117**(5): p. 734-738.

131. Wan, J., et al., *Controllable Microfluidic Production of Microbubbles in Water-in-Oil Emulsions and the Formation of Porous Microparticles.* Advanced Materials, 2008. **20**(17): p. 3314-3318.

132. Gong, X., W. Wen, and P. Sheng, *Microfluidic fabrication of porous polymer microspheres: dual reactions in single droplets.* Langmuir, 2009. **25**(12): p. 7072-7077.

133. Cohen, I., et al., *Using selective withdrawal to coat microparticles.* Science, 2001. **292**(5515): p. 265-267.

134. Dendukuri, D., et al., *Stop-flow lithography in a microfluidic device.* Lab on a Chip, 2007. **7**(7): p. 818-828.

135. Bhaskar, S. and J. Lahann, *Microstructured materials based on multicompartmental fibers.* Journal of the American Chemical Society, 2009. **131**(19): p. 6650-6651.

136. Owens, J.L., K.S. Anseth, and T.W. Randolph, *Compressed antisolvent precipitation and photopolymerization to form highly cross-linked polymer particles.* Macromolecules, 2002. **35**(11): p. 4289-4296.

137. Cai, Q., et al., *A novel porous cells scaffold made of polylactide–dextran blend by combining phase-separation and particle-leaching techniques.* Biomaterials, 2002. **23**(23): p. 4483-4492.

138. Kumari, A., S.K. Yadav, and S.C. Yadav, *Biodegradable polymeric nanoparticles based drug delivery systems.* Colloids Surf B Biointerfaces, 2010. **75**(1): p. 1-18.

139. Hans, M. and A. Lowman, *Biodegradable nanoparticles for drug delivery and targeting.* Current Opinion in Solid State and Materials Science, 2002. **6**(4): p. 319-327.

140. Kriven, W.M., et al., *Bio-resorbable nanoceramics for gene and drug delivery.* Mrs Bulletin, 2004. **29**(01): p. 33-37.

141. Liong, M., et al., *Multifunctional inorganic nanoparticles for imaging, targeting, and drug delivery.* ACS nano, 2008. **2**(5): p. 889-896.

142. van Rijt, S.H. and P.J. Sadler, *Current applications and future potential for bioinorganic chemistry in the development of anticancer drugs.* Drug discovery today, 2009. **14**(23): p. 1089-1097.

143. Carretero, M.I. and M. Pozo, *Clay and non-clay minerals in the pharmaceutical industry: Part I. Excipients and medical applications.* Applied Clay Science, 2009. **46**(1): p. 73-80.

144. Carretero, M.I., *Clay minerals and their beneficial effects upon human health. A review.* Applied Clay Science, 2002. **21**(3): p. 155-163.

145. Suresh, R., et al., *Nanoclay drug delivery system.* International Journal of Pharmaceutical Sciences and Nanotechnology, 2010. **3**(2): p. 901-905.

146. Morrison, K.D., R. Misra, and L.B. Williams, *Unearthing the antibacterial mechanism of medicinal clay: A geochemical approach to combating antibiotic resistance.* Scientific reports, 2016. **6**.

147. Ghadiri, M., W. Chrzanowski, and R. Rohanizadeh, *Biomedical applications of cationic clay minerals.* RSC Advances, 2015. **5**(37): p. 29467-29481.

148. Feng, S.-S., et al., *Poly (lactide)–vitamin E derivative/montmorillonite nanoparticle formulations for the oral delivery of Docetaxel.* Biomaterials, 2009. **30**(19): p. 3297-3306.

149. Cypes, S.H., W.M. Saltzman, and E.P. Giannelis, *Organosilicate-polymer drug delivery systems: controlled release and enhanced mechanical properties.* Journal of controlled release, 2003. **90**(2): p. 163-169.

150. Viseras, C., et al., *Biopolymer–clay nanocomposites for controlled drug delivery.* Materials Science and Technology, 2008. **24**(9): p. 1020-1026.

151. Viseras, C., et al., *Current challenges in clay minerals for drug delivery.* Applied Clay Science, 2010. **48**(3): p. 291-295.

152. Sun, B., B. Ranganathan, and S.-S. Feng, *Multifunctional poly (D, L-lactide-co-glycolide)/montmorillonite (PLGA/MMT) nanoparticles decorated by Trastuzumab for targeted chemotherapy of breast cancer.* Biomaterials, 2008. **29**(4): p. 475-486.

153. Dong, Y. and S.-S. Feng, *Poly (d, l-lactide-co-glycolide)/montmorillonite nanoparticles for oral delivery of anticancer drugs.* Biomaterials, 2005. **26**(30): p. 6068-6076.

154. Yang, Y., et al., *Nanoclay and modified nanoclay as sorbents for anionic, cationic and nonionic dyes.* Textile research journal, 2005. **75**(8): p. 622-627.

155. Roth, E.A., S. Agarwal, and R.K. Gupta, *Nanoclay-based solid sorbents for CO2 capture.* Energy & Fuels, 2013. **27**(8): p. 4129-4136.

156. Hussain, F., et al., *Review article: polymer-matrix nanocomposites, processing, manufacturing, and application: an overview.* Journal of composite materials, 2006. **40**(17): p. 1511-1575.

157. Bhattacharyya, K.G. and S. Sen Gupta, *Adsorption of a few heavy metals on natural and modified kaolinite and montmorillonite: A review.* Advances in Colloid and Interface Science, 2008. **140**(2): p. 114-131.

158. Kahr, G. and F. Madsen, *Determination of the cation exchange capacity and the surface area of bentonite, illite and kaolinite by methylene blue adsorption.* Applied Clay Science, 1995. **9**(5): p. 327-336.

159. Patel, H.A., et al., *Nanoclays for polymer nanocomposites, paints, inks, greases and cosmetics formulations, drug delivery vehicle and waste water treatment.* Bulletin of Materials Science, 2006. **29**(2): p. 133-145.

160. Czimerova, A., J. Bujdak, and R. Dohrmann, *Traditional and novel methods for estimating the layer charge of smectites.* Applied Clay Science, 2006. **34**(1-4): p. 2-13.

161. He, H.P., et al., *Organoclays prepared from montmorillonites with different cation exchange capacity and surfactant configuration.* Applied Clay Science, 2010. **48**(1-2): p. 67-72.

162. Mallakpour, S. and M. Dinari, *Synthesis and Properties of Biodegradable Poly(vinyl alcohol)/Organo-nanoclay Bionanocomposites.* Journal of Polymers and the Environment, 2012. **20**(3): p. 732-740.

163. Utracki, L., M. Sepehr, and E. Boccaleri, *Synthetic, layered nanoparticles for polymeric nanocomposites (PNCs).* Polymers for advanced technologies, 2007. **18**(1): p. 1-37.

164. Ray, S.S. and M. Okamoto, *Polymer/layered silicate nanocomposites: a review from preparation to processing.* Progress in polymer science, 2003. **28**(11): p. 1539-1641.

165. Lee, W.F. and L.L. Jou, *Effect of the intercalation agent content of montmorillonite on the swelling behavior and drug release behavior of nanocomposite hydrogels.* Journal of applied polymer science, 2004. **94**(1): p. 74-82.

166. Lee, W.F. and Y.T. Fu, *Effect of montmorillonite on the swelling behavior and drug-release behavior of nanocomposite hydrogels.* Journal of applied polymer science, 2003. **89**(13): p. 3652-3660.

167. Pongjanyakul, T. and S. Puttipipatkhachorn, *Sodium alginate-magnesium aluminum silicate composite gels: characterization of flow behavior, microviscosity, and drug diffusivity.* AAPS PharmSciTech, 2007. **8**(3): p. E158-E165.

168. Lee, W.F. and Y.C. Chen, *Effect of bentonite on the physical properties and drug-release behavior of poly (AA-co-PEGMEA)/bentonite nanocomposite hydrogels for mucoadhesive.* Journal of applied polymer science, 2004. **91**(5): p. 2934-2941.

169. Luckham, P.F. and S. Rossi, *The colloidal and rheological properties of bentonite suspensions.* Advances in Colloid and Interface Science, 1999. **82**(1): p. 43-92.

170. Abend, S. and G. Lagaly, *Sol–gel transitions of sodium montmorillonite dispersions.* Applied Clay Science, 2000. **16**(3): p. 201-227.

171. An, J.-H. and S. Dultz, *Adsorption of tannic acid on chitosan-montmorillonite as a function of pH and surface charge properties.* Applied Clay Science, 2007. **36**(4): p. 256-264.

172. Wang, X., et al., *Chitosan/organic rectorite nanocomposite films: Structure, characteristic and drug delivery behaviour.* Carbohydrate Polymers, 2007. **69**(1): p. 41-49.

173. Zimmermann, F., et al., *Acetone, methyl ethyl ketone, ethyl acetate, acetonitrile and other polar aprotic solvents are strong inducers of aneuploidy in Saccharomyces cerevisiae.* Mutation Research/Fundamental and Molecular Mechanisms of Mutagenesis, 1985. **149**(3): p. 339-351.

174. Ji, S.W., et al., *Transitional behavior of polymeric hollow microsphere formation in turbulent shear flow by emulsion diffusion method.* Polymer, 2012. **53**(1): p. 205-212.

175. Voorn, D.J., W. Ming, and A.M. van Herk, *Polymer-clay nanocomposite latex particles by inverse pickering emulsion polymerization stabilized with hydrophobic montmorillonite platelets.* Macromolecules, 2006. **39**(6): p. 2137-2143.

176. Teixeira, R.F.A., et al., *Pickering Emulsion Polymerization Using Laponite Clay as Stabilizer To Prepare Armored "Soft" Polymer Latexes.* Macromolecules, 2011. **44**(18): p. 7415-7422.

177. Song, A., et al., *Encapsulation of hydrophobic or hydrophilic iron oxide nanoparticles into poly (lactic acid) micro/nanoparticles via adaptable emulsion setup.* Journal of applied polymer science, 2016. **133**(45).

178. Hariharan, S., et al., *A study of the efficacy of diclofenac iontophoresis for providing effective topical analgesia.* The internet journal of pain, symptom control and palliative care, 2007. **5**(2).